FCT Fundação para a Ciência e Tecnologia
MINISTÉRIO DA EDUCAÇÃO E CIÊNCIA Portugal

Development of multifunctional coatings deposited on polymers based sensors for biomedical applicationsse
Sandra Mariana da Silva Marques
UMinho | 2016

Universidade do Minho
Escola de Engenharia

Sandra Mariana da Silva Marques

Development of multifunctional coatings deposited on polymers based sensors for biomedical applications

janeiro de 2016

Universidade do Minho
Escola de Engenharia

Sandra Mariana da Silva Marques

Development of multifunctional coatings deposited on polymers based sensors for biomedical applications

Tese de Doutoramento
Programa Doutoral em Engenharia de Materiais

Trabalho efectuado sob a orientação de
Professor Doutora Sandra Maria Fernandes Carvalho
Professor Doutor Senentxu Lanceros-Mendez
Professora Doutora Mariana Contente Rangel Henriques

janeiro de 2016

STATEMENT OF INTEGRITY

I hereby declare having conducted my thesis with integrity. I confirm that I have not used plagiarism or any form of falsification of results in the process of the thesis elaboration.

I further declare that I have fully acknowledged the Code of Ethical Conduct of the University of Minho.

University of Minho, _____

Full name: Sandra Mariana da Silva Marques

Signature: Sandra Mariana da Silva Marques

I dedicate this work to

Ricardo, my brother and my parents,

Thanks

Acknowledgements

During the journey of my PhD, in different ways, several people have contributed to make this moment possible. To them I owe my knowledge, my sensitivity, attitude, courage, my reasoning ... Thanks always involve a wide range of people who would be a waste of forgetting someone, however, there are human beings who need to be recorded in this document.

My first acknowledgment is for my supervisor Prof. Sandra Carvalho, I want to thanks the guide lines, ideas, availability, shared knowledge and most of all, the friendship revealed over all these years.

To my co-supervisors, Prof. Senentxu and Prof. Mariana Henriques, thank you for your friendship, sharing of experiences and encouragement for this work has more sense.

I would like to mention my colleagues/friends of Surface modification and functionalization research group for helping me along this time, always with a constructive and mutual aid spirit. In particular to Edgar Carneiro, Cristiana Alves, Sebastian Calderon, Isabel Carvalho, Isabel Ferreri, Noora Manninen and Rita Rebelo for their support and friendship.

I also want to thank Prof. Albano Cavaleiro for your friendship and all the scientific discussions that made this work better.

I want gratefully acknowledge the funding form the Portuguese national funds through the FCT- Fundação para a Ciência e a Tecnologia, (project SFRH/BD/71259/2010). Also thank support by FEDER through the COMPETE Program and by the Portuguese Foundation for Science and Technology (FCT) in the framework of the Strategic Project PEST-C/FIS/UI607/2011 and the project Matepro –Optimizing Materials and Processes", ref. NORTE-07-0124-FEDER-000037", co-funded by the "Programa Operacional Regional do Norte" (ON.2 – O Novo Norte), under the "Quadro de Referência Estratégico Nacional" (QREN), through the "Fundo Europeu de Desenvolvimento Regional" (FEDER).

I would like to thank the researchers at the Center for Biomaterials and Tissue Engineering of the Universitat Politècnica de València for the excellent reception and availability during my stay for the biological tests, especially to Prof. Jose Luis Ribelles, Patricia Rico and Hayk Mnatsakanyan.

To all of my friends, because it would be a huge fault to forget some, I am grateful for the kindness, words of encouragement and patience to hearing me many times... You are fundamental in my life.

Very special thanks to my parents for everything that have done for me, for all you tried to do and for all that will be done for me. What I am today I owe it to you.

I also want to thank to my dear aunt Tété, most of the times you are a second mother to me.

I want to thank to my brother Carlos for the support, encouragement and incentive that, in your own way, you always gave me.

Lastly but most important of all, I thank to my boyfriend/husband Ricardo that has been always my support, my refuge, my joy and my love. You sure make a difference in all aspects of my life, thank you mostly for your patience. Love you! :)

To all, my most sincere thanks...

Abstract

Within the framework of materials for biomedical applications, piezoelectric materials are interesting for the development of sensors and actuators in areas such as smart prosthesis, implantable biosensors and biomechanical signal monitoring, among others. However, for the acquisition/application of the electrical signal, suitable electrodes must be produced. Therefore, the aim of this work was the development of multifunctional coatings on a polymeric base substrate for biosensor applications.

The coatings were deposited by magnetron sputtering on polymers based sensors. The multifunctionality was achieved due to the good mechanical and electrical properties, together with the antibacterial characteristics obtained through silver clusters inclusions, without significantly changing the piezoelectric response of the polymers sensors. By changing the deposition conditions, it was possible to obtain coatings with different silver, titanium or nitrogen content, thus exploring the vast spectrum of their electrical, mechanical and biological properties as well as the piezoresistive response.

In this work, the different processing conditions allowed to obtain two different systems: $Ti_{1-x}Ag_x$ with different Ag/Ti atomic ratio and different Ag-TiN_x samples with increasing N content. These electrodes were deposited at room temperature on poly(vinylidene fluoride), PVDF, the all-round best piezoelectric polymer. For both series, results revealed that the deposition conditions preserved the polymer structure. In samples $Ti_{1-x}Ag_x$ it was suggested the presence of crystalline hcp-Ti phase in pure titanium coating, an fcc-Ag phase in pure silver coating and, besides these two phases, the possibility of a TiAg phase. On the other hand, for the Ag-TiN_x series, the results revealed the presence of crystalline fcc-TiN phase and fcc-Ag phase in samples with N_2 flow above 3 sccm. Only on Ag-TiN_x electrodes it was possible to found Ag clusters.

Sheet resistivity values showed a typical behavior of a binary alloy system for the $Ti_{1-x}Ag_x$ series, being low for coatings rich in Ti and Ag and slightly higher for coatings with a mixture of Ti and Ag. For the Ag-TiN_x series, increasing nitrogen flow lead to lower sheet resistivity values than in the sample without nitrogen.

Piezoelectricity of the different samples of $Ti_{1-x}Ag_x$ series presented similar values, but for the Ag-TiN_x series, the increase of nitrogen flow leads also to a decrease of the piezoelectric response. Despite this behavior, it was possible to conclude that the deposition conditions do not significantly affect the piezoelectric response of the polymer which maintain its suitable characteristics for sensor applications.

The mechanical and piezoresistive performance of the two series was assessed by uniaxial stretch tests and electrical resistance variation measurements during mechanical stimulus, respectively. It was possible to conclude that all electrodes show piezoresistive properties, with an increase of the electrical resistance as the applied strain increases. The sensitivity of the piezoresisitive materials can be characterized by the gauge factor (GF). The thin films deposited on β-PVDF polymer exhibit a similar performance with respect to the mechanical properties, where GF increases with increasing strain, being larger in the plastic zone than in elastic one. The Ag-TiN_x samples show higher GF values compared to the other series that can be explained by the presence of Ag nanoparticles/clusters imbedded in the TiN matrix. Higher GF values are desired for more sensitive sensors.

The antimicrobial activity of samples from both series was assessed by agar diffusion method (Halo test). Only electrodes from the Ag-TiN_x series presented antibacterial activity. As-deposited Ag-TiN_x electrodes exhibited silver clusters smaller than 4 nm and presented some Ag segregation in the TiN matrix, which disappeared after Halo test. This suggests that Ag nanoparticles aggregate and/or diffuse on the agar inhibiting bacterial growth. Therefore, Ag-TiN_x electrodes are more promising candidates to be used than $Ti_{1-x}Ag_x$ electrodes as these electrodes achieved the desired antibacterial activity.

Osteogenesis was also evaluated, in samples from both series, using MC3T3 osteoblastic cells. The results indicated lower cells attachment on the Ag-TiN_x electrodes compared with the $Ti_{1-x}Ag_x$ electrodes. The same behavior was observed for proliferation and differentiation tests. So, it was concluded that, the presence of silver nanoparticles in the surface of the Ag-TiN_x electrodes has a significant effect on antimicrobial activity as well as on the cell response.

So, as main conclusion of this work, a multifunctional electrode was achieved with antibacterial activity, which at an early stage does not promote animal cells adhesion and it still has proper electrical and mechanical properties. Further, it preserves the piezoelectric response of the polymer when deposited on PVDF and shows itself suitable and useful piezoresistive response for sensor applications.

Resumo

No âmbito dos materiais para aplicações biomédicas, os materiais piezoelétricos são interessantes para o desenvolvimento de sensores e atuadores em áreas como, próteses inteligentes, biossensores implantáveis, monitorização de sinais biomecânicos, entre outros. Contudo, para a aquisição/aplicação do sinal elétrico do sensor, terão de ser depositados elétrodos adequados. O objetivo deste trabalho visou assim, o desenvolvimento de revestimentos multifuncionais sobre uma base polimérica para aplicação em biossensores.

Os revestimentos foram depositados por pulverização catódica em polímeros. A multifuncionalidade foi conseguida devido às boas propriedades mecânicas e elétricas, assim como as características antibacterianas obtidas através da incorporação de nanopartículas de prata, sem alterar significativamente a resposta piezoelétrica dos polímeros base do sensor. Pela variação das condições de deposição foi possível obter revestimentos com diferentes teores de prata, titânio ou azoto, explorando desta forma o vasto espectro de propriedades elétricas, mecânicas e biológicas, assim como a resposta piezoresistiva.

Neste projeto, as diferentes condições de processamento, permitiam obter dois sistemas diferentes: $Ti_{1-x}Ag_x$ com diferentes razões atómicas Ag/Ti e Ag-TiN_x diferentes, com o aumento do teor de azoto. Estes elétrodos foram depositados à temperatura ambiente sobre fluoreto de polivinilideno (PVDF), o melhor polímero piezoelétrico. Para ambas as séries os resultados revelaram que as condições de deposição utilizadas preservaram a estrutura do polímero. Nas amostras de $Ti_{1-x}Ag_x$, foi sugerida a presença de uma fase cristalina hexagonal de Ti para o revestimento de titânio puro, uma fase de cfc-Ag para o revestimento de prata pura e para além destas fases, a possibilidade de uma fase TiAg. Por outro lado, para a série Ag-TiN_x, os resultados relevaram a presença das fases cristalinas cfc-TiN e cfc-Ag para amostras depositadas com fluxo de N_2 superior a 3 sccm. Apenas nos elétrodos da serie Ag-TiN_x foi possível observar pequenos aglomerados de prata à superfície.

Os resultados de resistividade mostraram um comportamento típico de uma liga metálica para a série $Ti_{1-x}Ag_x$, com valores baixos para as zonas ricas em Ti e em Ag e valores ligeiramente mais elevados para os revestimentos que exibem uma mistura de Ti e Ag. Relativamente á serie Ag-TiN_x, o aumento do teor de azoto induziu valores de resistividade mais baixos do que a correspondente amostra sem azoto.

A piezoeletricidade das diferentes amostras da serie $Ti_{1-x}Ag_x$ apresentam valores semelhantes, mas para a série Ag-TiN_x o aumento do fluxo de azoto leva a uma diminuição da resposta piezoelétrica. Apesar deste comportamento, foi possível concluir que as condições de

deposição não afetam significativamente a resposta piezoelétrica do polímero que mantém as características adequadas para aplicações em sensores.

O desempenho mecânico e piezoresistivo das duas séries foram avaliados através de ensaios de tração uniaxial e medições de variação da resistência elétrica durante o estímulo mecânico, respetivamente. Foi possível concluir que todos os elétrodos apresentam propriedades piezoresistivas, aumentando a resistência elétrica com o aumento da deformação aplicada. Os diferentes revestimentos depositados sobre o β-PVDF apresentam um desempenho semelhante no que diz respeito às propriedades mecânicas, em que o fator de sensibilidade do sensor aumenta com o aumento da deformação, sendo maior na zona plástica que na elástica. As amostras da série Ag-TiN_x apresentar valores de sensibilidade mais elevados em comparação com a outra série que pode ser explicado pela presença de nanopartículas de Ag embebidas numa matriz de TiN.

A atividade antimicrobiana de amostras de ambas as séries foi avaliada pelo método de difusão em ágar (teste de Halo). Somente os elétrodos da série Ag-TiN_x apresentaram atividade antibacteriana. Os elétrodos desta série exibem aglomerados de Ag menores que 4 nm e apresentaram segregação de Ag na matriz TiN que desaparecem após o teste. Isto sugere que as nanopartículas de Ag agregam e/ou difundem para o agar matando ou inibindo o crescimento bacteriano. Sendo assim, os elétrodos da série Ag-TiN_x são mais promissores como candidatos para serem utilizados como elétrodos do que a série $Ti_{1-x}Ag_x$, uma vez que estes elétrodos possuem a atividade antibacteriana desejada.

A osteogénese foi também avaliada, nas amostras das duas séries, usando células osteoblásticas MC3T3. Os resultados indicaram menos células aderidas nos elétrodos Ag-TiN_x em comparação com elétrodos $Ti_{1-x}Ag_x$. O mesmo comportamento foi observado para os ensaios de proliferação e de diferenciação. Assim, foi possível concluir que, a presença de nanopartículas de prata na superfície dos elétrodos de Ag-TiN_x tem um efeito significativo na atividade antimicrobiana assim como na resposta das células.

Assim, como conclusão principal deste trabalho, foi conseguido um elétrodo multifuncional com atividade antibacteriana, que numa fase inicial não promove adesão celular e ainda tem boas propriedades elétricas e mecânicas. Além disso, este revestimento permite preservar a resposta piezoelétrica do polímero quando depositado em PVDF e mostra resposta piezoresistiva adequada e útil para aplicações em sensores.

Table of contents

List of figures

List of tables

List of Symbols and Abbreviations

Description		Unit
d_{33}	Piezoelectricity	$pC.N^{-1}$
E	Young's Modulus	GPa
ε	Mechanical strain	%
F	Force	N
l	Length	m
J	Current density	mA/cm^2
R	Electrical resistance	Ω
t	Time	s
V	Electrical potential difference	V
v	Velocity	m/s
σ	Stress	MPa
λ	Wavelength	nm
ρ	Resistivity	Ω /sq

A

AFM – Atomic force microscopy

Ag – Silver

Ag^{+}- Silver ions

Al_2O_3 - Alumia

Ag NPs – Silver nanoparticles

Ag-TiN – Titanium nitride doped with silver

Ar – Argon

ARXPS – Angle-resolved X-ray photoelectron spectroscopy

B

BSE – Backcattered electron mode

C

CFU – Colony-forming unit

CVD – Chemical vapor depostition

D

DMEM – Dulbecco's modified eagle medium

DPBS – Dulbecco's phosphate buffered saline

E

ECM – Extracellular matrix

EDS – Energy dispersive spectroscopy

EPMA – Electron probe micro-analysis

F

FN – Fibronectin

G

GDOES – Glow discharge optical emission spectroscopy

GF – Gauge factor

H

HAP – Hydroxyapatite

N

N_2 – Nitrogen

O

OCN – Osteocalcin

OPN – Osteopontin

P

PBS – Phosphate buffered saline

PE – Polyethylene

PEEK - Polyetheretherketone

PET – Polyethylene terephthalate

PHEMA –Polyhydroxyethylmethacrylate

PLLA – Polylactic acid

PLGA – Poly(lactic-co-glycolic acid)

PMMA – Poly(methyl methacrylate)

4PP – 4 point probe

PP – Polypropylene

PTFE – Polytetrafluoroethylene

PVC - Polyvinyl chloride

PVD – Physical vapor deposition

PVDF – Polyvinylidene fluoride

PVDF-α – alpha phase of PVDF

PVDF-β – beta phase of PVDF

R

RBS – Rutherford backscattering spectrometry

Runx2 – Runt-related transcription factor 2

S

SEEY – Secondary electron emission yield

Sccm – Standart cubic centimeters per minute

SEM – Scanning electron microscopy

SSS – Sustained self-sputtering effect

T

TEM – Transmission electron microscopy

THR – Total hip replacement

Tm – Melting temperature

Tg – Glass transition temperature

Ti – Titanium

Ti-Ag – Tianium doped with silver

TiCN – Titanium carbonitride

TiN – Titanium nitride

TiO_2 – Titanium dioxide

U

UHMWPE – Ultra-high-molecular-weight polyethylene

UV – Ultraviolet

V

VDF – Vinylidene Fluoride

X

XPS – X-ray photoelectron spectroscopy

XRD – X-ray Diffraction

Z

Zol – Zone of inhibition

ZrO_2 – Zirconia

1. Introduction

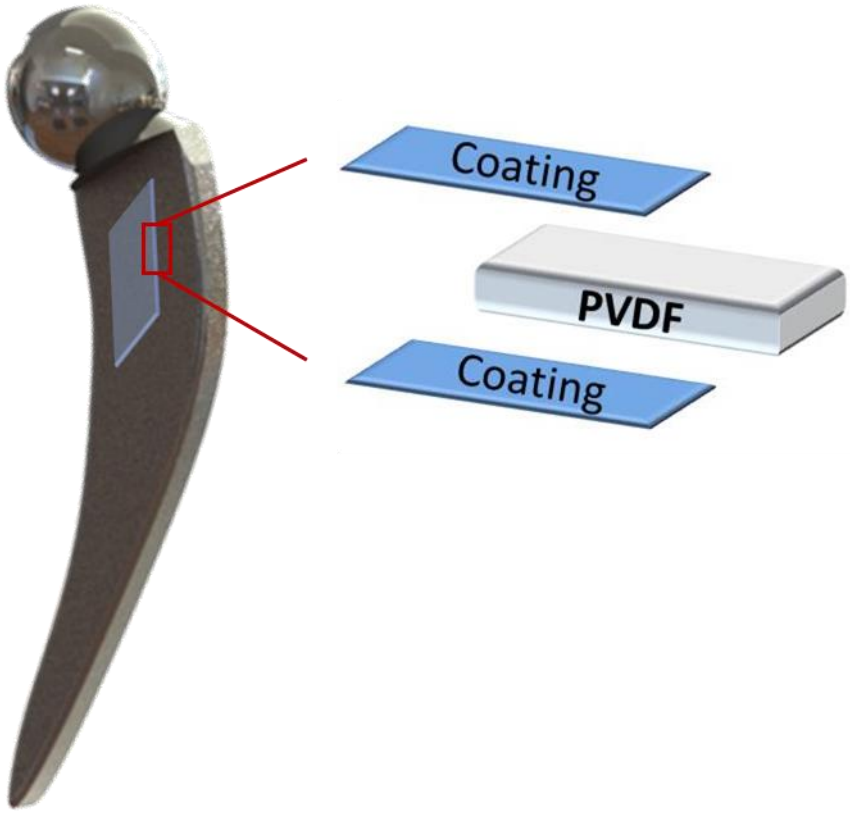

This chapter presents the motivation and the objectives of this research project. It also includes the description of the thesis structure and methodology.

1.1 Motivation

The increase of human average life expectancy has promoted an increasing incidence of joint diseases, often leading to the need for partial or total joint replacement by artificial implants. So, it becomes very important to choose suitable materials for these implants, in order to make them biocompatible, bioactive and with antibacterial properties that prevent the failure of these artificial implants by infections.

Thus, the challenge is to implement smart and functional implants, by application of sensors that early detect problems associated to the use of these artificial devices. The principal causes of failure of this artificial implants are: low resistance to stress, high wear that leads to release of small particles, corrosion resistance, infections by bacterial colonization and fractures. Owing the limitations of the materials currently used to comply these requirements, the use of smart materials and the development of coated materials have been increasingly considered as a solution to minimize the problems associated with artificial implants. Thus, it is mostly convenient to use smart implants, that early detect problems and communicate variations of relevant parameters (such as variations of pressure or bad interaction of prosthesis with surrounding tissues) to an acquisition system.

As mechanical dynamic loads is one of the most important requirement, the use of piezoelectric materials is interesting for the development of smart implants, since they react to mechanical and electrical applications and can be implemented without the need external applied power and may be used as sensors and actuators. However, for the acquisition of the electrical signal of the sensor suitable electrodes must be deposited.

Therefore, this research work aims to the development of multifunctional coatings based on $Ti_{1-x}Ag_x$ and Ag-TiN_x deposited on polymeric piezoelectric material, capable of detecting pressure variations for their incorporation in biomedical devices, more specifically smart prosthesis. The choice of these materials is justified by the properties of titanium, nitrogen and silver. Titanium, beyond its biocompatibility, was used as a good conductor, the incorporation of nitrogen aimed to promote mechanical strength and silver was used to ensure the antimicrobial activity.

1.2 Objectives

The main objective of this research is to develop multifunctional coatings based on two systems, $Ti_{1-x}Ag_x$ and Ag-TiN_x, with suitable mechanical and electrical properties as well as antibacterial activity. These coatings are deposited on piezoelectric polymer substrates whose function is to serve as sensors for biomedical applications.

The specific objectives of this work include:

- ✓ Deposition of two different systems by magnetron sputtering: (i) $Ti_{1-x}Ag_x$ with different Ag/Ti atomic ratio and (ii) Ag-TiN_x coatings with different nitrogen flow;
- ✓ Deposition of these coatings on piezoelectric polymer substrates (PVDF);
- ✓ Correlation of the structure, mechanical and electrical behavior with the deposition parameters and the atomic composition;
- ✓ Study of the piezoelectric response of different systems, ensuring that the coatings do not change significantly the piezoelectricity of the polymer;
- ✓ Evaluation of the mechanical and electromechanical responses of the two systems;
- ✓ Evaluation of the antimicrobial response;
- ✓ Assessment of the osteobastic cells response of the two systems.

A squematic representation of the different steps of the investigation are sumarized in Figure 1.1.

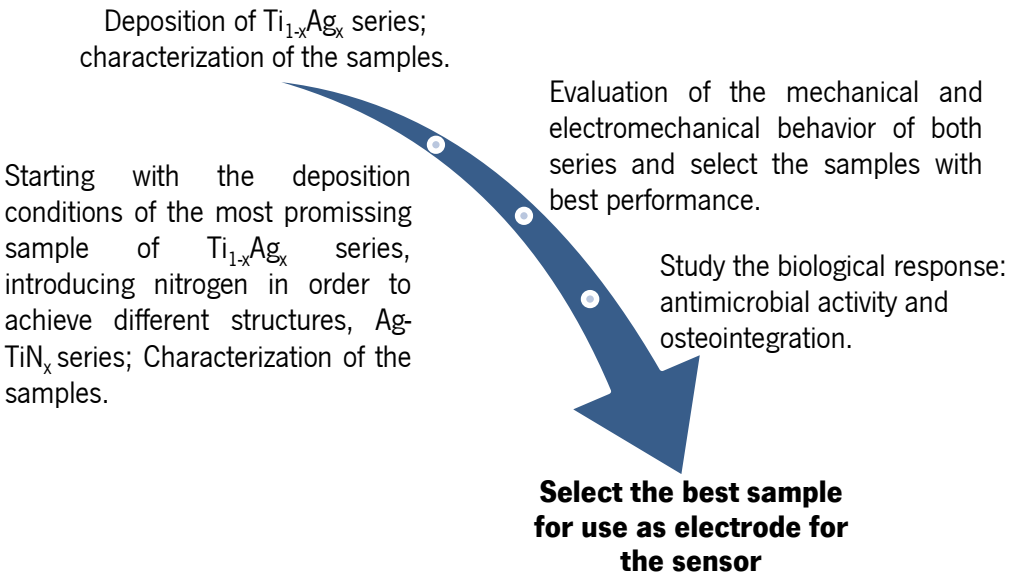

Figure 1.1 –Schematic representation of the steps of this investigation to achieve the best electrode.

1.3 Structure and methodology

The present thesis is divided in eight chapters with the objective to provide a comprehensive description of the progress achieved during this investigation. The chapters are presented in such a way that demonstrate the consecutive advance of the research. Five of those chapters are scientific articles published, submitted or ready-to-submission to international peer-reviewed journals. The development of different electrodes deposited on a polymer based sensor, their physical and chemical characterization, as well as mechanical and biological behavior are described as follows:

The present chapter (Chapter 1) describes the motivation, main objectives, and structure and methodology of this work.

Chapter 2 is divided in three main parts, consisting of (i): a review of the literature about the evolution of the materials used in prostheses over time, (ii) an explanation of the piezoelectric polymer used in this work and (iii) a description of the used multifunctional coatings for sensor devices, focusing on its function as electrodes. However, it should be pointed out that no extensive state-of-the-art or theoretical background is performed since the most specific bibliographic and theoretical concepts are included in the introduction section of each chapter.

On chapter 3 it is included the deposition parameters used for sputtering of $Ti_{1-x}Ag_x$ electrodes and their characterization regarding the chemical composition, structural analysis, topography, morphology, sheet resistivity and piezoelectricity.

Chapter 4 reports on the development of Ag-TiN_x electrodes and their characterization, following the same line used for the $Ti_{1-x}Ag_x$ previous system, characterized in chapter 3. Since the framework of these two chapters is very similar, their introductions sometimes show some repeated information.

Since these different electrodes will be subjected to mechanical solicitations, strain-stress tests were performed in order to assess the electrodes mechanical and piezoresistive properties. This study is described on chapter 5. The results obtained will enable the selection of the best coating for further characterization e.g. antimicrobial and osteogenic response.

Chapter 6 focus on the antibacterial behavior of the developed samples that present the best mechanical behavior.

Since the electrodes will be used in contact with the bone, osteogenesis of samples of the two different systems is analyzed. Chapter 7 focuses in adhesion, proliferation and differentiation tests using MC3T3 osteoblastic cells.

Finally, chapter 8 presents the overall conclusions and suggestions for the future work.

2. State of the art

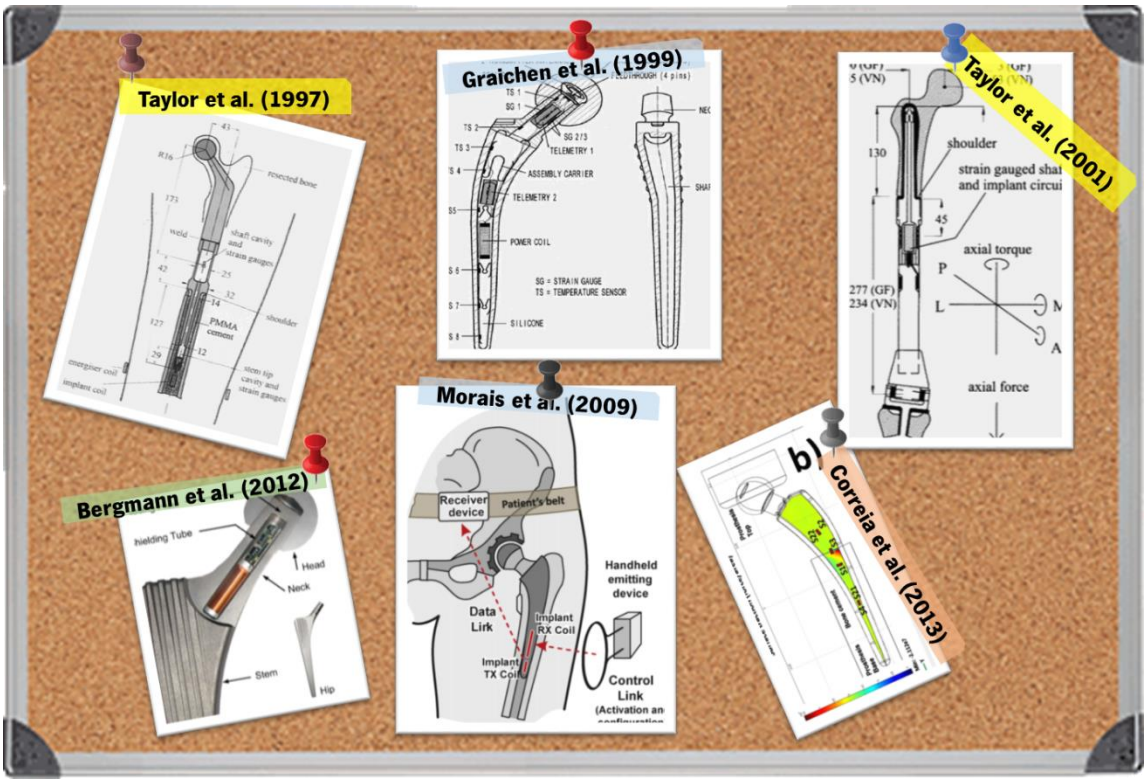

In the last decades, there has been a strong development of nanotechnology in materials science and engineering. The recent interest in the so-called multifunctional coatings is of increasing importance, not only scientifically but also for industrial applications. Such coatings are intended for applications in different areas to enhance the required properties. Currently, medicine and biomedical engineering are promising and exciting fields where the application of these coatings is very attractive. In a specific case, the current trend in the science of orthopedic implants is to use smart prosthesis. For this particular application, the choice of the coatings for their use as electrodes for sensors, is increasingly important.

In this chapter a review of the literature about the evolutions of the materials used in prostheses, main failures, the base material for the sensors and the choice of the multifunctional coatings used as electrodes is presented and is divided into three parts:

- ✓ Historical background on the evolution of materials used in prostheses and the main failures;
- ✓ Piezoelectric materials, focusing on the reasons for the choice of PVDF;
- ✓ Multifunctional coatings as promising electrodes, due to its electrical, mechanical and biological performance.

2.1 Historical background

The research in materials for application in artificial implants, such as prostheses, date from the first half of the XIX century. Since the problems associated with musculoskeletal system are of large interest, Table 2.1 presents a chronology of the main steps in the development and application of new materials for hip prostheses [1–3].

Table 2.1 - Chronology of the main steps in the development and evolution of materials used for hip prosthesis [1–3]

Year	*Main stages of development*
1890	Gluck introduced the femoral stem using ivory (hard, white materials from the teeth of animals) for the femoral head.
1919	Deblet, French surgeon used reinforced rubber for the femoral component.
1925	Smith-Petersen used for the first time, a hemispherical glass component to cover the femoral head in order to smooth the movement of the joint while promoting regeneration of the joint. Despite the high biocompatibility, low resistance to stress led to its quick failure.
1930	J. E. Pean, conducted an intensive study of the reaction of body to metal, giving unsatisfactory results in steel implants, due the release of small particles and / or ions (chemical degradation) which can accumulate in the tissues and cause inflammation. Despite the evolution, it is still a major cause of rejection of implants.
1936	Smith-Peterson used a cobalt-chromium alloy, called Vitallium®, which showed good mechanical properties and high corrosion resistance reasons why it is still used today.
1938	P. W. Wiles experienced a stainless steel in replacement of acetabular and femoral components of hip.
1950	The Judet brothers presented a short prosthesis made of poly(methyl methacrylate) PMMA. This prosthesis failed due to accumulation of wear debris and inflammation.
1958	It began the use of polytetrafluoroethylene (PTFE) polymer as the material for the acetabular component. The immediate results were very positive. However, the major limitation of this material are related to the high wear, which in many cases originated a negative reaction of the tissues.
1960	John Charnley introduced ultra-high molecular weight polyethylene (UHMWPE) as the polymeric material of the acetabular component. Its wear resistance was significantly higher than for PTFE.
1970	Charnley has begun to implement a "Low Friction Arthroplasty" model with a stainless steel femoral component and acetabular component of UHMWPE, which significantly reduces the coefficient of friction in the contact zone of the components.
1980	After the generalization of the hip prostheses implementation in the 70s, the concerns focused on the best tribological performance of the materials used. The study of ceramic materials for applications in prosthetics, such as alumina (Al_2O_3) and zirconia (ZrO_2) begins.
1992	Sedel has begun the use of joint pairs of ceramic/ceramic type, using alumina.
1995	Muller started using pairs of joint metal/metal, using cobalt-chromium alloy.
2000	The interest in hydroxyapatite (HAP) increases mainly as a coating on the external surface of the hip, to enhance bone ingrowth and biological fixation of the biomaterial.

Nowadays, total hip replacement (THP) is mainly composed by the elements illustrated in Figure 2.1.

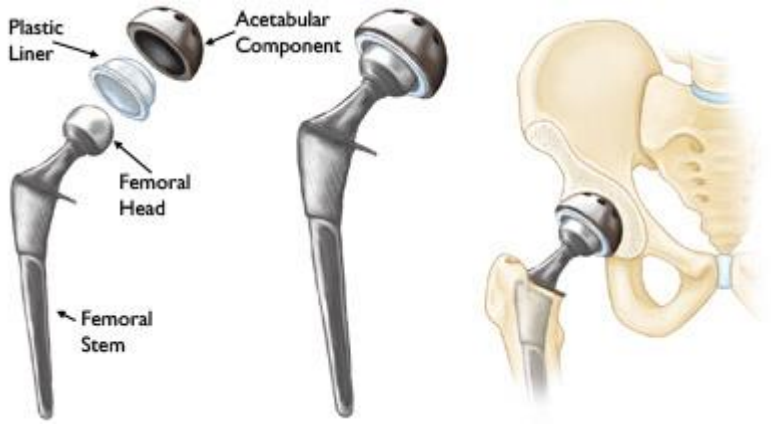

Figure 2.1 – Illustration of a total hip replacement: (left) Individual components of a total hip replacement; (center) components merged into an implant; (right) implant as it fits into the hip, adapted from [4].

There is a strong increase on the demand for new long lasting implants, because the information collected on total joint replacements surgery suggests that in 2030, the amount of total hip replacements can rise by 174% (572,000 procedures) [5].

Not solely the number of replacement surgeries have grown, but at the same time the number of revision surgery of hip and knee implants have additionally increased [6].

These revision surgeries that cause pain for the patient, are expensive and their success rate is still to be improved. The whole variety of hip revision surgery is anticipated to extend by 137% and knee revision surgery by 607% between the years 2005 and 2030 [5]. Therefore a really high boom in implant manufacturing is anticipated in coming years. Because of the steadily expanding request for implants, it is important that new biomaterials are quickly developed. This new biomaterials should show biocompatibility, higher corrosion resistance in body environment, high strength and low modulus, suitable fatigue and wear resistance, high plasticity and no toxicity [7–9]. Presently, the materials used (as stated in table 2.1) for these applications are 316L stainless steel, cobalt chromium alloys, and titanium-based alloys. These materials have, nevertheless, exhibited tendencies to fail due to various reasons like high modulus compared to the bone, low wear and high corrosion resistance [6]. Figure 2.2 shows the principal causes for implants failure that lead to revision surgeries.

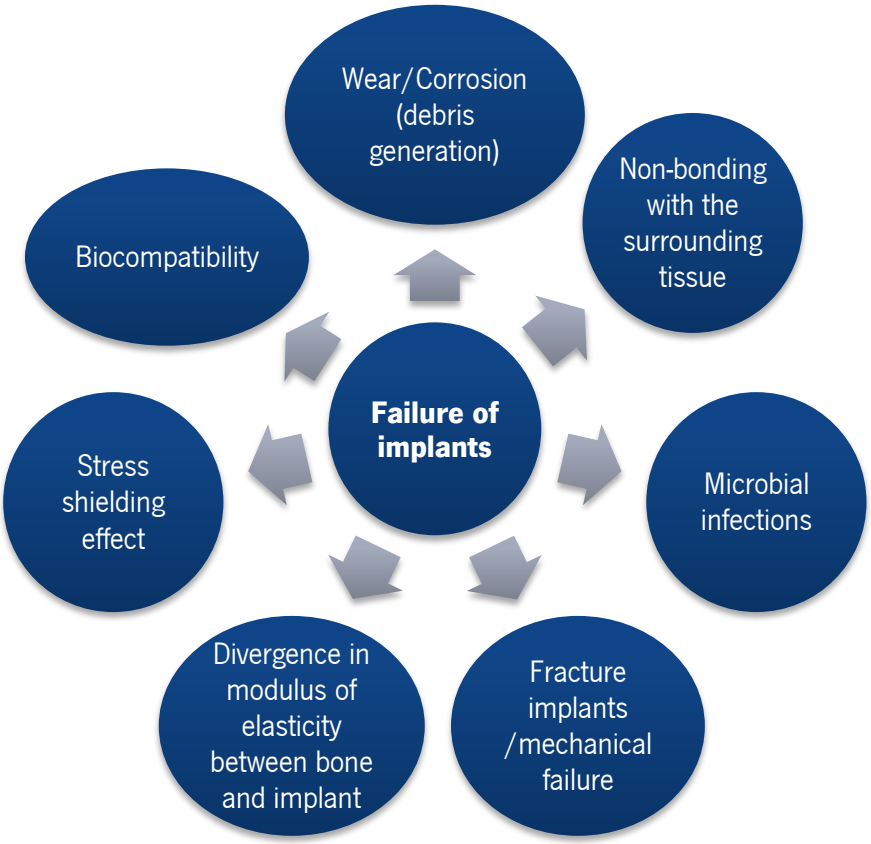

Figure 2.2 - Principal causes for failure of implants, adapted from [6].

Taking into account the strong application potential of polymer based sensors for biomedical applications, the interest will be focused in these materials. The development of this type of materials is based on the need to develop new materials specifically for biomedical applications, particularly in areas such as orthopedics, ophthalmology, plastic and reconstructive surgery, dentistry, cardiovascular surgery and neurosurgery [10]. In Table 2.2, the main synthetic polymers used in biomedical applications are listed.

Table 2.2 – Main synthetic polymers used in biomedical applications [10]

POLYMER	*APPLICATIONS*
Polyethylene (PE)	Hip, knee, shoulder joints (UHMWPE), catheters
Polypropylene (PP)	Sutures, reinforcing meshes, catheters
Polyvinyl chloride (PVC)	Catheters, shunts, tubing
Polytetrafluoroethylene (PTFE)	Vascular grafts, felts, membranes
Polymethyl methacrylate (PMMA)	Bone cement, intraocular lenses, artificial teeth
Polyhydroxiethyl methacrylate (PHEMA)	Contact lenses, membranes, drug delivery, coatings
Polymethyl 2-cyanoacrylate	Surgical adhesives
Polyethylene terephthalate (PET)	Sutures, vascular grafts, meshes, sewing rings
Polyether-ether ketone (PEEK)	Composite joints
Polyamides (Nylon 66 e Nylon 6))	Sutures
Polysiloxanes	Fingers joints, maxiofacial implants, heart valves, tubing shunts, adhesives, membranes

Currently, many strategies are adopted to determine the loosening status of the total hip replacement (THR) and to determine a basis for revision management. All of these techniques are based on imaging methods. Although the devices and technology are extremely developed, a 100% diagnostic accuracy is not achieved. For example, the period between the onset of an infection and the risk to spot any change inside the THR may be long.

Problems associated to THR should be diagnosed with precision and at an early state, so as to avoid massive osteolysis of the femur. In general, diagnostic methods can be divided into imaging and implant integrated sensors [11].

In recent decades, many researchers have focused their attention on the development of intelligent prosthesis, which are capable to detect early failures associated with the implant. Such prostheses have sensors that monitor certain key parameters to ensure that there are no problems associated with the artificial implant.

In the last decade, the number of studies related to the prevention mechanisms, based on sensors, increased. Figure 2.3 shows the work developed by Taylor et al. in 1997, where two proximal femoral replacements were instrumented to determine axial forces at two sites within the prostheses. The goal was to measure the changes in forces distribution over time. Inductive coupling between coil worn around the leg and a small implanted coil, was used in order to supply power to electronic circuit [12].

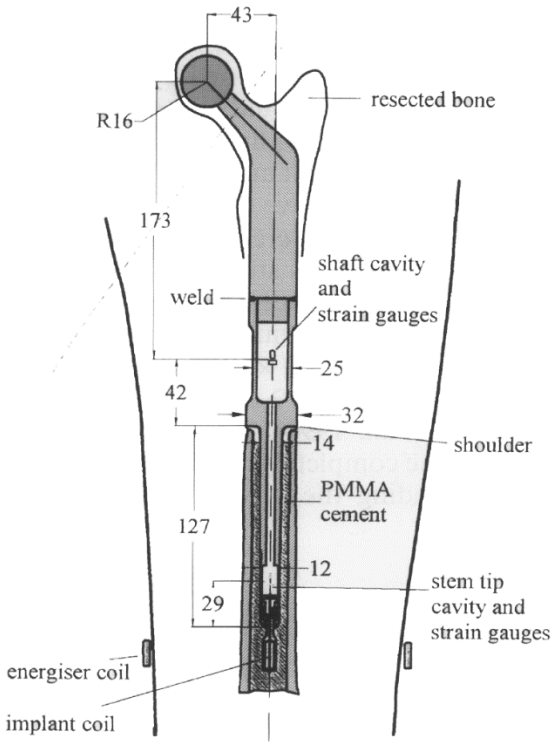

Figure 2.3 – Modified proximal femoral replacement showing strain gauge locations and inductive coils [12].

In 1999, Graichen et al [13] developed implants able to detect temperature variations caused by friction on the femur head (Figure 2.4). These are strain gauge sensors along with temperature sensors that allow the detection of temperature variations on the order of 2°C [13].

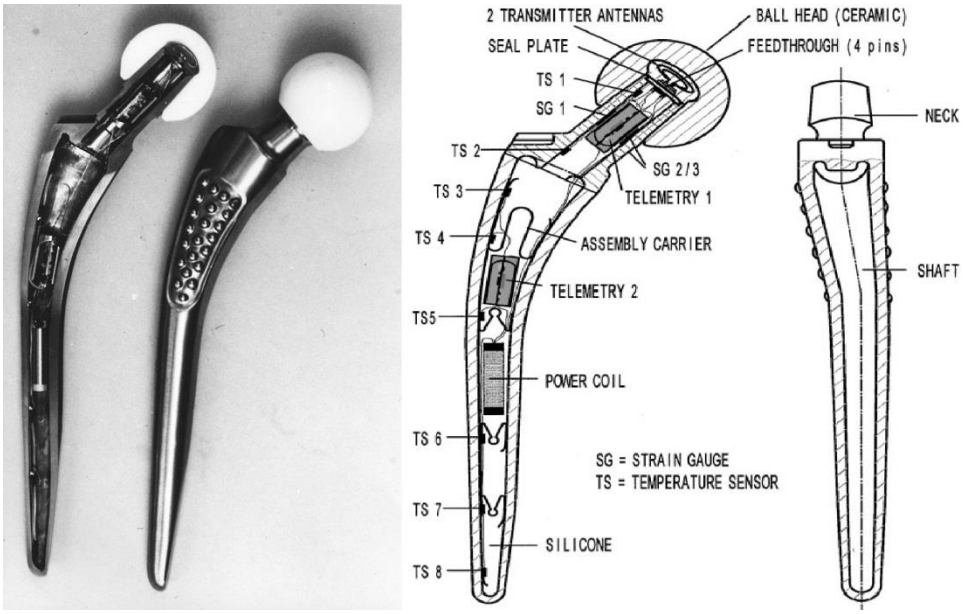

Figure 2.4 – Sensor model from F. Graichen et al, adapted from [13].

Another example of a prosthesis containing sensors, was developed by Burny et al in 2000 [14]. These are sensors for measuring three-dimensional forces in hip joints (Figure 2.5).

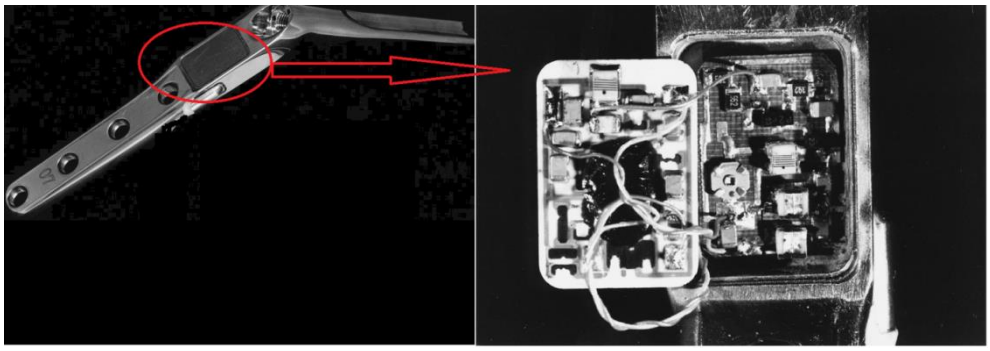

Figure 2.5 – Sensor developed by F. Burny et al, adapted from [14].

In 2001, Taylor and his co-workers proposed the production of a sensor that can detect shoulder prosthesis dislocation, preventing thereby serious consequences for patients. Like the other one proposed in 1997, it was also based on strain gauge and telemetric measurements [15] (Figure 2.6).

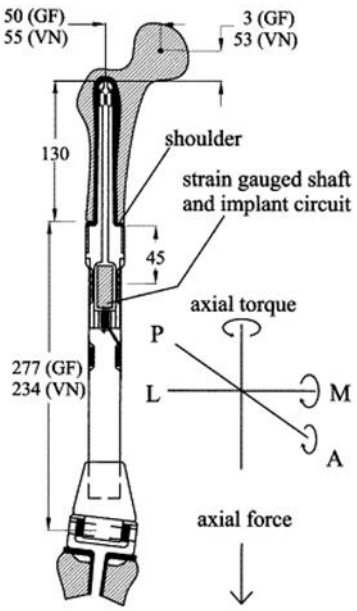

Figure 2.6 - Shoulder prosthesis with sensors for displacement detection, adapted from [15].

Concerning the problem associated to power supply of implantable devices, Morais et al. [16] in 2009, developed an activation circuit used to completely turn-off battery-power. In addition, it allows the reception of embed commands, suitable for calibration and sensor selection purposes. Results from an experimental device used as a smart hip prosthesis telemetry system for loosening detection, show the usefulness of the proposed activation concept. Figure 2.7 shows an illustration of the proposed activation circuit in a smart hip prosthesis. The implantable telemetry system is composed of four PVDF transducers and is externally activated and/or configured using a control unidirectional link provided by a handheld device. Prosthesis sensors data is then transmitted to a receiver device using a separated data link, which can be powered by a rechargeable battery or other power source [16].

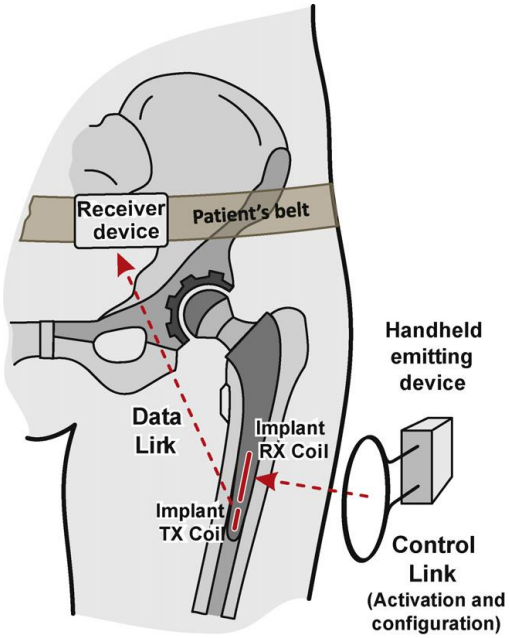

Figure 2.7 – Illustration of the proposed activation circuit in a smart hip prosthesis [16].

Later, in 2012, Bergmann et al. [17], developed an instrumented hip implant with telemetric data transfer to measure the implant temperature *in vivo*. It was able to measure temperature with an accuracy of 0.1°C in a range between 20°C and 58°C. The titanium hip endoprosthesis was modified to house the electronic inside its hollow neck and the electronics are powered by an external induction coil fixed around the joint as illustrated in Figure 2.8.

Figure 2.8 – Cross-section of the model of the modified hip implant and an image of the external equipment, adapted from [17].

More recently, in 2013, Ruther et al. [18] investigated a novel passive sensor array for implementation in endoprosthetic implants in order to identify implant loosening (Figure 2.9).

The proposed concept consists of several spring-mass-oscillators which are assembled by a flat spring and a permanent magnetic sphere. At the border of the bone-membrane system, the sound characteristics appear dependent on the condition of implant fixation [18].

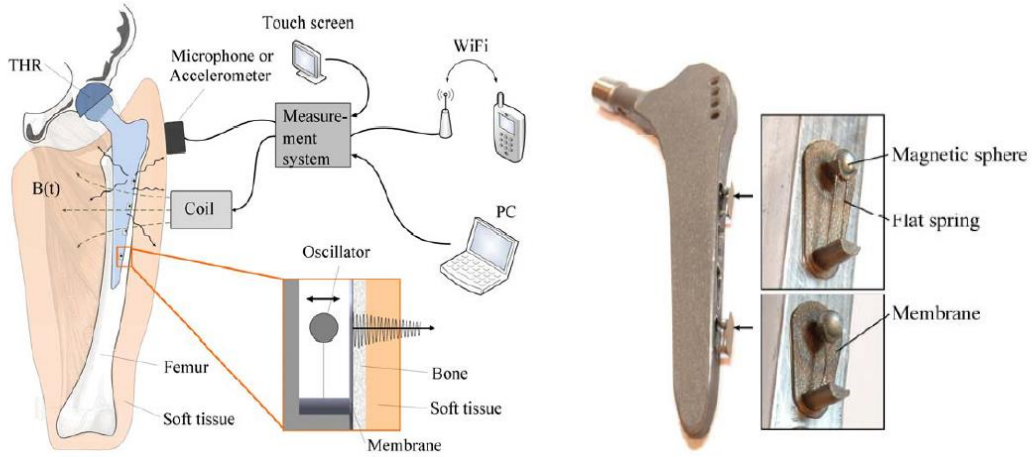

Figure 2.9 – Schematic illustration of the passive sensor array and the arrangement of the sensor inside the total hip stem, adapted from [18].

Also in 2013, Correia et al. [19], developed a piezoresistive sensor for force mapping of hip-prostheses. The goal of this investigation was to monitor mechanical stresses over time, in prosthesis. For this purpose, high sensitive silicon piezoresistive thin-films were fabricated and attached to prosthesis (Figure 2.10) [19].

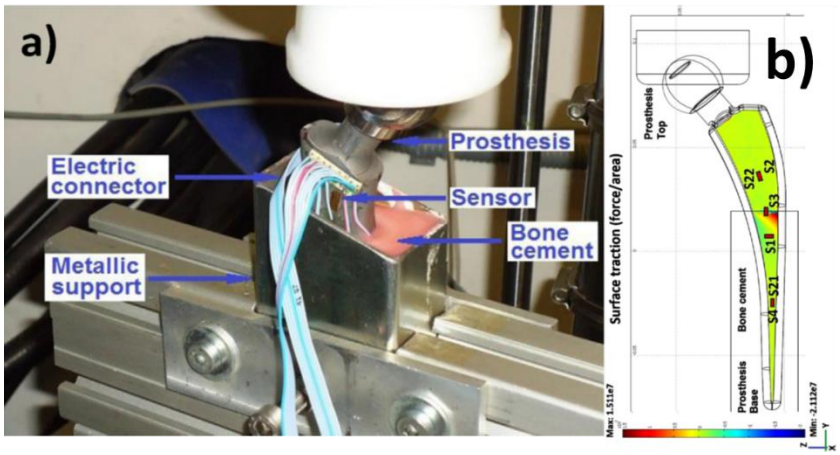

Figure 2.10 – Image of the hip-joint prosthesis in the stress-strain experimental setup (a) and a simulation of the stress distribution (b), adapted from [19].

In addition to this type of prostheses whose focus is to determine the load that this type of implant are subject, there are other types of sensors capable of detecting, for example, variations in temperature or pH.

These information is important because it allows to early detect implant rejection mechanisms that cause change in these parameters. One example is bacterial colonization leading to biofilm formation [12].

The data obtained from this type of sensors are important for developing computational models, to improve surgical techniques and to allow the education of patients for a more secure life after surgery. However, these pressure sensors have some limitations such as low resolution and the need for an external power supply [13,14].

Therefore, it is safe to argue that, the future of prostheses requires the implementation of preventive mechanisms based on sensors capable of acquiring information on a wide range of rejections signals of artificial implants [20,21].

Taking into account these developments, the field of research that uses piezoelectric materials for pressure and force sensors in various applications should be considered. These sensors are very accurate for sensory applications having the advantage of not requiring external power supply, since piezoelectric materials can even offer power to the system [22].

Piezoelectric materials are able to transform mechanical strains into electrical signals, requiring conductive electrodes to promote the acquisition of the signal. However, since these sensors are used in implantable prostheses, they should have characteristics compatible with biomedical applications, including biocompatibility, corrosion resistance and antibacterial properties.

2.2 Piezoelectric materials: Poly(vinylidene fluoride)

One of the possible solutions for the problems associated to rejection of prosthesis passes by the use of sensors being able, earlier as possible, to detect and communicate variations of specific parameters, such as pressure, of defective interaction of the prosthesis with surrounding tissues to a computer [16]. These measurements can rely on piezoelectric materials.

In 1880 Jacques and Pierre Curie [23] discovered the piezoelectricity in non-symmetrical crystals. Piezoelectricity (that means, “electrical charge produced by an applied mechanical stress”) is the property of some dielectric materials to develop or change their potential difference when subjected to a mechanical strain.

The opposite is also true, if an electrical field is applied to this material, it will generate a mechanical strain. According to these properties a piezoelectric element is an electromechanical transducer (energy converter) (Figure 2.11) [24].

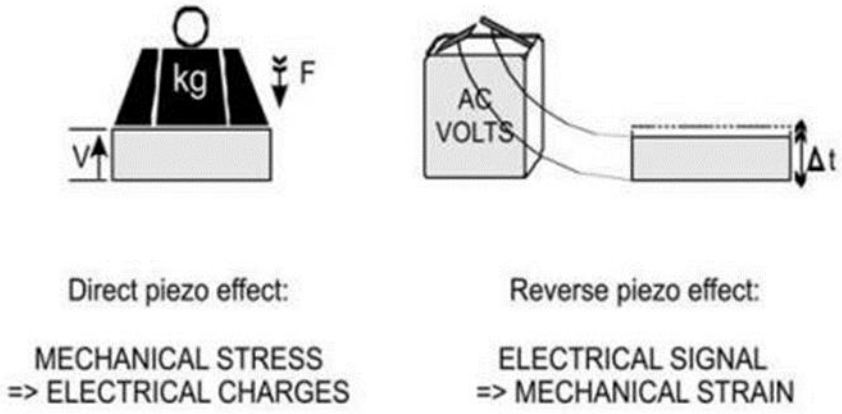

Figure 2.11 – Direct and reverse piezoelectric effect, adapted from [24].

These materials are even more interesting in sensor applications, since they do not require external power, being even able to provide power to the circuit, keeping the system operating for long periods of time [22].

There are a few polymers presenting this piezoelectric properties, including, Nylon-11, polylactic acid (PLLA) and poly(lactic-co-glycolic acid) (PLGA), poly(vinylidene fluoride) (PVDF) and its copolymers. PVDF and its copolymers, having the best electroactive properties, are the main choice for an increasing number of applications [25,26]. Poly (vinylidene fluoride), PVDF, is characterized by its piezo and pyroelectric properties, which offer a wide variety of applications in the field of sensors and actuators. The piezoelectricity of PVDF was first reported by Kawai in 1969 [27]. PVDF is a semicrystalline polymer of high molecular weight whose monomer is the vinylidene fluoride (VDF), illustrated in Figure 2.12.

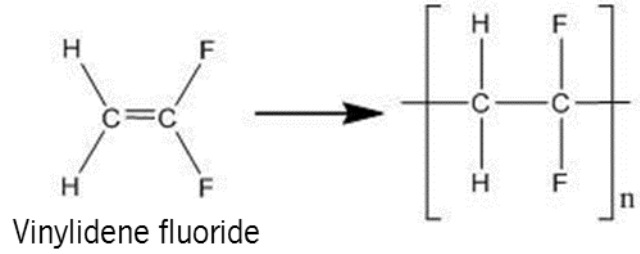

Figure 2.12 - Schematic representation of VDF monomer and PVDF.

PVDF is produced by polymerization chain reaction, its glass transition temperature, Tg, is -34 °C and its melting temperature, Tm, is between 160 - 190°C, depending on the processing conditions [28]. This is a crucial aspect to be taken into account when deposition conditions of electrodes are set.

PVDF is in a semi-crystalline form, with a degree of crystallinity between 40 and 50% that generally crystallize in a spherulitic structure. Spherulites are composed of a set of lamellae that, during crystallization, grow radially from a common center [29]. In Figure 2.13 a spherulite is shown and the highlight shows three lamellae constituting the crystalline region, between which are located regions of amorphous material.

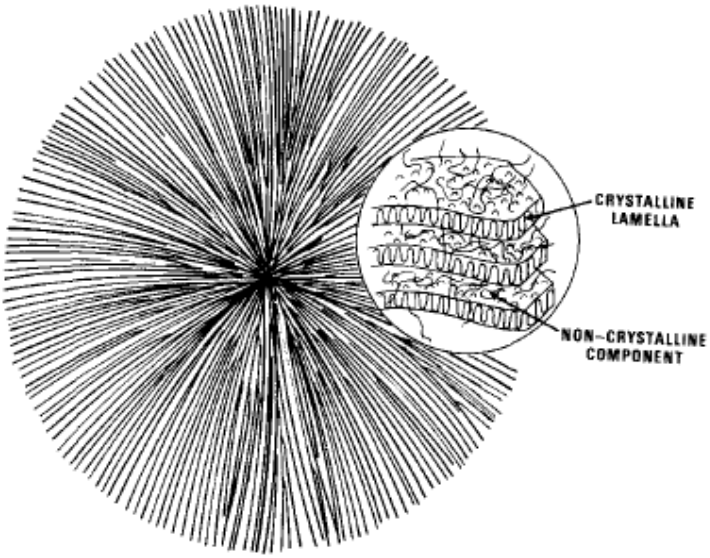

Figure 2.13 – Schematic representation of a spherulite [29].

PVDF is a linear polymer having permanent dipoles almost perpendicular to the chains direction. These dipoles are formed by the difference in electronegativity between fluorine atoms and those of carbon and hydrogen atoms [25,30,31] .

There have been reported five crystalline phases for PVDF, but only four crystal modifications are described with a permanent dipole moment (polar crystals): β, γ, δ and ε phases. In the α phase, the molecular dipoles are anti-parallel, so this phase is apolar [25,28,30,32,33] .

The polar β phase is the most desirable for sensor and actuator applications as it shows the highest piezoelectric response [25,34–36]. Therefore, this phase has attracted technological interest and it is now used in common components for both sensors and actuators [32,37].

This phase can be obtained by different techniques, the most important one being the mechanical stretching of α-phase film at a certain percentage elongation at a given temperature [25,30,38].

In PVDF α-phase the chains are organized in a trans-gauche conformational type where the molecules are arranged in a helical configuration, thus allowing a larger separation between the atoms of fluorine arranged along the chain. On the other hand, β-phase has a chain conformation designed as all trans-planar zigzag. [25,30,39]. The configuration of this PVDF phase is characterized by the arrangement of the fluorine atoms, which are at the same side of the chain and on the opposite side of the hydrogen atoms. Figure 2.14 shows a schematic representation of the α and β phases of PVDF.

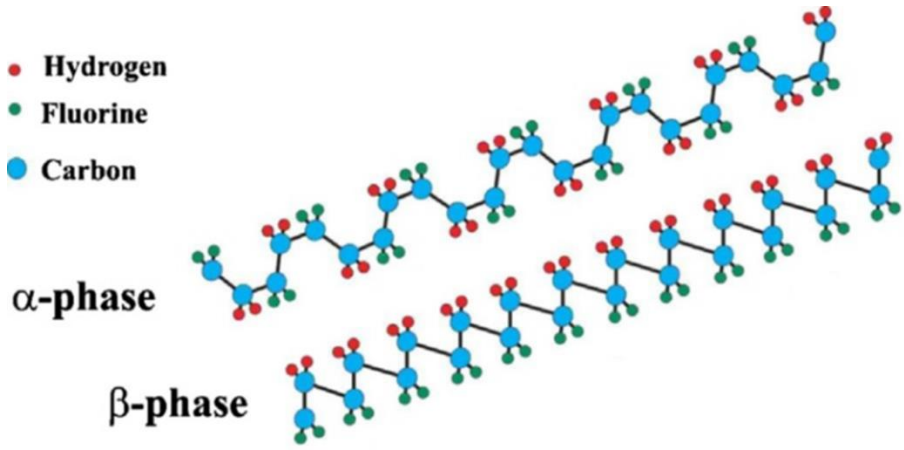

Figure 2.14 – Schematic representation of the chain conformation of the α and β phases of PVDF, adapted from [25].

Once the β-phase is obtained, the dipolar moments are randomly oriented. Further, the piezoelectric response of the β-phase is improved by the application of an electric field, leading to a preferred orientation of the dipoles along the field direction, increasing the electroactive response of the material [32,36–38,40,41].

As the piezoelectric material can transform mechanical loads into electrical signals, they need electrodes for the acquisition of the signal. Electrodes for medical applications, must possess certain properties such as: good electrical conductivity, biocompatibility, antibacterial properties and resistance to corrosion [36,42–48].

2.3 Multifunctional coatings

As the piezoelectric material can transform mechanical loads into electrical signals, they need electrodes for the acquisition of the signal. It is important to select the correct materials that will perform as electrodes, since they have first the function of conducting the electrical signal generated by the sensor, but must also show suitable physical, chemical, mechanical and biological properties. Such properties include:

- High adhesion between coating and polymeric substrate;
- Good mechanical properties (elasticity, elastic modulus (stiffness) and hardness;
- Low wear rate;
- Chemical resistance to biological fluids;
- Antimicrobial activity;
- Biocompatibility;
- Nontoxicity.

In order to fulfill these requirements, it has become necessary to develop new multifunctional coatings, which are able to match specific applications. Magnetron sputtering technology is one of the most well-known and wide used techniques for thin films production, both in research and industry. Top quality, skillfulness, reliability, inexpensive production, environment friendly, good adhesion and wear resistance, there are a number of the multiple advantages offered by PVD techniques [49–53]. Among the large variety of potential applications of thin films fabricated by PVD, the special emphasis goes for the medical field, specifically for biosensor and bioelectrode devices.

In this research, two different systems were deposited to produce the electrodes:

- $Ti_{1-x}Ag_x$ system with different Ag/Ti atomic ratios;
- Ag-TiN_x system, using different flows of nitrogen.

Depositions are performed using the custom made PVD sputtering system shown in Figure 2.15.

Figure 2.15 – Sputtering deposition system in the Functional Coatings Laboratory II, Physics Department, University of Minho.

Titanium was selected for this application since it, together with its alloys, has been widely used in artificial implants due to its biocompatibility, good corrosion resistance, strength and elasticity, excellent thermal and chemical stability. Additionally, it shows a bulk Ti electrical resistivity in the range 43 μΩ cm [42,54–56]. However, despite the good biocompatibility, Ti coatings do not prevent the adhesion of microorganisms.

The antibacterial effect of silver ions (Ag^+) is well known and these are hypoallergenic and non-toxic to living mammalian tissue at certain concentrations [57]. Moreover, not only silver ions present antibacterial effect, also silver nanoparticles and silver compounds (as silver sulfadiazine and silver zeolite) have this property [58,59]. The antibacterial property of silver is related to the amount of silver and the rate of silver released. In its metallic state, silver is inert but it can react with the body fluids and can get ionized (Ag^+) and Ag^+ is very reactive. In this form, silver binds to the bacterial cell wall and cell membrane and inhibits the respiration process [58]. In nanoparticle form, silver attaches to the cell membrane and also penetrates inside the bacteria. The bacterial membrane contains proteins and silver nanoparticles interact with these proteins in the cell. So, the nanoparticles release silver ions in the bacterial cells which enhance their bactericidal activity [57,58].

Nonetheless, despite the advantages of silver, some limitations were found such as the interference of silver salts and in the case of metallic silver, the impossibility of continuously releasing sufficient concentrations of silver ions. These limitations can be overcome by the use of Ag nanoparticles. These have the advantage of a higher surface area, which increases its antimicrobial effectiveness.[58,60,61].

Despite the high antimicrobial effect of Ag^{+}, it is sometimes difficult to achieve the desired ionization from Ag nanoparticles within the body, since this effect is dependent on pH levels, microgalvanic pair formation and the location of the Ag nanoparticles in a matrix, among other [62–64].

Thus, introducing silver as an external component to Ti films may improve the well-known properties of pure Ti by the formation of intermetallic-like compounds. The useful properties of intermetallic compounds or alloys are typically enhanced when compared to those of standard metals, particularly at high temperatures, attributable to their mixed bonding (metallic, valence and ionic) and specific stoichiometry [65,66]. Titanium–silver ($Ti_{1-x}Ag_x$) is one of such systems, where the mixture of titanium biocompatibility with the antimicrobial properties of silver is attracting increasing attention. A visible example comes from the dental sector of orthodontic area , namely in implants and dental prosthesis, where the Ti–Ag system is being increasingly considered and tested [61,67,68]. The importance of this binary intermetallic-like compound comes from the fact that it can offer a multifunctional response by providing a set of proper chemical, electrical, thermal and mechanical properties, along with excellent biocompatibility and good resistance to wear and corrosion [61,67,68].

The Ag-TiN_x system can be achieved by the incorporation of nitrogen. It is expected a completely change in the structure and/or the disappearance of the intermetallic-like compounds achieved by the deposition conditions of the $Ti_{1-x}Ag_x$ system. The suppression of TiAg intermetallic compounds is expected and explained by the higher enthalpy of formation of TiAg (-1.6±2.4 kJ/mol) [66,69] in comparison with the enthalpy of formation of TiN (-330 kJ/mol) [70,71]. Nitrogen incorporation can increase the mechanical resistance of titanium.

Tests of biocompatibility of TiN, have also classified them as suitable for orthopedic implants, blood contacting materials and the material of choice for hard coatings of dental implants and dental surgery tools [72–74]. Furthermore, TiN is a good electrically conductive coating making it an interesting material for microelectronic applications, due to its extreme hardness, high strength, good chemical stability and remarkable resistance to wear and corrosion [71,74–76].

The inclusion of silver in the Ag-TiN_x system, together with the antibacterial characteristics already mentioned, can offer the possibility to tailor the mechanical properties of TiN, regarding the sputtering on flexible substrates, since Ag increases the plasticity of TiN [44,77]. Additionally, silver incorporation can also modify the materials electrical conductivity, which may be very important to electrodes for biosensor applications [44,46]. Since silver is immiscible with TiN, when these materials are reactively co-deposited, coatings tend to form a nanocomposite structure that consists of a TiN matrix surrounding nanoparticles of silver, opening the way for the use of these coatings for biomedical applications with antimicrobial activity [78–80].

Currently, different coatings produced by magnetron sputtering are proposed as potential candidates as functional conductive electrodes in polymeric sensors. Lopes et al. [42,81–83], developed $TiAg_x$ thin films for lower limb prosthesis pressure sensors in order to monitor the strain or pressure fields that established all over the contact surface between the patient and the prosthesis. This allows the optimization of the prosthesis in terms of shape and alignment of the socket, contributing to increase patient's comfort. Also Ferreira et al. [48], used the same system (Ti-Ag) as electrodes for large deformation sensors applications using carbon nanotube/poly(vinylidene fluoride) composites (CNT/PVDF).

Later, Lopes et al. [47] investigated a protective Ag:TiO_2 thin films for pressure sensors in orthopedic prosthesis. The goal was to monitor pressure fields at the prosthesis/limb interface in order to optimize the use of the prosthesis by the amputees. Moreover, Pedrosa et al. [43,44,46,84–86] reported the used of Ag:TiN thin films for dry biopotential electrodes for electroencephalographic (EEG) signal monitoring. These recent investigation were developed in different substrates and for different purposes.

An interesting effect normally used for the development of deformation sensors is the change of electrical resistance due to an applied load, which was first discovered by Lord Kelvin in 1856 in metals, being the large piezoresistive effect first discovered in 1954 with the use of single crystals silicon and germanium [87].

As in the case of metals, also the semiconductors change their resistivity as a function of strain. The sensibility of a piezoresistive sensor is generally termed the gauge factor. This is a dimensionless quantity and is given by (Equation 1):

$$GF = \frac{\text{relative change in resistance}}{\text{applied strain}} = \frac{\Delta R/R}{\Delta L/L} = \frac{\Delta R/R}{\varepsilon} \qquad \textit{(Equation 1)}$$

Where, R is the initial resistance of the piezoresistive sensor and ΔR is the change in resistance. $\Delta L/L$ is, by definition, the applied strain denoted as ε.

The typical gauge factor values of the main materials used for strain sensors described in the literature are presented in Table 2.3.

Table 2.3 – Typical gauge factor values of the main materials used for strain sensors

Sensor Material	***Gauge factor***
Thin film metal [88]	2
Crystalline silicon [89]	±50-150
Thin film crystalline silicon [90]	±15
Polymer [91]	18

Thus, it is relevant to evaluate the GF of the $Ti_{1-x}Ag_x$ and Ag-TiN_x systems and, therefore, their suitability for sensor applications.

The biocompatibility of biomaterials is very closely related to cell behavior on contact with them and particular to cell adhesion on their surface [92]. In this particular case, the study of osteoblastic cells response seems important because these sensors will be implemented on prosthesis that will be in contact with the bone, since the different performances of these electrodes will influence the cells' capacity to adhere, proliferate and differentiate. Thus attachment, adhesion and spreading have a place with the first stage of cell/material interaction and the quality of the first stage will affect the cell's capacity to proliferate and to differentiate itself in contact with the sensor [92].

2.4 References

[1] Mathys | Hip Joint | General | History of orthopaedics, Mathys Ltd Bettlach. (2015). http://www.my-artificial-joint.com/en/hip-joint.96/general/history.html (accessed August 21, 2015).

[2] B.D. Ratner, A.S. Hoffman, F.J. Schoen, J.E. Lemons, Biomaterials Science: An Introduction to Materials in Medicine, Academic Press Publications, 2012. https://books.google.com/books?id=8hBq-dLLaxwC&pgis=1 (accessed August 21, 2015).

[3] S.R. Knight, R. Aujla, S.P. Biswas, Total Hip Arthroplasty - over 100 years of operative history, Orthop. Rev. (Pavia). 3 (2011) e16. doi:10.4081/or.2011.e16.

[4] J.R. Foran, Total Hip Replacement-OrthoInfo - AAOS, (2015). http://orthoinfo.aaos.org/topic.cfm?topic=A00377&webid=24DAE050 (accessed August 31, 2015).

[5] S.M. Kurtz, K.L. Ong, J. Schmier, F. Mowat, K. Saleh, E. Dybvik, et al., Future Clinical and Economic Impact of Revision Total Hip and Knee Arthroplasty, J. Bone & Jt. Surg. 89 (2007) 144–151. http://jbjs.org/content/89/suppl_3/144.abstract.

[6] M. Geetha, a. K. Singh, R. Asokamani, A.K. Gogia, Ti based biomaterials, the ultimate choice for orthopaedic implants – A review, Prog. Mater. Sci. 54 (2009) 397–425. doi:10.1016/j.pmatsci.2008.06.004.

[7] J.C. Sánchez-López, M.D. Abad, I. Carvalho, R. Escobar Galindo, N. Benito, S. Ribeiro, et al., Influence of silver content on the tribomechanical behavior on Ag-TiCN bioactive coatings, Surf. Coat. Technol. 206 (2012) 2192–2198. doi:10.1016/j.surfcoat.2011.09.059.

[8] C. Oliveira, L. Gonçalves, B.G. Almeida, C.J. Tavares, S. Carvalho, F. Vaz, et al., XRD and FTIR analysis of Ti–Si–C–ON coatings for biomedical applications, Surf. Coatings Technol. 203 (2008) 490–494. doi:10.1016/j.surfcoat.2008.06.121.

[9] F. Guimarães, C. Oliveira, E. Sequeiros, M. Torres, M. Susano, Structural and Mechanical properties of Ti – Si – C – ON for biomedical applications, Technology. 202 (2008) 2403 – 2407. doi:10.1016/j.surfcoat.2007.08.056.

[10] A.F. von Recum, Handbook of Biomaterials Evaluation: Scientific Technical and Clinical Testing of implant Materials, 2nd Editio, Taylor & Francis, 1999.

[11] C. Ruther, U. Timm, H. Ewald, W. Mittelmeier, R. Schmelter, A. Lohrengel, et al., Current Possibilities for Detection of Loosening of Total Hip Replacements and How Intelligent Implants Could Improve Diagnostic Accuracy, in: S.K. Fokter (Ed.), Recent Adv. Arthroplast., InTech, 2012: pp. 363–386. doi:10.5772/1445.

[12] S.J.G. Taylor, J.S. Perry, J.M. Meswania, N. Donaldson, P.S. Walker, S.R. Cannon, Telemetry of forces from proximal femoral replacements and relevance to fixation, J. Biomech. 30 (1997) 225–234. doi:10.1016/S0021-9290(96)00141-8.

[13] F. Graichen, G. Bergmann, A. Rohlmann, Hip endoprosthesis for in vivo measurement of joint force and temperature, J. Biomech. 32 (1999) 1113–1117. doi:10.1016/S0021-9290(99)00110-4.

[14] F. Burny, M. Donkerwolcke, F. Moulart, R. Bourgois, R. Puers, K. Van Schuylenbergh, et al., Concept, design and fabrication of smart orthopedic implants, Med. Eng. Phys. 22 (2000) 469–479. doi:10.1016/S1350-4533(00)00062-X.

[15] S.J.. Taylor, P.. Walker, Forces and moments telemetered from two distal femoral replacements during various activities, J. Biomech. 34 (2001) 839–848. doi:10.1016/S0021-9290(01)00042-2.

[16] R. Morais, C.M. Frias, N.M. Silva, J.L.F. Azevedo, C.A. Serôdio, P.M. Silva, et al., An activation circuit for battery-powered biomedical implantable systems, Sensors Actuators A Phys. 156 (2009) 229–236. doi:10.1016/j.sna.2009.06.008.

[17] G. Bergmann, F. Graichen, J. Dymke, A. Rohlmann, G.N. Duda, P. Damm, et al., High-Tech Hip Implant for Wireless Temperature Measurements In Vivo., PLoS One. 7 (2012) 1–7. 10.1371/journal.pone.0043489.

[18] C. Ruther, C. Schulze, A. Boehme, H. Nierath, H. Ewald, W. Mittelmeier, et al., Investigation of a passive sensor array for diagnosis of loosening of endoprosthetic implants, Sensors. 13 (2013) 1–20. doi:10.3390/s130100001.

[19] V. Correia, V. Sencadas, M.S. Martins, C. Ribeiro, P. Alpuim, J.G. Rocha, et al., Piezoresistive sensors for force mapping of hip-prostheses, Sensors Actuators A Phys. 195 (2013) 133–138. doi:10.1016/j.sna.2013.03.013.

[20] R. Branemark, P.-I. Branemark, B. Rydevik, R.R. Myers, Osseointegration in skeletal reconstruction and rehabilitation, J. Rehabil. Res. Dev. 38 (2001) 1–8.

[21] S.P.S.P. Mohanty, E. Kougianos, Biosensors: a tutorial review, Potentials, IEEE. 25 (2006) 35–40.

[22] S. Kon, K. Oldham, R. Horowitz, Piezoresistive and Piezoelectric MEMS Strain Sensors for Vibration Detection, Sensors Smart Struct. Technol. Civil, Mech. Aerosp. Syst. 6529 (2007) 1–11. doi:10.1117/12.715814.

[23] J. Curie, P. Curie, Development, via compression, of electric polarization in hemihedral crystals with inclined faces, Bull. La Soc. Minerol. Fr. 3 (1880) 90–93.

[24] Ueberschlag, Pierre, PVDF piezoelectric polymer, Sens. Rev. 21 (2001) 118–126. doi:10.1108/02602280110388315.

[25] P. Martins, A.C. Lopes, S. Lanceros-Mendez, Electroactive phases of poly(vinylidene fluoride): Determination, processing and applications, Prog. Polym. Sci. 39 (2014) 683–706. doi:10.1016/j.progpolymsci.2013.07.006.

[26] A. Lovinger, Poly(Vinylidene Fluoride), in: D.C. Bassett (Ed.), Dev. Cryst. Polym. SE - 5, Springer Netherlands, 1982: pp. 195–273. doi:10.1007/978-94-009-7343-5_5.

[27] H. Kawai, The Piezoelectricity of Poly (vinylidene Fluoride), Jpn. J. Appl. Phys. 8 (1969) 975. http://stacks.iop.org/1347-4065/8/i=7/a=975.

[28] R. Gregorio Jr., R.C. Capitão, Morphology and phase transition of high melt temperature crystallized poly (vinylidene fluoride), J. Mater. Sci. 35 (2000) 299–306.

[29] M.G. Broadhurst, G.T. Davis, J.E. Mckinney, R.E. Collins, Piezoelectricity and pyroelectricity in polyvinylidene fluoride — A model, J. Appied Phys. 49 (1978) 4992–4997. doi:10.1063/1.324445.

[30] A. Salimi, A.A. Yousefi, FTIR studies of b-phase crystal formation in stretched PVDF film, Polym. Test. 22 (2003) 699–704. doi:10.1016/S0142-9418(03)00003-5.

[31] E. Giannetti, Semi-crystalline fluorinated polymers, Polym. Int. 50 (2001) 10–26. doi:10.1002/1097-0126(200101)50:1<10::AID-PI614>3.0.CO;2-W.

[32] B. Mohammadi, A.A.Y. Ã, S.M. Bellah, A.A. Yousefi, S.M. Bellah, A.A.Y. Ã, Effect of tensile strain rate and elongation on crystalline structure and piezoelectric properties of PVDF thin films, Polym. Test. 26 (2007) 42–50. doi:10.1016/j.polymertesting.2006.08.003.

[33] J. Gomes, J. Serrado Nunes, V. Sencadas, S. Lanceros-Mendez, Influence of the β-phase content and degree of crystallinity on the piezo- and ferroelectric properties of poly(vinylidene fluoride), Smart Mater. Struct. 19 (2010) 065010 (7pp). doi:10.1088/0964-1726/19/6/065010.

[34] P. Sajkiewicz, A. Wasiak, Z. Gocłowski, Phase transitions during stretching of poly(vinylidene fluoride), Eur. Polym. J. 35 (1999) 423–429. doi:10.1016/S0014-3057(98)00136-0.

[35] V.K. Tiwari, P.K. Kulriya, D.K. Avasthi, P. Maiti, Radiation-resistant behavior of poly(vinylidene fluoride)/layered silicate nanocomposites., ACS Appl. Mater. Interfaces. 1 (2009) 311–8. doi:10.1021/am800040q.

[36] S.M. Marques, N.K. Manninen, S. Ferdov, S. Lanceros-Mendez, S. Carvalho, Ti1−xAgx electrodes deposited on polymer based sensors, Appl. Surf. Sci. 317 (2014) 490–495. doi:10.1016/j.apsusc.2014.08.142.

[37] D.M. Esterly, B.J. Love, Phase Transformation to Beta-Poly (vinylidene fluoride) by Milling, J. Polym. Sci. Part B Polym. Phys. 42 (2004) 91–97.

[38] V. Sencadas, R. Gregorio, S. Lanceros-Méndez, α to β Phase Transformation and Microestructural Changes of PVDF Films Induced by Uniaxial Stretch, J. Macromol. Sci. Part B. 48 (2009) 514–525. doi:10.1080/00222340902837527.

[39] A.J. Lovinger, Ferroelectric polymers, Science (80-.). 220 (1983) 1115–1121. http://www.scopus.com/inward/record.url?eid=2-s2.0-0001506123&partnerID=tZOtx3y1.

[40] S.M. Marques, C.J. Tavares, S. Lanceros-Mendez, Z. Denchev, X-ray Scattering Experiments on Sputtered Titanium Dioxide Coatings onto PVDF Polymers for Self-Cleaning Applications, J. Appl. Polym. Sci. 119 (2011) 726–731. doi:10.1002/app.

[41] C.J. Tavares, S.M. Marques, L. Rebouta, S. Lanceros-Mendez, V. Sencadas, C.M. Costa, et al., PVD-Grown photocatalytic TiO2 thin films on PVDF substrates for sensors and actuators applications, Thin Solid Films. 517 (2008) 1161–1166. doi:10.1016/j.tsf.2008.06.024.

[42] C. Lopes, C. Gonçalves, P. Pedrosa, F. Macedo, E. Alves, N.P. Barradas, et al., TiAgx thin films for lower limb prosthesis pressure sensors: Effect of composition and structural changes on the electrical and thermal response of the films, Appl. Surf. Sci. 285 (2013) 10–18. doi:10.1016/j.apsusc.2013.07.021.

[43] D. Machado, P. Pedrosa, C. Fonseca, N. Martin, F. Vaz, Structural and Morphological Changes in Ag:TiN Nanocomposite Films Promoted by In-Vacuum Annealing, J. Nano Res. 25 (2013) 67–76. doi:10.4028/www.scientific.net/JNanoR.25.67.

[44] P. Pedrosa, D. Machado, C. Lopes, E. Alves, N.P. Barradas, N. Martin, et al., Nanocomposite Ag:TiN thin films for dry biopotential electrodes, Appl. Surf. Sci. 285 (2013) 40–48. doi:10.1016/j.apsusc.2013.07.154.

[45] S.M. Marques, N.K. Manninen, S. Lanceros-Mendez, S. Carvalho, Ag-TiNx electrodes deposited on piezoelectric poly(vinylidene fluoride) for biomedical sensor applications, Sensors Actuators A Phys. 234 (2015) 1–8. doi:10.1016/j.sna.2015.08.016.

[46] P. Pedrosa, E. Alves, N.P. Barradas, N. Martin, P. Fiedler, J. Haueisen, et al., Electrochemical behaviour of nanocomposite Agx:TiN thin films for dry biopotential electrodes, Electrochim. Acta. 125 (2014) 48–57. doi:10.1016/j.electacta.2014.01.082.

[47] C. Lopes, P. Fonseca, T. Matamá, a. Gomes, C. Louro, S. Paiva, et al., Protective Ag:TiO2 thin films for pressure sensors in orthopedic prosthesis: the importance of composition, structural and morphological features on the biological response of the coatings, J. Mater. Sci. Mater. Med. 25 (2014) 2069–2081. doi:10.1007/s10856-014-5251-z.

[48] A. Ferreira, C. Lopes, N. Martin, S. Lanceros-Méndez, F. Vaz, Nanostructured functional Ti-Ag electrodes for large deformation sensor applications, Sensors Actuators A Phys. (2014). doi:10.1016/j.sna.2014.09.031.

[49] D.M. Mattox, Handbook of physical vapor deposition (PVD) pocessing, Noyes Publications, Albuquerque, New Mexico, 1998.

[50] E. Lugscheider, C. Barimani, C. Wolff, S. Guerreiro, G. Doepper, Comparison of the structure of PVD-thin films deposited with different deposition energies, Surf. Coatings Technol. 86-87 (1996) 177–183. doi:10.1016/S0257-8972(96)03041-1.

[51] P.H. Mayrhofer, C. Mitterer, L. Hultman, H. Clemens, Microstructural design of hard coatings, Prog. Mater. Sci. 51 (2006) 1032–1114. doi:10.1016/j.pmatsci.2006.02.002.

[52] G.K. Hubler, J.A. Sprague, Energetic particles in PVD technology: particle-surface interaction processes and energy-particle relationships in thin film deposition, Surf. Coatings Technol. 81 (1996) 29–35. doi:10.1016/0257-8972(95)02617-7.

[53] H.A. Jehn, PVD and ECD-competition, alternative or combination?, Surf. Coatings Technol. 112 (1999) 210–216. doi:10.1016/S0257-8972(98)00750-6.

[54] C.F.A. Alves, F. Oliveira, I. Carvalho, a. P. Piedade, S. Carvalho, Influence of albumin on the tribological behavior of Ag–Ti (C, N) thin films for orthopedic implants, Mater. Sci. Eng. C. 34 (2014) 22–28. doi:10.1016/j.msec.2013.09.031.

[55] B.B. Zhang, Y.F. Zheng, Y. Liu, Effect of Ag on the corrosion behavior of Ti-Ag alloys in artificial saliva solutions., Dent. Mater. 25 (2009) 672–7. doi:10.1016/j.dental.2008.10.016.

[56] Y.-Y. Chang, H.-L. Huang, C.-H. Lai, J.-T. Hsu, T.-M. Shieh, A.Y.-J. Wu, et al., Analyses of Antibacterial Activity and Cell Compatibility of Titanium Coated with a Zr–C–N Film, PLoS One. 8 (2013) 1–8. doi:10.1371/journal.pone.0056771.

[57] K.D. Secinti, H. Özalp, A. Attar, M.F. Sargon, Nanoparticle silver ion coatings inhibit biofilm formation on titanium implants., J. Clin. Neurosci. 18 (2011) 391–5. doi:10.1016/j.jocn.2010.06.022.

[58] M. Rai, A. Yadav, A. Gade, Silver nanoparticles as a new generation of antimicrobials, Biotechnol. Adv. 27 (2009) 76–83. doi:10.1016/j.biotechadv.2008.09.002.

[59] a Simchi, E. Tamjid, F. Pishbin, a R. Boccaccini, Recent progress in inorganic and composite coatings with bactericidal capability for orthopaedic applications., Nanomedicine. 7 (2011) 22–39. doi:10.1016/j.nano.2010.10.005.

[60] B.S. Necula, L.E. Fratila-Apachitei, S. a J. Zaat, I. Apachitei, J. Duszczyk, In vitro antibacterial activity of porous TiO2-Ag composite layers against methicillin-resistant Staphylococcus aureus., Acta Biomater. 5 (2009) 3573–80. doi:10.1016/j.actbio.2009.05.010.

[61] A. Ewald, S.K. Glückermann, R. Thull, U. Gbureck, Antimicrobial titanium/silver PVD coatings on titanium., Biomed. Eng. Online. 5 (2006) 22. doi:10.1186/1475-925X-5-22.

[62] H. Cao, X. Liu, F. Meng, P.K. Chu, Biological actions of silver nanoparticles embedded in titanium controlled by micro-galvanic effects, Biomaterials. 32 (2011) 693–705. doi:10.1016/j.biomaterials.2010.09.066.

[63] M.V.D.Z. Park, A.M. Neigh, J.P. Vermeulen, L.J.J. De, H.W. Verharen, J.J. Briedé, et al., Biomaterials The effect of particle size on the cytotoxicity , inflammation , developmental toxicity and genotoxicity of silver nanoparticles, Biomaterials. (2011) 1–8. doi:10.1016/j.biomaterials.2011.08.085.

[64] E.-J. Park, E. Bae, J. Yi, Y. Kim, K. Choi, S. Hee, et al., Repeated-dose toxicity and inflammatory responses in mice by oral administration of silver nanoparticles, Environmenntal Toxicol. Pharmacol. 30 (2010) 162–168. doi:10.1016/j.etap.2010.05.004.

[65] A.M. Russell, Ductility in Intermetallic Compounds, Adv. Eng. Mater. 5 (2003) 629–639. doi:10.1002/adem.200310074.

[66] S.V. Meschel, O.J. Kleppa, Thermochemistry of some binary alloys of noble metals (Cu, Ag, Au) and transition metals by high temperature direct synthesis calorimetry, J. Alloys Compd. 350 (2003) 205–212. doi:10.1016/S0925-8388(02)00983-0.

[67] M. Takahashi, M. Kikuchi, Y. Takada, O. Okuno, Grindability and mechanical properties of experimental Ti–Au, Ti–Ag and Ti–Cu alloys, Int. Congr. Ser. 1284 (2005) 326–327. doi:10.1016/j.ics.2005.06.006.

[68] M. Kikuchi, M. Takahashi, O. Okuno, Machinability of experimental Ti-Ag alloys., Dent. Mater. J. 27 (2008) 216–220. doi:10.4012/dmj.27.216.

[69] M. Li, C. Li, F. Wang, W. Zhang, Experimental study and thermodynamic assessment of the Ag–Ti system, Comput. Coupling Phase Thermochem. 29 (2005) 269–275. doi:10.1016/j.calphad.2005.09.002.

[70] K. Zeng, R. Schimid-Fetzer, Critical assessment and thermodynamic modeling of the Ti-N system, Zeitschrift Für Met. 87 (n.d.) 540–554. http://cat.inist.fr/?aModele=afficheN&cpsidt=3153564 (accessed August 5, 2015).

[71] L. Tan, T.R. Allen, P. Demkowicz, High temperature interfacial reactions of TiC, ZrC, TiN, and ZrN with palladium, Solid State Ionics. 181 (2010) 1156–1163. doi:10.1016/j.ssi.2010.06.054.

[72] S. Mandl, B. Rauschenbach, Improving the biocompatibility of medical implants with plasma immersion ion implantation, Surf. Coatings Technol. 156 (2002) 276–283.

[73] D. V Shtansky, E.A. Levashov, N.A. Glushankova, S.A. Kulinich, M.I. Petrzhik, F. Rossi, Structure and properties of CaO- and ZrO 2 -doped TiCxNy coatings for biomedical applications, Surf. Coatings Technol. 182 (2004) 101–111. doi:10.1016/S0257-8972(03)00813-2.

[74] S. Piscanec, L. Ciacchi, E. Vesselli, G. Comelli, O. Sbaizero, S. Meriani, et al., Bioactivity of TiN-coated titanium implants, Acta Mater. 52 (2004) 1237–1245. doi:10.1016/j.actamat.2003.11.020.

[75] F. Vaz, J. Ferreira, E. Ribeiro, L. Rebouta, S. Lanceros-Méndez, J.A. Mendes, et al., Influence of nitrogen content on the structural, mechanical and electrical properties of TiN thin films, Surf. Coatings Technol. 191 (2005) 317–323. doi:10.1016/j.surfcoat.2004.01.033.

[76] S. Konstantinidis, RF amplified magnetron source for efficient titanium nitride deposition, Surf. Coatings Technol. 174-175 (2003) 100–106. doi:10.1016/S0257-8972(03)00528-0.

[77] R.C. Adochite, D. Munteanu, M. Torrell, L. Cunha, E. Alves, N.P. Barradas, et al., The influence of annealing treatments on the properties of Ag:TiO2 nanocomposite films prepared by magnetron sputtering, Appl. Surf. Sci. 258 (2012) 4028–4034. doi:10.1016/j.apsusc.2011.12.095.

[78] T. de los Arcos, P. Oelhafen, U. Aebi, a Hefti, M. Düggelin, D. Mathys, et al., Preparation and characterization of TiN–Ag nanocomposite films, Vacuum. 67 (2002) 463–470. doi:10.1016/S0042-207X(02)00232-4.

[79] P.J. Kelly, H. Li, K. a. Whitehead, J. Verran, R.D. Arnell, I. Iordanova, A study of the antimicrobial and tribological properties of TiN/Ag nanocomposite coatings, Surf. Coatings Technol. 204 (2009) 1137–1140. doi:10.1016/j.surfcoat.2009.05.012.

[80] P.J. Kelly, H. Li, P.S. Benson, K.A. Whitehead, J. Verran, R.D. Arnell, et al., Comparison of the tribological and antimicrobial properties of CrN/Ag, ZrN/Ag, TiN/Ag, and TiN/Cu nanocomposite coatings, Surf. Coatings Technol. 205 (2010) 1606–1610. doi:10.1016/j.surfcoat.2010.07.029.

[81] C. Gonçalves, C. Lopes, C. Fonseca, A. Guedes, F. Vaz, Structural and morphological evolution in TiAgx thin films as a function of in-vacuum thermal annealing, J. Nano Res. (2013).

[82] C. Lopes, C. Gonçalves, J. Borges, T. Polcar, M.S. Rodrigues, N.P. Barradas, et al., Evolution of the functional properties of titanium–silver thin films for biomedical applications: Influence of in-vacuum annealing, Surf. Coatings Technol. 261 (2015) 262–271. doi:10.1016/j.surfcoat.2014.11.020.

[83] C. Lopes, P. Pedrosa, N. Martin, N.P. Barradas, E. Alves, F. Vaz, Study of the electrical behavior of nanostructured Ti–Ag thin films, prepared by Glancing Angle Deposition, Mater. Lett. 157 (2015) 188–192. doi:10.1016/j.matlet.2015.05.067.

[84] P. Pedrosa, C. Lopes, N. Martin, C. Fonseca, F. Vaz, Electrical characterization of Ag:TiN thin films produced by glancing angle deposition, Mater. Lett. 115 (2014) 136–139. doi:10.1016/j.matlet.2013.10.044.

[85] P. Pedrosa, D. Machado, P. Fiedler, E. Alves, N.P. Barradas, J. Haueisen, et al., Electrochemical and structural characterization of nanocomposite Agy:TiNx thin films for dry bioelectrodes: the effect of the N/Ti ratio and Ag content, Electrochim. Acta. 153 (2015) 602–611. doi:10.1016/j.electacta.2014.12.020.

[86] P. Pedrosa, D. Machado, J. Borges, M.S. Rodrigues, E. Alves, N.P. Barradas, et al., Agy:TiNx thin films for dry biopotential electrodes: the effect of composition and structural changes on the electrical and mechanical behaviours, Appl. Phys. A. 119 (2015) 169–178. doi:10.1007/s00339-014-8943-9.

[87] S. Beeby, G. Ensell, M. Kraft, N. White, MEMS Mechanical Sensors, Artech House, 2004. https://books.google.com/books?id=6wg5oXzks9UC&pgis=1 (accessed September 3, 2015).

[88] M. Cremona, L.. Gazola, L.. Scavarda do Carmo, J.T.. Castro, C.. Achete, In situ hard coatings strain measurement using a commercial strain-gage device, Thin Solid Films. 377-378 (2000) 436–440. doi:10.1016/S0040-6090(00)01271-2.

[89] L. Zhou, S. Jung, E. Brandon, T.N. Jackson, Flexible substrate micro-crystalline silicon and gated amorphous silicon strain sensors, IEEE Trans. Electron Devices. 53 (2006) 380–385. doi:10.1109/TED.2005.861727.

[90] G. Schultes, R. Koppert, D. Goettel, O. Freitag-Weber, A.C. Probst, U. Werner, New perspectives for pressure and force sensors Thin films combining high guage factor and low TCR, Proc. SPIE. 7362 (2009) 73620W. doi:10.1117/12.820496.

[91] P. Costa, J. Silva, V. Sencadas, R. Simoes, J.C. Viana, S. Lanceros-Méndez, Mechanical, electrical and electro-mechanical properties of thermoplastic elastomer styrene–butadiene–styrene/multiwall carbon nanotubes composites, J. Mater. Sci. 48 (2012) 1172–1179. doi:10.1007/s10853-012-6855-7.

[92] K. Anselme, Osteoblast adhesion on biomaterials, Biomaterials. 21 (2000) 667–681. doi:10.1016/S0142-9612(99)00242-2.

[93] S.M. Marques, I. Carvalho, M. Henriques, T. Polcar, S. Carvalho, PVD-grown antibacterial Ag-TiN films on piezoelectric PVDF substrates for sensor applications, Surf. Coatings Technol. 281 (2015) 117–124. doi:10.1016/j.surfcoat.2015.09.057.

3. $Ti_{1-x}Ag_x$ electrodes deposited on polymer based sensor

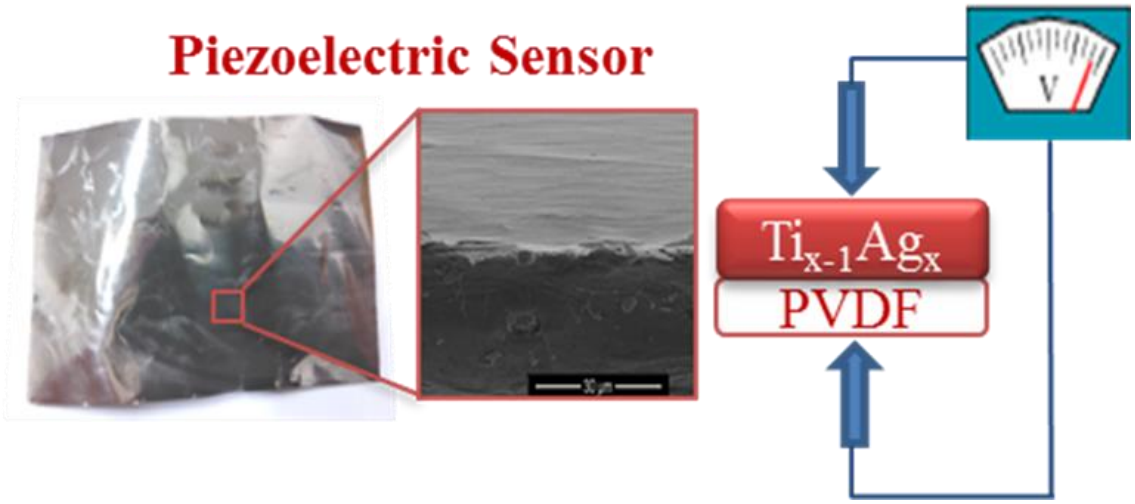

This chapter is based on the publication: S.M. Marques, N.K. Manninen, S. Ferdov, S. Lanceros-Mendez, S. Carvalho, *$Ti_{1-x}Ag_x$ electrodes deposited on polymer based sensors*, Appl. Surf. Sci. 317 (2014) 490–495. doi:10.1016/j.apsusc.2014.08.142. Q1, Impact factor: 2.711

The following chapter refers to the deposition and characterization of different $Ti_{1-x}Ag_x$ samples. Samples with different Ag/Ti atomic ratios (silver content ranging between 0 and 100 at %) were deposited by d.c. and pulsed magnetron sputtering on β-PVDF poled polymeric substrates. No temperature or bias voltage were used in order to do not damage the polymeric substrates. All samples were analyzed in relation to chemical composition, roughness, structural, topography and morphological properties. To finalize, sheet resistivity and piezo d33 response were evaluated.

The main conclusion is that $Ti_{1-x}Ag_x$ samples can be deposited by sputtering on PVDF substrates without modifying the piezoelectric response of the material. According to the results obtained from scanning electron microscopy (SEM) analysis, the coatings are homogeneous and no silver clusters were found; since β-PVDF is anisotropic, the deposited coatings replicate the underlying substrate surface.

When a mixture of Ti and Ag is achieved (with Ag/Ti between 0.22 and 0.69), XRD analysis suggested the presence of a TiAg phase. Which in turn, can explain the typical behavior of a binary alloy observed in the sheet resistivity data for this system. The piezoelectricity of the different samples showed similar values.

Keywords: *Sensors, Ag nanoparticles, piezoelectric polymers, sputtering.*

3.1 Introduction

Implant failure represents a large problem for both patients and health agencies, since it results in repeated surgeries with consequent discomfort and human pain, being also responsible for a large economic burden for society. This failure can be attributed to excessive wear, wear debris and microbial infection [1]. The future of prosthetic implants pass through the implementation of prevention mechanisms based on the application of sensor systems, which allow to obtain valuable information about a wide range of biomechanical signals [2,3]. An example of this evolution relays on piezoresistive [4,5] and piezoelectric materials to serve as strain and force sensor [6] for various applications. These sensors are suitable for the above-mentioned application, adding the fact that the piezoelectric materials do not need external power supply, being even able to provide energy to the circuit, keeping the system operational for longer periods of time [7,8].

Poly (vinylidene fluoride), PVDF, is well-known for its piezo and pyroelectric properties, useful for a wide variety of applications in the field of sensors and actuators. For the four known polymorphs of PVDF, the β - phase is the one with the largest piezoelectric response [9,10] and it was the one used as substrate material in this work. This phase can be obtained in different ways [9], being the most common the uniaxial stretching of α-phase (non-electroactive) PVDF [11,12]. Further, for improving the piezoelectric response, the material must be poled, i.e. the alignment of the randomly organized dipolar moments against the applied electric field [11,12].

As this piezoelectric material transforms mechanical loads into electrical signals, conductive electrodes are necessary on both sides for signal acquisition. Such electrodes must show good electrical conductivity and, since they are to be used within the human body, they must be biocompatible. Titanium and its alloys have been widely used on artificial implants due to their biocompatibility and good corrosion resistance [13], and Ti shows electrical conductivity in the range 43 $\mu.\Omega$ cm [14].

These implants show a high failure rate, mainly caused by microbial adhesion and colonization [13]. Thus, it becomes essential to create strategies that prevent bacterial adhesion in the first place. In addition, infections caused by *Staphylococcus epidermidis* and other coagulases-negative *Staphylococcus* (CNS) are also known as one of the most common causes of serious hospital acquired infections [13,15]. This is related to the ability of microorganisms to adhere to medical devices and forming biofilm.

Despite various efforts to develop effective medical treatments against infections caused by biofilms [16], the physical removal of an infected medical device (such as implants) is often necessary, which entails extra costs, as well as physical discomfort of the patient. Over the past years a considerable interest in increasing biodevices lifetime, trough inhibition of biofilm, has raised. In order to achieve this goal, different concepts based on the incorporation of Ag in nanoparticles and coatings have been proposed, due to the effective antibacterial activity of this metal [13,17–19].

Presently, different coatings produced by magnetron sputtering are proposed as potential candidates as functional conductive electrodes in polymeric sensors. Regarding biomedical applications, Ag-TiN_x [20–22] and $Ti_{1-x}Ag_x$ [14,23] coatings have been proposed for prosthesis pressure sensors and dry biopotential electrodes, respectively, due to their interesting electrical and biological properties. However, in the above mentioned reports the coatings were deposited on silicon and glass substrates.

In fact, the high temperatures associated with magnetron sputtering process represent the major limitation in the development of functional electrode coatings in piezoelectric PVDF substrates, due to the eventual structural changes promoted by temperature, as well as eventual depolarization of the sample, leading to the loss of the piezoelectric response. Thus, the major innovation of the present report is the deposition of $Ti_{x-1}Ag_x$ electrodes on PVDF substrates, while maintaining the piezoelectric response of the polymer.

This report focus on the development of polymer based sensors for biomedical devices, which allow detecting early failure and/or to monitor implants and biomechanical signals. Taking into account the good electrical conductivity of Ti and Ag, $Ti_{1-x}Ag_x$ coatings represent a good candidate for electrode materials. In addition, Ti is biocompatible, while Ag has been pointed as an effective antibacterial agent, able to improve the lifetime of the biodevices. Thus, Ti, Ag and $Ti_{1-x}Ag_x$ coatings, with different Ag/Ti atomic ratios were deposited by magnetron sputtering on piezoelectric PVDF substrates. The electric and piezoelectric responses of these thin films were evaluated, together with their structure and morphology.

3.2 Materials and methods

$Ti_{1-x}Ag_x$ coatings were deposited by d.c./pulsed magnetron sputtering onto ultrasonically cleaned silicon (used for AFM, and EPMA tests) and PVDF thin films with a thickness of approximately 28 μm (used for SEM, XRD analysis, Four Point Probe technique and piezoelectric response (d_{33}) tests) . One pure Ti target (99.99 %) and one Ag target (purity 99.99%)) (both with 200x100 mm^2) were used in argon atmosphere with the substrates rotating at 70 mm from the target at a constant speed of 7 rpm.

During deposition, the pressure in the deposition chamber was about 0.17 Pa and the argon flow was kept constant at 60 sccm. To vary the Ag content in the films, the current density applied to each target was varied, as indicated in Table 3.1. The Ti target was connected to the pulsed d.c. power supply, while the Ag target was connected to a d.c. power supply. For the deposition of the pure silver coating and the $Ti_{1-x}Ag_x$ coating with lowest Ag content (coating Ag/Ti 0.02), the pulsed d.c. power supply was connected to the Ag target and for the latter case the d.c. power supply to the Ti target. The frequency and reverse time were fixed at 200 kHz and 1536 ns, respectively, corresponding to a duty cycle of 69 %.

The deposition time was varied in order to obtain a final thickness ranging between 150 nm to 200 nm. In order to avoid the structural damage of the polymer substrate, the substrate temperature must be ideally kept below ≈100°C (far from the melt transition temperature of PVDF) [25]. In this sense, the depositions were performed without any external heating of the substrate and no bias polarization was applied on the substrate holder.

Chemical characterization was performed with a Cameca SX 50 electron probe microanalysis (EPMA) apparatus. Five punctual measurements were randomly performed on the samples surface, with an acceleration voltage of 10 kV. Since the depth of analysis at 10kV is about 300 nm for pure Ag and 700 nm for pure titanium, $Ti_{1-x}Ag_x$ coatings with a thickness of 1 μm were deposited for EPMA analysis. The morphology/topography of the coatings, was evaluated by atomic force microscopy (AFM) using a NanoScope III apparatus (Digital Instruments) operating in tapping mode. AFM images were taken over scanning areas of 5x5 μm^2. The roughness values are an average of three measurements. The surface morphology and thickness were by examined by scanning electron microscopy (SEM) with a NanoSEM – FEI Nova 200 (FEG/SEM). The structure and phase distribution of the coatings were analyzed by powder X-rays diffraction (XRD) using a Bruker D8 Discover diffractometer (CuKα radiation – λ =1.5406 Å, step 0.04°, time per step 1s and 6-60 2θ interval).

The sheet resistivity was tested by Four-Point-Probe technique, in three randomly distributed points with a d.c. current and voltage calibrator. The piezoelectric response (d_{33}) of the poled samples was analyzed with a wide range d_{33}-meter (model 8000, APC Int Ltd).

3.3 Results and discussion

3.3.1 Chemical composition vs. deposition parameters

The synthesis conditions together with the coating chemical composition, deposition rate, roughness and sheet resistivity are summarized in Table 3.1.

Table 3.1 – Chemical composition, resistivity, roughness of $Ti_{1-x}Ag_x$ coatings and some experimental details; for Ag/Ti(0.02) sample, Ag target was connected to the pulse power (■) and Ti target connected to a d. c. power (□)

Coating	Zone	J_{Ti} (mA/cm²)	J_{Ag} (mA/cm²)	J_{Ag}/J_{Ti}	Deposition rate (nm/h)	Chemical Composition (at. %)		Ag/Ti	Resistivity (Ω/sq)	Roughness (nm)
						Ti	Ag			
Ti		5	0	0	437.2	100	0	0	10.62±0.48	5.30
Ag/Ti (0.02)	Z1	4□	0.05■	0.0125	590.0	98.0	2.0	0.02	20.30±0.12	
Ag/Ti (0.11)		7.5	0.05	0.0067	891.8	89.8	10.2	0.11	13.87±0.29	3.55
Ag/Ti (0.21)	Z2	5	0.05	0.0100	507.0	82.7	17.3	0.21	27.09±1.13	
Ag/Ti (0.69)		3.5	0.15	0.0430	336.7	59.2	40.8	0.69	28.05±0.17	1.97
Ag/Ti (1.27)		3	0.25	0.0830	405.2	44.0	56.0	1.27	10.24±0.06	
Ag/Ti (1.70)	Z3	4	0.5	0.1250	752.0	37.1	62.9	1.70	6.91±0.33	
Ag/Ti (3.71)		2.5	0.5	0.2000	629.6	21.2	78.8	3.71	4.21±0.11	3.42
Ag		0	2.5	-	658.6	0	100	-	0.12±0.01	3.93

Through the deposition time and coatings thickness estimated by SEM analysis, it was possible to determine the deposition rate. The $Ti_{1-x}Ag_x$ coatings were labeled according to the Ag/Ti atomic ratio, while pure titanium and pure silver coatings are labeled as Ti and Ag, respectively. The coatings were divided in three different zones: Z1 (Ag/Ti < 0.11), Z2 (0.11 < Ag/Ti > 0.69) and Z3 (Ag/Ti>0.69) according to the variations in the resistivity values. Since Ag and Ti show high sputtering yields (3.12 and 0.51, when bombarded with Ar at 0.5 keV, respectively [24]) the deposition of these elements results in high deposition rates.

The use of pulsed d.c. power supply promotes a reduction in the deposition rate, thus, allowing to control the chemical composition of the coatings, achieving a low Ag content, in the case of Ag/Ti (0.02), and low Ti contents in the coatings of zone 3.

As shown in Table 3.1, the current density (J_{Ag}) applied on the Ag target was 0.05 mA/cm^2 for the deposition of Ag/Ti (0.02) and Ag/Ti (0.11), however, in the first case the pulsed d.c. power supply was connected to the Ag target, while in the coating with Ag/Ti (0.11) the d.c. power supply was connected to the Ag target. Despite the similar current density applied to Ag target (J_{Ag}) and the decrease on the current density applied to Ti target (J_{Ti}) in the deposition of Ag/Ti(0.11), the silver content was five times higher in relation to the coating Ag/Ti (0.02), which demonstrates the reduction in the sputtering rate with the use of pulsed d.c. power supply, as used on Ag/Ti (0.02) sample deposition.

Regarding the coatings deposited in similar deposition conditions (with a pulsed d.c. and a d.c. power supply connected to Ti and Ag targets, respectively) it can be found from Figure 3.1 that the Ag content increases with the J_{Ag}/J_{Ti} ratio, along with a decrease in the Ti content.

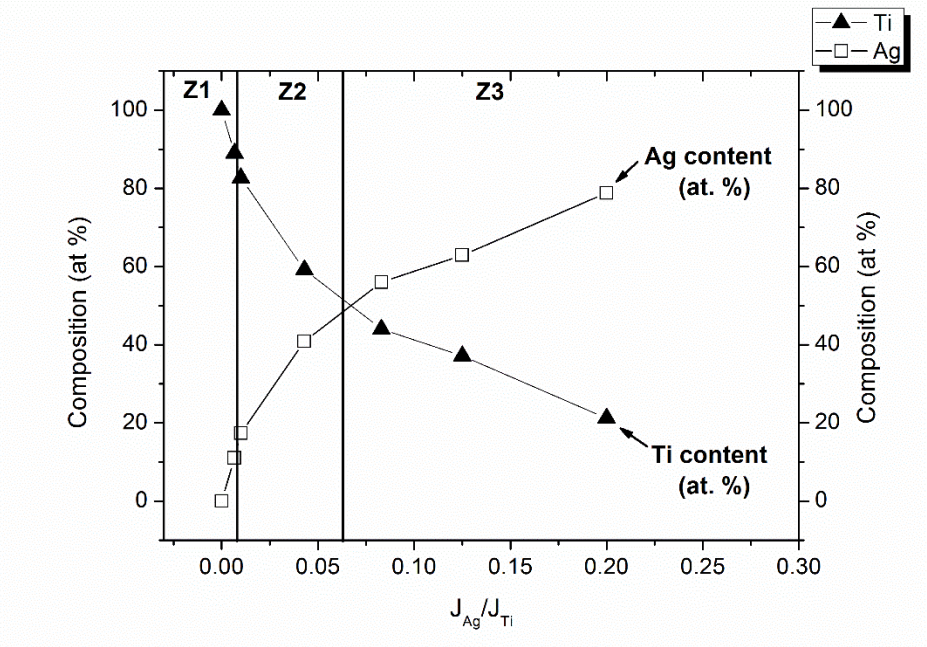

Figure 3.1 – Variation of Ti and Ag content (at.%) with the current density ratio (J_{Ag}/J_{Ti}).

The relation between current density and sputter efficiency is well described in [25] discussing that higher current densities applied on Ti and other material targets induce the sustained self-sputtering (SSS) effect meaning that during target bombardment by inert gas, in this case argon (Ar), secondary electrons, photons, neutral and excited particles are extracted from target surface contributing to sputtering along with the inert gas, promoting a higher sputter effect [25].

According to the chemical composition, it is observed that with increasing current density applied on Ag target, the Ag content increases being this effect already explained previously.

3.3.2 Structural analysis

The crystalline structure of the coatings was evaluated by means of XRD analysis and the results are shown in Figure 3.2, where the main identified crystalline phases are depicted, namely Ti (ICDD 181718) and Ag (ICDD 181730), together with the crystalline peaks of PVDF [9].

The XRD analysis was performed on pure Ti and Ag coatings and also in $Ti_{1-x}Ag_x$ coatings representative of the different zones defined previously.

XRD peaks corresponding to atomic planes (200) and (110) of β-PVDF (Figure 3.2a) indicate that the deposition conditions do not induce any phase change in the polymer. This means that the piezoelectric phase of PVDF is still present, and that, if not depoling of the material is induced during the deposition of the films, the piezoelectric response will be maintained (see later, Section 3.3.4). It can be seen a peak shift to the left, possible due to the compressive residual stress in the coatings [26]. Pure Ti coating crystallizes in a hexagonal closed packed structure, which represents the most stable titanium phase [27–29]. The XRD pattern of Ag coating suggests the presence of crystalline fcc-Ag. A magnification of the XRD patterns is shown in Figure 3.2b, where the Ag, Ti, TiAg (ICDD 605934) and Ti_2Ag (ICDD 605935) crystalline peaks are identified. According to Figure 3.2a) and b) the $Ti_{1-x}Ag_x$ coatings present very similar XRD patterns, with the most intense peak at about 37.8°, which is close to the TiAg (013) diffraction peak.

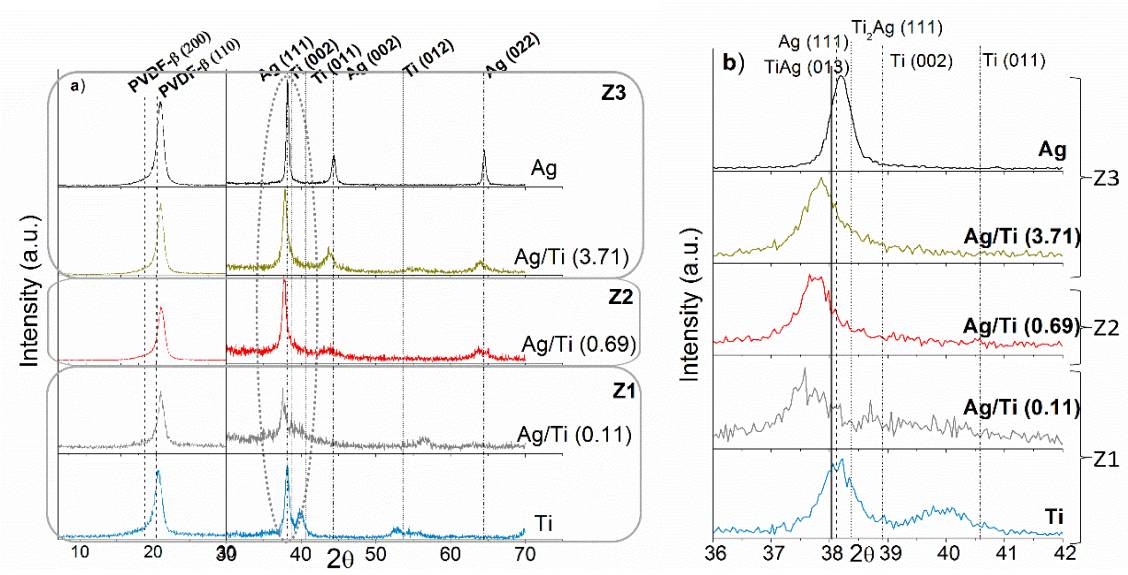

Figure 3.2 – XRD patterns of $Ti_{1-x}Ag_x$ coatings deposited with different Ag/Ti atomic ratios (Cukα radiation). Magnifications of the XRD patterns are show in b.

The formation of TiAg phase was previously reported for TiAg coatings deposited by magnetron sputtering [14]. However, taking into account that the titanium, silver and TiAg peaks show similar values, it is difficult to accurately identify the presence of the different phases. In the Ag/Ti(0.11) coating, in addition to the TiAg phase, the presence of Ti(002) peak can also be identified, which suggests that the coating is composed by a mixture of crystalline TiAg and Ti phases.

This was somehow predictable since the amount of Ti present in the coating is high (89.8 at.%), which means that the TiAg phase is formed until the Ag is consumed and the remaining titanium forms a crystalline Ti phase. Regarding the coatings with higher Ag contents (40.8 at.% Ag (Ag/Ti(0.69)) and 78.8 at.% Ag (Ag/Ti(3.71)), it can be found that the diffraction peak of Ti(002) disappears, which suggests that the crystalline titanium phase is not present in these coatings. In fact, the diffraction patterns of $Ti_{1-x}Ag_x$ coatings representative of zone 2 and 3 are very similar, both showing comparable full width at half maximum (FWHM). The only difference in these two coatings is the presence of a diffraction peak at about 43° for the coating Ag/Ti(3.71) (see Figure 3.2a), which corresponds to the diffraction peak of TiAg(110), thus suggesting a change in the orientation. The diffraction patterns of Ag/Ti(0.69) and Ag/Ti(3.71), suggest the presence of TiAg phase, however, the presence of both Ti and Ag cannot be discarded, especially for the coating with higher Ag content, where Ag phases should be present taking into account the high Ag content (78.8 at.%).

3.3.3 Topography and Morphology

SEM and AFM analyses were performed in order to evaluate surface characteristics and detect the presence of Ag clusters on the surface. The SEM micrographs of coatings representative of different Zones (identified in Figure 3.1) are depicted in Figure 3.3.

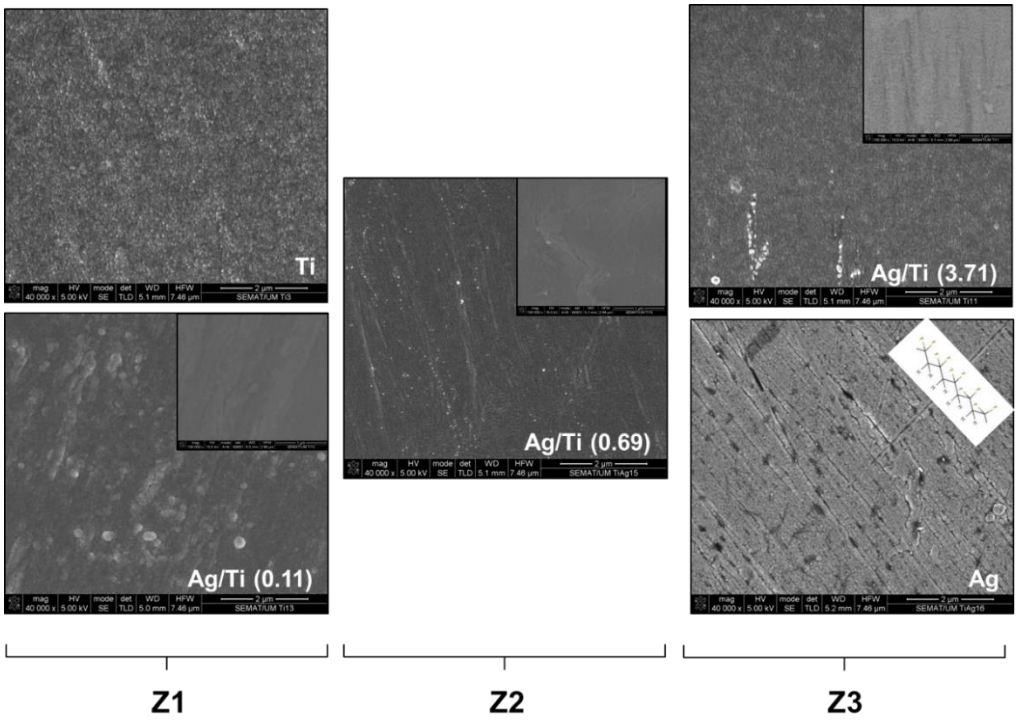

Figure 3.3 – SEM micrographs on SE mode of different $Ti_{1-x}Ag_x$ thin films on PVDF representative of the three different zones. The inceptions are micrographs in BSE mode for coatings Ag/Ti(0.11), Ag/Ti(0.69) and Ag/Ti(3.71).

Since β-PVDF is anisotropic, the deposited thin film ($Ti_{1-x}Ag_x$) replicates the underlying substrate surface showing a preferential accumulation of thin film along the crest of the longitudinal polymer microstructure obtained during the mechanical stretching to obtain the β polymer phase [9,12,30]. The co-deposition of Ag and titanium nitride (TiN) [31]; carbonitride (TiCN) [32] and oxide (TiO_2) [33] results in the formation of nanocomposites with Ag nanoparticles embedded in the matrix coating, being the size of these nanoparticles strongly dependent on the amount of silver incorporated in the coating. The formation of Ag nanoparticles is related to the immiscibility of Ag in these matrixes. It was reported [14] that TiAg coatings were composed of TiAg clusters segregated from the Ti grain boundaries, which appear as bright spots in SEM micrographs.

In order to clarify if clusters of different phases (Ag or TiAg) were present, SEM analysis was performed with magnifications up to 200.000x (not shown) and also in backscattered electron mode (BSE) (shown in the inset), which allows to obtain the elemental contrast between elements of different atomic mass, where heavier phases should appear brighter.

The XRD analysis suggested the formation of crystalline TiAg phases, combined with crystalline Ti phase (coatings of zone 1) and the formation of TiAg phases possibly combined with Ag and Ti phases in the coatings of zone 2 and 3. However, according to the results obtained from SEM analysis (Figure 3.3), the coatings are homogeneous and no clusters were found.

Figure 3.4 shows AFM images of the Ti, Ag and $Ti_{1-x}Ag_x$ films deposited on silicon. The AFM images suggest that the coatings of zone 1 and zone 3 show similar topographies, with roughness values between 3 nm to 5 nm, while the coating of zone 2 shows a smoother surface with a slightly lower roughness value (2 nm). Still, no large variations are observed between the tested coatings.

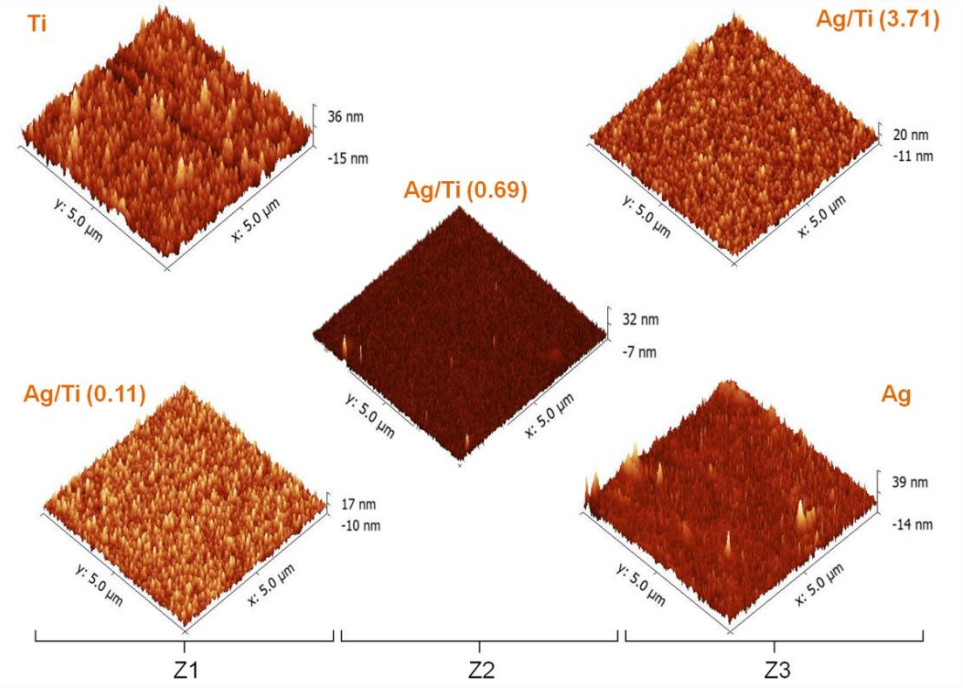

Figure 3.4 – AFM images of coatings deposited on silicon substrates with a scan range of 5µm x 5µm.

3.3.4 Sheet resistivity and piezoelectric d_{33} response

Figure 3.5 shows the coatings resistivity and piezoelectric response as a function of silver content in the coatings. Sheet resistivity shows a typical behavior of a binary alloy, according to literature [34].

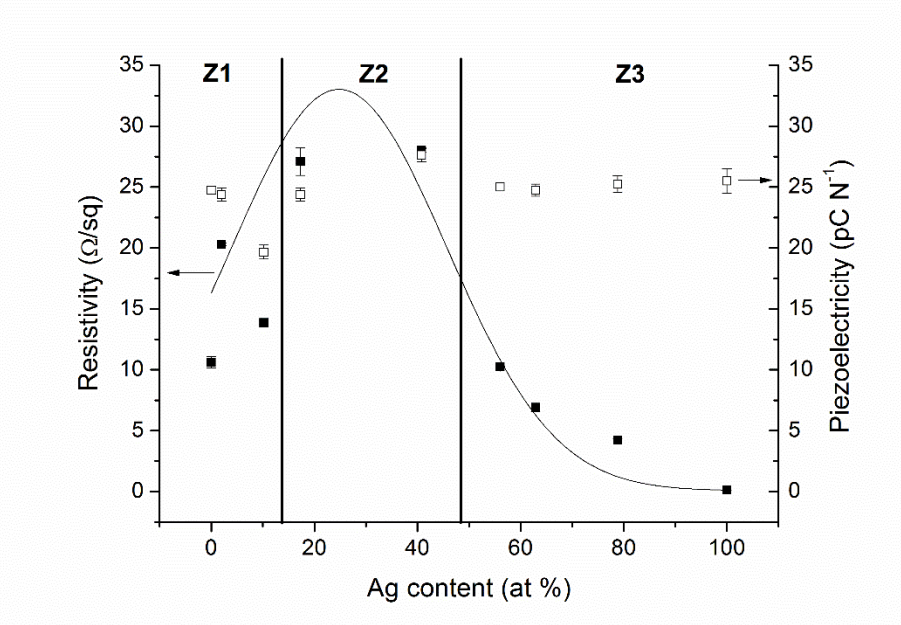

Figure 3.5 – Relationship between sheet resistivity (■), piezoelectric coefficients (d_{33}) (□) and the Ag content of the different thin films.

When Ag is added to titanium, the sheet resistivity will increase with increasing Ag concentration. It is apparent that when it reach 100 at. % of Ag and consequently 0 at. % of Ti, the electrode behaves as a pure metal so the resistivity must be small. Thus, the resistivity vary from 10.62 Ω /sq for 100 % of Ti and 0.12 Ω /sq for 100% of Ag. Therefore, resistivity versus Ag content must pass through a maximum, which for the Ti-Ag alloy is around ≈ 40 at. %. The coated polymer piezoelectric d_{33} response as a function of silver content is similar for the different samples. The values of the piezoelectric response vary from 19.6 pC N^{-1} to 27.6 pC N^{-1}. Taking into account the typical range of piezoelectric d_{33} values obtained for these materials [9], it is concluded that the deposition process does not modify the piezoelectric response of the base material (polymer) [30]. Thus, the electrodes deposited by magnetron sputtering on the PVDF surface under the conditions proposed in this investigation, allow maintaining the functional piezoelectric response of the polymer and its use for sensor and actuator applications.

3.4 Conclusions

Ti, Ag and $Ti_{1-x}Ag_x$ thin films with different Ag/Ti atomic ratios were deposited on piezoelectric PVDF polymers by magnetron sputtering.

The main goal of this investigation is to determine: i) if it is possible to deposit electrodes in PVDF polymeric films without causing any structural damage on the polymeric substrate and keeping the piezoelectric properties inherent to PVDF and ii) to evaluate the effect of thin films composition on the electrical response of PVDF coated sensors.

$Ti_{1-x}Ag_x$ thin films were divided in three different zones, according to the variations in the chemical composition, structure and electrical response: zone 1, with Ti rich coatings, with Ag/Ti atomic ratios ranging from 0 to 0.11, zone 2 which consists in a mixture of Ag and Ti (with Ag/Ti between 0.22 and 0.69) and zone 3, with silver rich coatings (Ag/Ti atomic ratios ranging from 1.27 to 3.71). XRD analysis suggested the presence of crystalline hcp-Ti phase in pure titanium coating and fcc-Ag phase in pure silver coating. The coatings of zone 1 are characterized by the presence of crystalline TiAg phase and hcp-Ti phase, while $Ti_{1-x}Ag_x$ thin films of zone 2 and zone 3 show similar XRD patterns, which suggest the formation of TiAg phase. However, since all the possible crystalline phases (Ti, Ag and TiAg), show very similar XRD patterns it is difficult to accurately identify the phases present in these thin films. Another important feature is the presence of β-PVDF phase diffraction peaks, which indicate that the deposition conditions did not damage the polymeric substrate.

SEM images revealed that the topography of the anisotropic polymer (β-PVDF) tends to enhance a preferred nucleation of the $Ti_{1-x}Ag_x$ thin films on the longitudinal crest of the polymer microstructure. The AFM analysis suggested that the coatings show very similar morphologies, with surface roughness ranging from 2 nm to 5 nm.

Sheet resistivity values show a typical behavior of a binary alloy system, with low resistivity values for coatings of zone 1 (Ti rich) and zone 3 (Ag rich) and a slightly higher resistivity values in zone 2. The piezoelectricity of the different samples are very similar and presented values from 19.6 6 $pC.N^{-1}$ to 27.6 $pC.N^{-1}$.

3.5 References

[1] C. Oliveira, L. Gonçalves, B.G. Almeida, C.J. Tavares, S. Carvalho, F. Vaz, et al., XRD and FTIR analysis of Ti–Si–C–ON coatings for biomedical applications, Surf. Coatings Technol. 203 (2008) 490–494. doi:10.1016/j.surfcoat.2008.06.121.

[2] R. Branemark, P.-I. Branemark, B. Rydevik, R.R. Myers, Osseointegration in skeletal reconstruction and rehabilitation, J. Rehabil. Res. Dev. 38 (2001) 1–8.

[3] S.P. Mohanty, E. Kougianos, Biosensors: a tutorial review, Potentials, IEEE. 25 (2006) 35–40.

[4] V. Correia, V. Sencadas, M.S. Martins, C. Ribeiro, P. Alpuim, J.G. Rocha, et al., Piezoresistive sensors for force mapping of hip-prostheses, Sensors Actuators A Phys. 195 (2013) 133–138.

[5] P. Alpuim, V. Correia, E.S. Marins, J.G. Rocha, I.G. Trindade, S. Lanceros-Mendez, Piezoresistive silicon thin film sensor array for biomedical applications, Thin Solid Films. 519 (2011) 4574–4577. doi:10.1016/j.tsf.2011.01.300.

[6] V. Correia, C. Caparros, C. Casellas, L. Francesch, J.G. Rocha, S. Lanceros-Mendez, Development of inkjet printed strain sensors, Smart Mater. Struct. 22 (2013) 105028. doi:10.1088/0964-1726/22/10/105028.

[7] J. Nunes-Pereira, V. Sencadas, V. Correia, J.G. Rocha, S. Lanceros-Méndez, Energy harvesting performance of piezoelectric electrospun polymer fibers and polymer/ceramic composites, Sensors Actuators A Phys. 196 (2013) 55–62. doi:10.1016/j.sna.2013.03.023.

[8] J.G. Rocha, L.M. Gonçalves, P.F. Rocha, M.P. Silva, S. Lanceros-Mendez, Energy Harvesting From Piezoelectric Materials Fully Integrated in Footwear, Ind. Electron. IEEE Trans. 57 (2010) 813–819. doi:10.1109/TIE.2009.2028360.

[9] P. Martins, A.C. Lopes, S. Lanceros-Mendez, Electroactive phases of poly(vinylidene fluoride): Determination, processing and applications, Prog. Polym. Sci. 39 (2014) 683–706. doi:10.1016/j.progpolymsci.2013.07.006.

[10] V.K. Tiwari, P.K. Kulriya, D.K. Avasthi, P. Maiti, Radiation-resistant behavior of poly(vinylidene fluoride)/layered silicate nanocomposites., ACS Appl. Mater. Interfaces. 1 (2009) 311–8. doi:10.1021/am800040q.

[11] C.J. Tavares, S.M. Marques, L. Rebouta, S. Lanceros-Mendez, V. Sencadas, C.M. Costa, et al., PVD-Grown photocatalytic TiO2 thin films on PVDF substrates for sensors and actuators applications, Thin Solid Films. 517 (2008) 1161–1166. doi:10.1016/j.tsf.2008.06.024.

[12] S.M. Marques, C.J. Tavares, S. Lanceros-Mendez, Z. Denchev, X-ray Scattering Experiments on Sputtered Titanium Dioxide Coatings onto PVDF Polymers for Self-Cleaning Applications, J. Appl. Polym. Sci. 119 (2011) 726–731. doi:10.1002/app.

[13] C.F.A. Alves, F. Oliveira, I. Carvalho, a. P. Piedade, S. Carvalho, Influence of albumin on the tribological behavior of Ag–Ti (C, N) thin films for orthopedic implants, Mater. Sci. Eng. C. 34 (2014) 22–28. doi:10.1016/j.msec.2013.09.031.

[14] C. Lopes, C. Gonçalves, P. Pedrosa, F. Macedo, E. Alves, N.P. Barradas, et al., TiAgx thin films for lower limb prosthesis pressure sensors: Effect of composition and structural changes on the electrical and thermal response of the films, Appl. Surf. Sci. 285 (2013) 10–18. doi:10.1016/j.apsusc.2013.07.021.

[15] N. Cerca, S. Martins, G.B. Pier, R. Oliveira, J. Azeredo, The relationship between inhibition of bacterial adhesion to a solid surface by sub-MICs of antibiotics and subsequent development of a biofilm, Res. Microbiol. 156 (2005) 650–655. doi:10.1016/j.resmic.2005.02.004.

[16] B. Jansen, K.G. Kristinsson, S. Jansen, G. Peters, G. Pulverer, In-vitro efficacy of a central venous catheter complexed with iodine to prevent bacterial colonization., J. Antimicrob. Chemother. 30 (1992) 135–139.

[17] H. Cao, X. Liu, F. Meng, P.K. Chu, Biological actions of silver nanoparticles embedded in titanium controlled by micro-galvanic effects, Biomaterials. 32 (2011) 693–705. doi:10.1016/j.biomaterials.2010.09.066.

[18] P.J. Kelly, H. Li, K. a. Whitehead, J. Verran, R.D. Arnell, I. Iordanova, A study of the antimicrobial and tribological properties of TiN/Ag nanocomposite coatings, Surf. Coatings Technol. 204 (2009) 1137–1140. doi:10.1016/j.surfcoat.2009.05.012.

[19] D.M. Eby, H.R. Luckarift, G.R. Johnson, Hybrid Antimicrobial Enzyme and Silver Nanoparticle Coatings for Medical Instruments, ACS Appl. Mater. Interfaces. 1 (2009) 1553–1560. doi:10.1021/am9002155.

[20] P. Pedrosa, C. Lopes, N. Martin, C. Fonseca, F. Vaz, Electrical characterization of Ag:TiN thin films produced by glancing angle deposition, Mater. Lett. 115 (2014) 136–139. doi:10.1016/j.matlet.2013.10.044.

[21] P. Pedrosa, E. Alves, N.P. Barradas, N. Martin, P. Fiedler, J. Haueisen, et al., Electrochemical behaviour of nanocomposite Agx:TiN thin films for dry biopotential electrodes, Electrochim. Acta. 125 (2014) 48–57. doi:10.1016/j.electacta.2014.01.082.

[22] P. Pedrosa, D. Machado, C. Lopes, E. Alves, N.P. Barradas, N. Martin, et al., Nanocomposite Ag:TiN thin films for dry biopotential electrodes, Appl. Surf. Sci. 285 (2013) 40–48. doi:10.1016/j.apsusc.2013.07.154.

[23] C. Gonçalves, C. Lopes, C. Fonseca, A. Guedes, F. Vaz, Structural and morphological evolution in TiAgx thin films as a function of in-vacuum thermal annealing, (n.d.).

[24] M. Ohring, The Materials Science of Thin Films, 2nd ed., Academic Press, San Diego, 2002.

[25] W.M. Posadowski, Sustained self sputtering d.c. magnetron materials using d.c. magnetron, Vacuum. 46 (1995) 1017–1020.

[26] J.C. Sánchez-López, M.D. Abad, I. Carvalho, R. Escobar Galindo, N. Benito, S. Ribeiro, et al., Influence of silver content on the tribomechanical behavior on Ag-TiCN bioactive coatings, Surf. Coat. Technol. 206 (2012) 2192–2198. doi:10.1016/j.surfcoat.2011.09.059.

[27] M. Li, C. Li, F. Wang, W. Zhang, Experimental study and thermodynamic assessment of the Ag–Ti system, Comput. Coupling Phase Thermochem. 29 (2005) 269–275. doi:10.1016/j.calphad.2005.09.002.

[28] J.L. Murray, K.J. Bhansali, The Ag-Ti (Silver-Titanium) System Ag-Ti, Bull. Alloy Phase Diagrams. 4 (1983) 178–183.

[29] D.A. Young, Phase diagrams of the elements, Lawrence L, University of California, 1975.

[30] J. Gomes, J. Serrado Nunes, V. Sencadas, S. Lanceros-Mendez, Influence of the β-phase content and degree of crystallinity on the piezo- and ferroelectric properties of poly(vinylidene fluoride), Smart Mater. Struct. 19 (2010) 065010 (7pp). doi:10.1088/0964-1726/19/6/065010.

[31] T. de los Arcos, P. Oelhafen, U. Aebi, a Hefti, M. Düggelin, D. Mathys, et al., Preparation and characterization of TiN–Ag nanocomposite films, Vacuum. 67 (2002) 463–470. doi:10.1016/S0042-207X(02)00232-4.

[32] R. Escobar Galindo, N.K. Manninen, C. Palacio, S. Carvalho, Advanced surface characterization of silver nanocluster segregation in Ag-TiCN bioactive coatings by RBS, GDOES, and ARXPS., Anal. Bioanal. Chem. 405 (2013) 6259–69. doi:10.1007/s00216-013-7058-z.

[33] V.S.K. Chakravadhanula, C. Kübel, T. Hrkac, V. Zaporojtchenko, T. Strunskus, F. Faupel, et al., Surface segregation in TiO2-based nanocomposite thin films., Nanotechnology. 23 (2012) 495701 (7 pp). doi:10.1088/0957-4484/23/49/495701.

[34] S.O. Kasap, Principles of Electronic Materials and Devices, McGraw-Hill Companies, 2002.

4. Ag-TiN$_x$ electrodes deposited on piezoelectric(vinylidene fluoride) for biomedical sensor applications

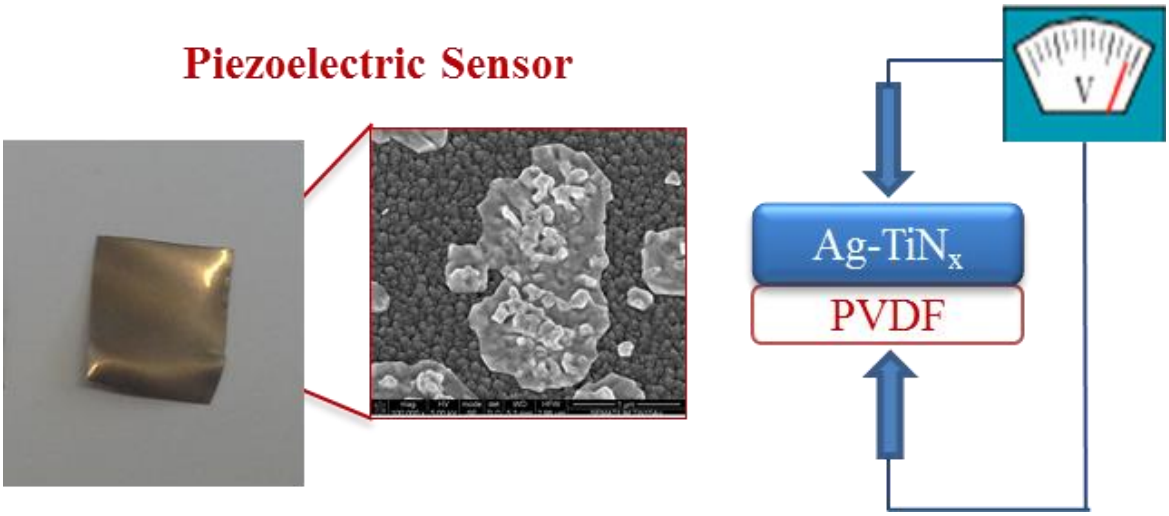

This chapter is based on the publication: S.M. Marques, N.K. Manninen, S. Lanceros-Mendez, S. Carvalho, *Ag-TiN$_x$ electrodes deposited on piezoelectric poly(vinylidene fluoride) for biomedical sensor applications*, Sensors Actuators A Phys. 234 (2015) 1–8. Doi:10.1016/j.sna.2015.08.016. Q1, Impact factor: 1.903

In this chapter an Ag-TiN_x system was deposited on PVDF to produce the electrodes. The characterization of these samples was performed using the same techniques used for $Ti_{1-x}Ag_x$ system (chapter 3) in order to compare the different coatings achieved.

From chapter 3, resulted that the Ag/Ti (0.11) sample showed an interesting behavior: the presence of a TiAg phase cannot be discarded and the silver content (10 at.%) should not present cytotoxicity problems, in contrast with further increments on silver contents. So, it seemed relevant to investigate the Ag-TiN_x series to evaluate whether nitrogen incorporation in this system promote significant changes in terms of structural and sheet resistivity.

Thus, Ag-TiN_x electrodes were deposited, by d.c. and pulsed reactive magnetron sputtering at room temperature on PVDF with increasing N_2 flow, from 0 to 15 sccm. The TiN0Ag sample (ϕ_{N2} = 0 sccm), has exactly the same deposition conditions of Ag/Ti(0.11). The different electrodes obtained were characterized in terms of chemical composition, deposition rate, roughness, structural, topography, and morphology. Additionally, the sheet resistivity and the piezoelectric d_{33} response, were also evaluated.

The most important conclusions for this chapter, relays in the presence of Ag clusters, segregated from the TiN cubic grain boundaries, being the largest structural change promoted by the incorporation of nitrogen on the $Ti_{1-x}Ag_x$ *system. The deposition conditions preserved the polymer structure and suggested the presence of crystalline fcc-TiN phase and fcc-Ag phase in samples with N_2 flow above 3 sccm. The new structural arrangement promoted a slight decrease on the sheet resistivity value. Furthermore, the piezoelectric response decreased, although not compromising the piezoelectric response for the required application.*

Keywords: *Sensors, Ag nanoparticles, piezoelectric polymers, sputtering.*

4.1 Introduction

Although the use of hip implants is continuously increasing, implant failure represents a large problem for patients and health agencies, since it results in repeated surgeries with consequent discomfort and human pain, being also responsible for a large economic burden for society. This failure can be attributed to excessive wear, wear debris and microbial infection [1,2]. The future of prosthetic implants pass through the implementation of prevention mechanisms based on the implementation of sensor systems, which allow to obtain valuable information about a wide range of biomechanical signals [3,4].

This evolution can rely on piezoresistive [5,6] and piezoelectric materials to serve as strain and force sensor [7] for various applications. These sensors are suitable for the above-mentioned applications, adding the fact that the piezoelectric materials do not need external power supply, being even able to provide energy to the circuit, through mechano-electrical conversion, keeping the system operational for longer periods of time [8,9].

Due to its important pyro and piezoelectric properties, poly(vinylidene fluoride) (PVDF) has been widely investigated [10] and is being implemented in a wide variety of applications in the field of sensors and actuators. From the different polymorphs of PVDF, the β phase is the one with the largest piezoelectric response [11,12] and it was the one used as substrate material in this work. This phase can be obtained in different ways [11], being the most common the uniaxial stretching of the non-polar α-phase [13,14]. Further, for improving the piezoelectric response, the material must be poled, i.e. alignment of the randomly oriented dipolar moments with an applied electric field [13,14].

Beyond the specific nature and characteristics of the sensing material (PVDF), there is still the need for its surface functionalization, namely in terms of electrodes. The present approach consists in using a magnetron sputtered conductive thin layer to serve as electrode for signal acquisition or actuation of the piezoelectric response of the polymer [15]. Taking into account the main requirements of the targeted application, the selected electrodes must show good electrical conductivity and since they are to be used within the human body, in the case of specific biomedical applications, they must be biocompatible. Furthermore, coated polymers will be subjected to mechanical and/or electrical solicitations that can cause degradation of the coating, affecting its functional performance [15].

In order to overcome the aforementioned potential limitations, the Ag-TiN_x system was selected as the material for electrode fabrication. A similar study in $Ti_{1-x}Ag_x$ electrodes has been recently performed by the authors [16] being found that Ti, Ag and $Ti_{1-x}Ag_x$ coatings with different Ag/Ti atomic ratios are suitable electrodes own to their good electrical conductivity. Moreover, the coatings were successfully deposited on PVDF substrates, without compromising its piezoelectric response. In this report the influence of nitrogen incorporation in $Ti_{1-x}Ag_x$ coatings is evaluated. In fact, despite the good electrical conductivity of Ti coatings the low chemical stability of this metal in corrosive environments, such as those found within the human body, may promote its degradation with consequent loss if its functional properties.

Conversely, ceramic TiN coatings are chemically inert, and thus stable within human body conditions, still showing good electrical conductivity and biocompatibility, which represent the main requirements for the envisaged application. The inclusion of silver, with low Young's Modulus and high conductivity [17], within the TiN films may offer the possibility to tailor the Young's Modulus of the electrode [18] since Ag increases the plasticity of TiN (a brittle material) [19], opening a wide range of possible applications, especially those related to coatings on polymers (flexible devices) [20]. Silver is also known as an antibacterial agent [21–24] particular in its nanocrystalline form [25,22] and an excellent material for biosensor applications [19].

Thus, Ag-TiN_x coatings, using different flows of nitrogen were deposited by magnetron sputtering on piezoelectric PVDF-β poled substrates. The electrical properties of the films were evaluated, together with their structure and morphology. Finally, the influence of film deposition on the piezoelectric response of the polymer was determined.

4.2 Materials and methods

Ag-TiN_x coatings were deposited by d.c./pulsed d.c. reactive magnetron sputtering onto ultrasonically cleaned silicon substrates (monocrystalline silicon wafers (100 P-type/B) with resistivity 1-100 Ω .cm) and commercial PVDF-β poled thin films (Precision Acoustics Ltd, with a thickness of approximately 28 μm). Silicon substrates were used for atomic force microscopy (AFM), and energy dispersive spectroscopy (EDS) tests and PVDF substrates for the analyses by scanning electron microscopy (SEM), X-ray diffraction (XRD) analysis, Four-Point-Probe technique and piezoelectric response (d_{33}) tests.

A pure Ti target (99.99 %) and an Ag target (99.99%)) (both with 200x100 mm^2) were used in Ar + N_2 mixture, with the substrates rotating at 70 mm from the target at a constant speed of 7 rpm. The base pressure in the deposition chamber was about $5x10^{-4}$ Pa, which increased up to $1.7x10^{-1}$ Pa during deposition. The argon flow was kept constant at 60 sccm while the reactive gas flux, N_2, was changed in the range of 0-15 sccm. The current density applied to each target was maintained constant at 7.5 mA/cm^2 for Ti target and 0.05 mA/cm^2 for Ag target, respectively. The Ti target was connected to the pulsed d.c. power supply, while the Ag target was connected to a d.c. power supply. The frequency and reverse time were fixed at 200 kHz and 1536 ns, respectively, corresponding to a duty cycle of 69 %. The deposition time was varied in order to obtain a final thickness.

In order to avoid the structural damage of the polymer substrate, the substrate temperature must be ideally kept below ≈ 100 °C (below the α -relaxation and far from the melt transition temperature of PVDF) [11]. In this sense, the depositions were performed without any external heating of the substrate and no bias polarization was applied on the substrate holder.

Chemical composition estimation was performed with an EDAX - Pegasus X4M - EDS apparatus coupled with a SEM. Since the depth of analysis at 10kV is about 300 nm for pure Ag and 700 nm for pure titanium, Ag-TiN_x coatings with a thickness of 1 μm were deposited onto Si substrate for EDS analysis. The topography of the coatings was evaluated by AFM using a NanoScope III apparatus (Digital Instruments) operating in tapping mode. AFM images were taken over scanning areas of 5 × 5 μm^2. The roughness values are an average of three measurements. The surface morphology and thickness were examined by SEM through a NanoSEM – FEI Nova 200 (FEG/SEM). The structure and phase distribution of the coatings were analyzed by XRD using a Bruker D8 Discover diffractometer (Cu Kα radiation – λ=1.5406 Å, step 0.04°, time per step 1s and 6-60 2θ interval). Glow discharge optical emission spectroscopy (GDOES) was performed in order to determine the Ag depth profile. GDOES was performed in a Horiba Jobin Yvon RF GD Profi ler equipped with a 4-mm diameter copper anode, operating at radiofrequency discharge pressure of 650 Pa (in argon atmosphere) and a power of 40 W. The sheet resistivity was tested by Four-Point-Probe technique, in three randomly distributed points with a Time Electronics 9818 d.c. Current Voltage Calibrator current source and a Keithley 2182 nanovoltmeter. The piezoelectric response (d_{33}) of the samples was analyzed with a wide range d_{33}-meter (model 8000, APC Int Ltd).

4.3 Results and discussion

4.3.1 Chemical composition vs. deposition parameters

The synthesis conditions together with the coatings chemical composition, deposition rate, roughness, sheet resistivity and the piezoelectric d_{33} values are summarized in Table 4.1.

Table 4.1 - Chemical composition, resistivity, roughness of Ag-TiN$_x$ coatings and some relevant experimental details. The Ag-TiN$_x$ coatings were labeled according to the N_2 flow applied e.g. TiN2Ag was deposited with a nitrogen flow of 2 sccm

Coating	Zone	N_2 flow (sccm)	Thickness on polymers (nm)	Deposition rate (nm/h)	Chemical Composition (at. %)			N/Ti	Resistivity (Ω/sq)	Piezoelectric d_{33} (pC.N^{-1})	Roughness (nm)
					Ti	Ag	N				
TiN0Ag	Metallic mode	0	200.8	803.3	93	7	0	0	12.00±0.96	-19.5±0.48	5
TiN1Ag		1	211.7	846.7	68	7	25	0.4	3.85±0.23	-17.8±0.50	3
TiN2Ag	Transition mode	2	227.5	910.0	57	6	37	0.7	3.21±0.44	-16.9±0.54	21
TiN3Ag		3	141.7	566.7	44	18	38	0.9	6.08±1.22	-13.0±0.58	22
TiN4Ag	Reactive mode	4	102.2	460.0	41	20	40	1.0	3.93±0.89	-13.5±0.58	23
TiN6Ag		6	84.9	436.7	41	20	39	1.0	2.21±0.39	-17.25±0.73	25
TiN8Ag		8	75.8	390.0	42	18	40	1.0	2.91±0.56	-17.13±1.12	25
TiN10Ag		10	80.6	322.5	42	18	40	1.0	3.04±0.42	-14.38±0.66	21
TiN15Ag		15	86.7	346.7	42	18	40	1.0	2.76±0.20	-13.63±0.54	26

Through the deposition time and coatings thickness estimated by SEM cross-sectional imaging on silicon substrate, it was possible to determine the deposition rate. All the coatings were deposited with constant power density applied to silver (J_{Ag}) and titanium (J_{Ti}) targets of 0.05 mA/cm^2 and 7.5 mA/cm^2, respectively, while the N_2 flow was varied as indicated in Table 4.1, in order to achieve different chemical compositions. The presence of oxygen in sputtered coatings occurs as result of contamination, thus, the oxygen content was found below 7 at.%. Moreover, no great differences in oxygen content were found between the different coatings.

The target potential provides valuable information about the physical processes occurring during the reactive magnetron sputtering process, which have a strong influence on both deposition rate and chemical composition and consequently on phase formation. In fact, the determination of these values represents a simple method for selection of deposition parameters and also for quality control [26].

The variation of the titanium target potential values for different nitrogen flows are depicted in Figure 4.1(a), while the N/Ti atomic ratios, Ag content (at.%) and deposition rate (see inset) are shown in Figure 4.1(b).

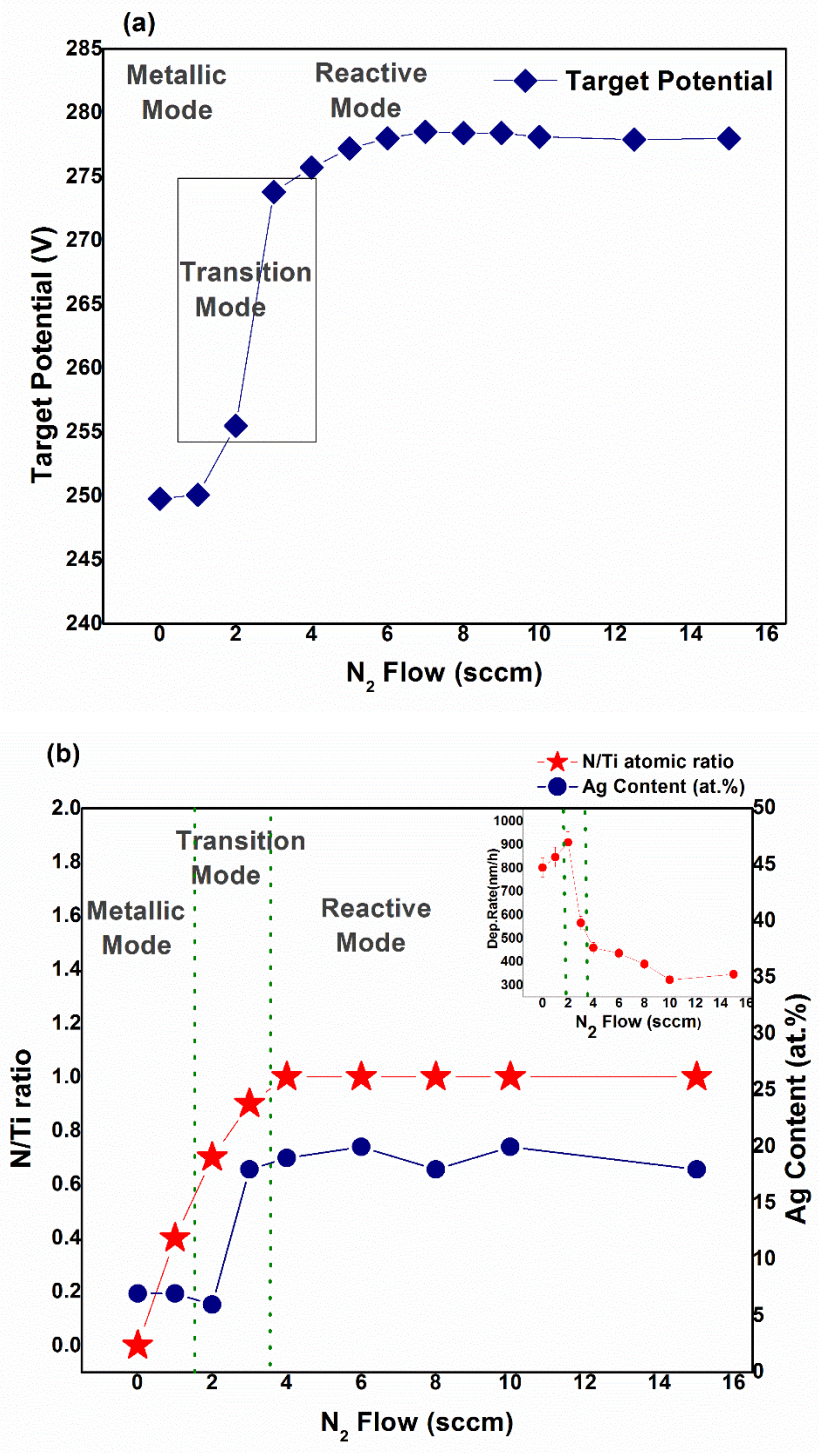

Figure 4.1 - (a) Variation of Ti target potential for different N_2 flows and (b) variation of N/Ti atomic ratio and Ag content with N_2 flow and on influence of nitrogen flow on deposition rate (inset).

The results shown in Figure 4.1(a) indicate that the target potential shows an approximately constant value (about 250 V) for nitrogen flows between 0 to 2 sccm; while increasing the nitrogen flow up to 3 sccm promotes an increase in the target potential up to 275 V, which remains almost constant up to 15 sccm.

The variations in cathode voltage are related to the target chemical composition, since this value is related to the secondary electron emission yield (SEEY) from target surface, which varies inversely with the target potential [27]. When the reactive gas flow rate (N_2) is increased, the target surface state evolves from metallic (or clean) to poisoned mode following the percentage of nitrogen added [28]. The poisoned state corresponds to the formation of a titanium nitride compound on the target surface, which shows a lower secondary electron emission yield (SEEY) in relation to metallic titanium; thus promoting an increase in the target voltage [27,28]. In this sense, the deposition in metallic mode (clean metallic target) and reactive mode (formation of a compound on the target), were determined being found that the transition occurs at a nitrogen flow between 2 and 3 sccm.

Regarding the Ag target, it was found that the target potential values were almost constant for different nitrogen flows, which was somehow predictable, since Ag shows a very low affinity to bind with nitrogen [27,29]. Based on these observations, different coatings were deposited in metallic mode (with nitrogen flow lower than 2 sccm) and in reactive mode (with nitrogen flow higher than 3 sccm). The variations in the coatings chemical composition (see Figure 4.1(b)) are well correlated with the conceptual model of reactive magnetron sputtering process proposed by Spencer et al [30]. In metallic mode, the increase in N_2 flow promotes a gradual increase in N/Ti ratio, which increases from 0 up to 0.7 corresponding to the formation of metal rich coatings; while in reactive mode the N/Ti ratio is almost constant, with a value close to 1, which corresponds to the formation of stoichiometric films. For low nitrogen flows the reactive gas is consumed by the growing film and the N/Ti increases linearly with the N_2 flow, until a saturation regime is achieved, which corresponds to a flow rate higher than the rate of the sputtered metal. At this point, a stoichiometric film is formed and excessive reactive gas begins to react with the target forming the poisoned layer. In this regime the deposition rate decreases, due to the lower sputtering rate of the compound layer in relation to the metallic Ti, in fact, the inset of figure 4.1(b) suggests a constant deposition rate in metallic mode (about 800-900 nm/h) while in reactive mode the deposition rate decreases continuously from 567 nm/h to 347 nm/h.

The Ag content is also influenced by the deposition mode, being found that in metallic mode the Ag content remains almost constant with a value around 6 to 7 at.%, while in reactive mode the silver content increases up to 20 at.%. This variation in silver content is mainly attributed to the changes in target composition and consequently on their sputtering rates.

In fact, in reactive mode the titanium content decreases, due to the target poisoning effect, while the Ag target is not affected by the nitrogen flow, which means that its sputtering rate remains constant irrespective to the nitrogen flow. As consequence, the Ti content decreases (from 57 at.% to 44 at.%) along with an increase in Ag (from 6 at.% to 18 at.%) content during the transition from metallic to reactive deposition mode.

The coatings were divided in 3 different zones, based on the variations on their chemical composition, which has a strong effect on phase formation and coatings morphology, as discussed in sections 4.3.2 and 4.3.3. In fact, it can be observed that the coating TiN2Ag shows a deposition rate, target potential values and Ag content very close to the ones achieved in metal rich coatings of Metallic mode; however, the nitrogen content in this coating is very similar to the nitrogen contents achieved in gas rich coatings of Transition mode, which have a strong influence on phase formation as discussed below.

4.3.2 Structural analysis

XRD analysis was performed in order to: i) evaluate the PVDF structure after the deposition process and ii) identify the phase composition in AgTiN coatings for different nitrogen flows. The coatings XRD patterns are depicted in Figure 4.2. Figure 4.2(a) presents the results for detailed analysis of PVDF phases, while Figure 4.2(b) shows the detailed information concerning the Ag and TiNx phases. The reference peaks of the main crystalline phases identified are namely hcp-Ti (ICDD 00-044-1294), fcc-Ag (ICDD 00-004-0783), tetragonal TiAg (ICDD 00-006-0560), stoichiometric fcc-TiN (ICDD 00-038-1420) and $TiN_{0.88}$ (ICDD 01-087-0630) together with the crystalline peaks of PVDF (ICDD 00-042-1649).

XRD peaks corresponding to atomic planes (200) and (110) of β-PVDF (Figure 4.2(a)) indicate that the deposition conditions do not induce any phase change in the polymer. This means that the piezoelectric phase of PVDF is still present.

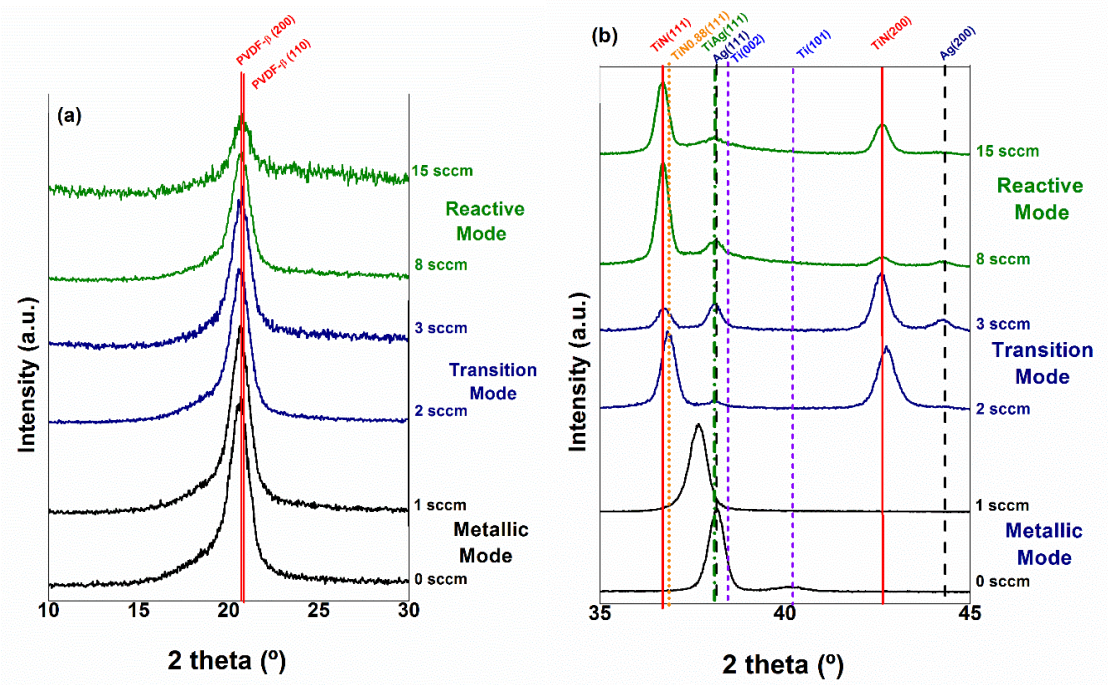

Figure 4.2 - XRD patterns of Ag-TiN$_x$ coatings deposited with different N_2 flow (Cu Kα radiation). (a) present the crystalline peaks of PVDF-β (from 10 to 30°) and in (b), from 35 to 45°, the peaks from coating crystalline phases.

The XRD pattern of TiN0Ag coating indicates that the most intense peak is located at 38.1°, which is very close to the TiAg(111) and Ag(111) peak (see Figure 4.2(b)). Previous studies in $Ti_{1-x}Ag_x$ coatings deposited by magnetron sputtering, suggested the formation of the TiAg crystalline phase; however, the accurate phase identification in $Ti_{1-x}Ag_x$ coatings is quite complex, since the Ag, hcp-Ti (which represents the most stable titanium phase) and TiAg phases show very similar diffraction patterns. In addition to the TiAg phase, the presence of the Ti(002) peak can also be identified, which suggests that the coating is composed by a mixture of crystalline TiAg and Ti phases. This was somehow predictable since the amount of Ti present in the coating is high (93 at.%), which means that the TiAg phase is formed until the Ag is consumed and the remaining titanium forms a crystalline Ti phase [16].

For TiN1Ag coating, the only visible peak is found at 36.9°, which should be related to sub-stoichiometric TiN phase, which is in good agreement with the low N/Ti atomic ratio (0.4), although the presence of Ag phase cannot be excluded. A further increase in N_2 flow up to 2 sccm results in the shift of TiN peak to lower angular position, which is attributed to the increase of N/Ti atomic ratio to 0.7 (see Table 4.1). The appearance of a second crystalline phase, attributed to fcc-Ag phase, is now evident.

The suppression of TiAg intermetallic phase, which becomes clear for coatings deposited with N_2 flows above 2 sccm, can be explained by the higher enthalpy of the formation of TiAg (-1.6±2.4 kJ/mol) [31,32] in comparison with the enthalpy of formation of TiN phase (-330 kJ/mol) [33,34]. Thus takings into account this thermodynamically parameter, when nitrogen is introduced in the deposition chamber the Ti atoms will preferentially bind to N atoms than to Ag atoms, thus, the formation of the TiAg phase is suppressed by the formation of TiN phase as soon as nitrogen is introduced in the system. In addition, Ag will grow as a second phase. Regarding the coatings of reactive mode the presence of two crystalline fcc phases can be clearly identified: a stoichiometric TiN and an Ag phases.

4.3.3 Topography, morphology and Ag in depth distribution

SEM top-view analysis was performed in order to evaluate surface characteristics and the presence of Ag nanoparticles on the surface. The SEM micrographs of representative coatings from different zones are depicted in Figure 4.3.

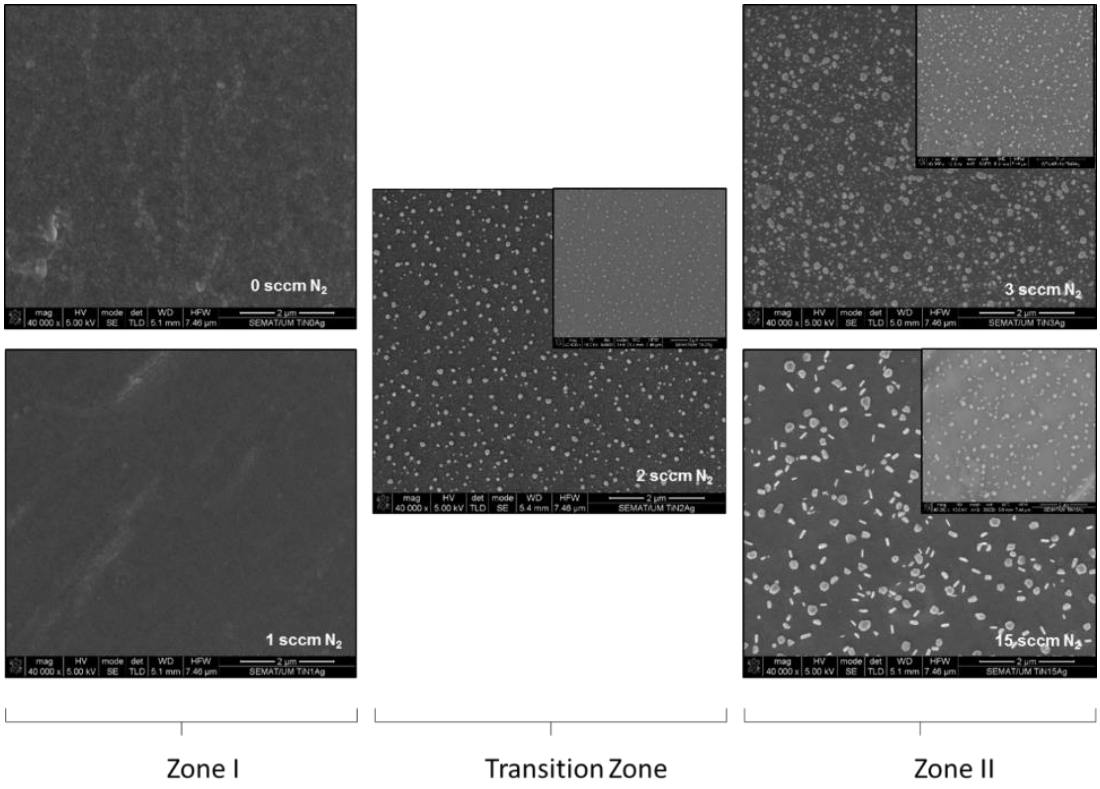

Figure 4.3 - SEM micrographs on SE mode of different Ag-TiN$_x$ thin films deposited on PVDF. The insets are micrographs in BSE mode for the coatings TiN2Ag, TiN3Ag and TiN15Ag.

According to the results obtained from SEM analysis (Figure 4.3), the coatings deposited under metallic mode are homogeneous presenting a very smooth surface, while the coatings deposited on Transition mode and Reactive mode are composed by nanoparticles embedded in a matrix coating. Lopes et al [15] reported that Ag-TiN_x coatings were composed of Ag clusters segregated from the TiN cubic grain boundaries, which appear as bright spots in the SEM micrographs. In order to clarify if the nanoparticles visible in SEM micrographs are Ag, SEM analysis was performed in backscattered electron mode (BSE) (shown in the inset), which allows to obtain the elemental contrast between elements of different atomic mass, where heavier phases (in this case Ag) appear brighter. These results are well correlated with the structural characterization performed by XRD analysis, which suggested the presence of one phase in the coatings deposited in Metallic mode, while the coatings deposited in Reactive mode and Transition mode are composed by two phases: one $Ti_{1-x}N_x$ phase, which represents the matrix, and the second Ag phase grows forming nanoparticles, according to the results obtained in SEM analysis. It should be pointed out that the "absence" of second phases in the coatings of Metallic zone (TiN1Ag sample) might be related to the formation of very small Ag nanocrystals (< 2 nm), which cannot be detected either in SEM or XRD analysis, due to the limitations related with the resolution of the above mentioned techniques. The co-deposition of Ag and titanium nitride (TiN) [35], carbonitride (TiCN) [36] and oxide (TiO_2) [37] results in the formation of nanocomposites with Ag nanoparticles embedded in the matrix coating, which related to the immiscibility of Ag in these matrixes.

Other common feature observed in sputtered Ag nanocomposite coatings is the heterogeneous distribution of Ag along the coatings depth, being reported that silver clusters are able to diffuse in the base coating, which leads to a non-uniform Ag distribution along the coatings thickness. Escobar Galindo et al [36] and Chakravadhanula et al [37] reported that Ag nanoparticles are able to segregate to coatings surface, being found that bigger Ag nanoparticles grow at coatings top-surface at expenses of smaller Ag clusters located in the first nanometers below the top surface layer. Escobar Galindo et al [36] found through GDOES, angle-resolved X-ray photoelectron spectroscopy (ARXPS) and Rutherford backscattering (RBS) analyses that Ag-TiCN coatings were composed of a Ag rich top-surface layer (with a thickness of few nanometers) followed by a depletion zone of few nanometers and aftermost the Ag showed a uniform distribution along the coatings depth.

As a result, in order to clarify how Ag is distributed along the coatings depth, a qualitative GDOES depth profile analysis was performed in different coatings representative of different analyzed zones (Metallic, Transition and Reactive) and the results are shown in Figure 4.4.

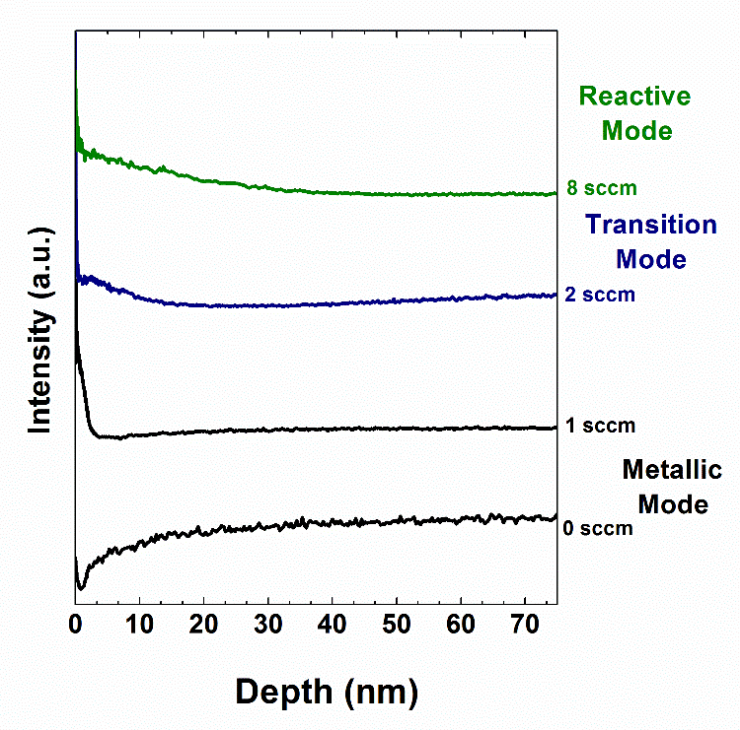

Figure 4.4 - Silver composition by GDOES depth profiles of Ag-TiN$_x$ coatings.

The results suggest that in all coatings the first 10 nm show a different Ag distribution in relation to the matrix coating. In fact, the TiNOAg thin film shows a lower amount of Ag in the top surface layer in relation to the bulk coatings, while an opposite trend is observed in Ag-TiN$_x$ coatings containing N. The lower amount of Ag and Ti in coatings surface is mainly attributed to the presence of high amounts of oxygen (result not shown), which is somehow expectable due to the metallic nature of the alloy thin film. The nitride coatings show an Ag rich surface layer, as previously reported by other authors [36,37]; nevertheless, no Ag depletion zone is observed as reported by Escobar Galindo et al [36], which means that no Ag surface segregation is occurring. In this sense, the Ag rich surface layer might be attributed to the presence of Ag nanoparticles which are exposed to the outer surface and not completely embedded in the bulk; thus, during the GDOES analysis these particles are first analyzed.

Figure 4.5 shows AFM images of the Ag-TiN$_x$ films deposited on silicon.

The AFM images suggest that the coatings deposited with 0 sccm of N_2 and 1 sccm of N_2 show similar morphologies, with roughness values between 4 nm to 2 nm, while the coatings deposited with 3 sccm of N_2 to 15 sccm of N_2 show a roughness around ≈ 20 nm due to the presence of silver nanoparticles on the surface of the thin film as it was confirmed by the SEM images presented on Figure 4.3.

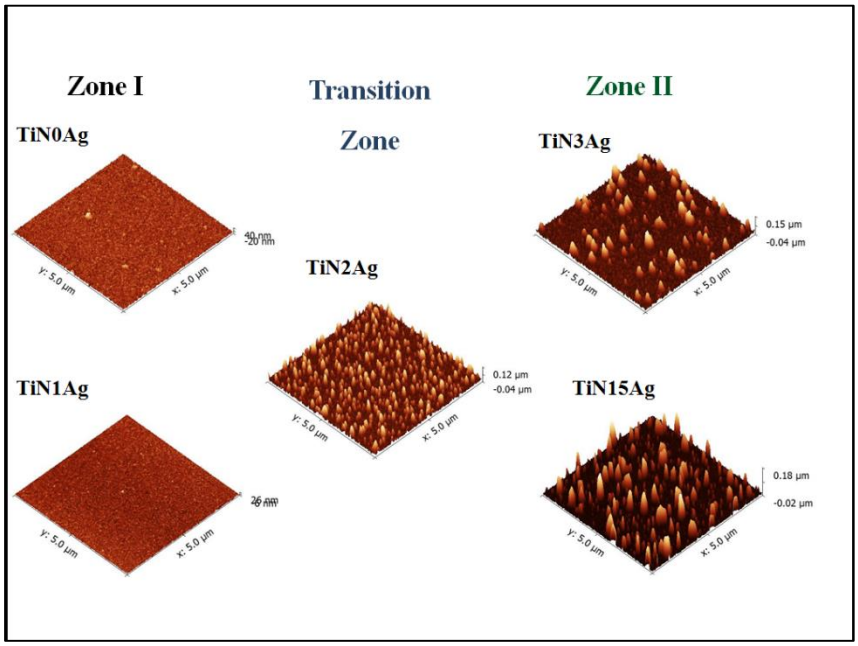

Figure 4.5 - AFM images of the coatings on silicon substrate with a scan range of 5 µm x5 µm.

4.3.4 Sheet resistivity of the films and piezoelectric d_{33} response of the polymer

Figure 4.6 shows the coatings electrical resistivity and piezoelectric response as a function of the nitrogen flow applied in the deposition of the different samples.

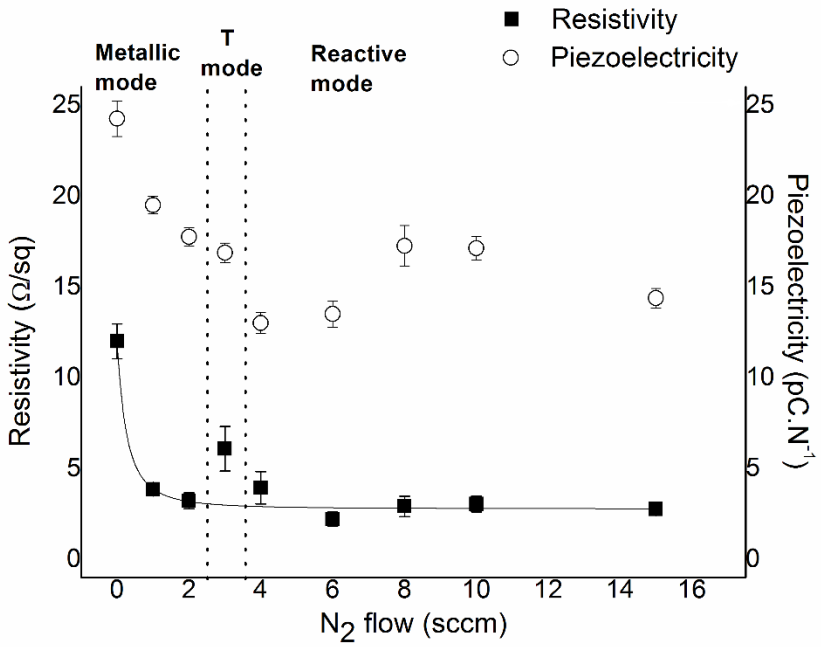

Figure 4.6 - Relationship between sheet resistivity (■) of the deposited films, piezoelectric coefficients (d_{33}) of the polymer (○) and the N_2 flow for different thin films.

The resistivity for the samples with 0 sccm of nitrogen flow, presents a value of 12.0 Ω /sq, but when more nitrogen is introduced, the resistivity tends to decrease to values between 2.21 Ω /sq and 6.08 Ω /sq. The results for 0 sccm of nitrogen flow, is in agreement with results reported previously [16]. This deep drop of the resistivity is explained by the Ag distribution within the TiN matrix. The Ag segregation phenomenon explained in (section 4.3.3), possibly gives rise to electronic path-ways between clusters that will contribute to an improvement of the electrical conductivity [19,20] because Ag acts as a high conductivity dopant [18]. The values of the piezoelectric response vary from 24.25 to 13.00 pC N^{-1}.

Taking into account the typical range of piezoelectric d_{33} values obtained for this materials, 25.19 pC N^{-1} [11], there is a small decrease in the value of piezoelectricity for samples deposited with higher nitrogen flow. Some depoling of the material might have been induced during the deposition of the films, and then the piezoelectric response is lower. For higher flows of nitrogen, higher target potential is observed.

More energy can lead to increased heating of the sample, leading to greater dipole mobility and, if the temperature is sufficiently high, greater depoling leading to a lower d_{33} value. The decrease of the piezoelectric response is attributed to depoling of the samples. There is no phase transformation under those deposition conditions or an additional capacitive layer.

The most common effect in PVD sputtered film deposition, leading to a decrease of the piezoelectric signal, is the local heating of the sample due to the harsh deposition conditions. Local heating of the samples above certain temperatures leads to a decrease of the piezoelectric signal due essentially to dipole misalignment [38]. However, this slight variation do not compromise the piezoelectric response for the required application, so, it is possible to conclude that the deposition process does not modifies significantly the piezoelectric response of the material [39]. So, the electrodes deposited by magnetron sputtering on the PVDF surface under the conditions proposed in this investigation, allow maintaining the functional piezoelectric response of the polymer and its use for sensor and actuator applications.

4.4 Conclusions

Ag-TiN_x thin films were deposited on piezoelectric PVDF polymers by magnetron sputtering.

In this investigation, it is evaluated the possibility of depositing electrodes in PVDF polymer films without causing structural damage on the polymeric substrate and keeping the piezoelectric properties of PVDF, as well as the effect of thin films composition on its electrical properties.

XRD analysis suggested the presence of crystalline TiAg phase in addition to the hcp-Ti phase, in sample with 0 sccm of N_2 flow. Also, in this sample, an fcc-Ag phase cannot be excluded, indicating that this coating is composed by a mixture of crystalline phases. For samples deposited with more than 3 sccm of N_2 flow, XRD analysis suggested the formation of crystalline fcc-TiN phases, combined with crystalline fcc-Ag phase. According to the results obtained from SEM analysis the coatings are homogeneous, presenting a TiN matrix with Ag clusters visible on the surface.

Another important feature is the presence of β-PVDF phase diffraction peaks, which indicate that the deposition conditions did not damage the polymeric substrate. SEM images revealed the presence of Ag nanoparticles segregated from the TiN cubic grain boundaries, which appear as bright spots in SEM micrographs.

The AFM analysis suggested that the coatings deposited with 0 and 1 sccm of N_2 show similar morphologies, with roughness values of 4 nm and 2 nm, respectively, while the coatings of samples deposited from 3 to 8 sccm of N_2 shows a roughness around ≈ 20 nm due silver nanoparticles on the surface of the thin film.

Sheet resistivity values are different if nitrogen is present or not. For the sample without nitrogen, resistivity is high, 12.0 Ω /sq but when more nitrogen is introduced, the resistivity tends to decrease for values that vary from 6.08 Ω /sq to 2.21 Ω /sq. This deep drop of the resistivity is explained by the Ag distribution on the TiN matrix because Ag acts as a high conductivity dopant. The values of the piezoelectric response vary from 24.25 to 13.00 pC N^{-1}. Taking into account the typical range of piezoelectric d_{33} values obtained for this materials there is a small decrease in the value of piezoelectricity for samples deposited with higher nitrogen flow. However, this slight variation thus not compromise the piezoelectric response for the required application, so, it is possible to conclude that the deposition process does not significantly modify the piezoelectric response of the material.

4.5 References

[1] C. Oliveira, L. Gonçalves, B.G. Almeida, C.J. Tavares, S. Carvalho, F. Vaz, et al., XRD and FTIR analysis of Ti–Si–C–ON coatings for biomedical applications, Surf. Coatings Technol. 203 (2008) 490–494. doi:10.1016/j.surfcoat.2008.06.121.

[2] J.C. Sánchez-López, M.D. Abad, I. Carvalho, R. Escobar Galindo, N. Benito, S. Ribeiro, et al., Influence of silver content on the tribomechanical behavior on Ag-TiCN bioactive coatings, Surf. Coat. Technol. 206 (2012) 2192–2198. doi:10.1016/j.surfcoat.2011.09.059.

[3] R. Branemark, P.-I. Branemark, B. Rydevik, R.R. Myers, Osseointegration in skeletal reconstruction and rehabilitation, J. Rehabil. Res. Dev. 38 (2001) 1–8.

[4] S.P.S.P. Mohanty, E. Kougianos, Biosensors: a tutorial review, Potentials, IEEE. 25 (2006) 35–40.

[5] V. Correia, V. Sencadas, M.S. Martins, C. Ribeiro, P. Alpuim, J.G. Rocha, et al., Piezoresistive sensors for force mapping of hip-prostheses, Sensors Actuators A Phys. 195 (2013) 133–138. doi:10.1016/j.sna.2013.03.013.

[6] P. Alpuim, V. Correia, E.S. Marins, J.G. Rocha, I.G. Trindade, S. Lanceros-Mendez, Piezoresistive silicon thin film sensor array for biomedical applications, Thin Solid Films. 519 (2011) 4574–4577. doi:10.1016/j.tsf.2011.01.300.

[7] V. Correia, C. Caparros, C. Casellas, L. Francesch, J.G. Rocha, S. Lanceros-Mendez, Development of inkjet printed strain sensors, Smart Mater. Struct. 22 (2013) 105028. doi:10.1088/0964-1726/22/10/105028.

[8] J. Nunes-Pereira, V. Sencadas, V. Correia, J.G. Rocha, S. Lanceros-Méndez, Energy harvesting performance of piezoelectric electrospun polymer fibers and polymer/ceramic composites, Sensors Actuators A Phys. 196 (2013) 55–62. doi:10.1016/j.sna.2013.03.023.

[9] J.G. Rocha, L.M. Gonçalves, P.F. Rocha, M.P. Silva, S. Lanceros-Mendez, Energy Harvesting From Piezoelectric Materials Fully Integrated in Footwear, Ind. Electron. IEEE Trans. 57 (2010) 813–819. doi:10.1109/TIE.2009.2028360.

[10] R. Gregorio Jr., R.C. Capitão, Morphology and phase transition of high melt temperature crystallized poly (vinylidene fluoride), J. Mater. Sci. 35 (2000) 299–306.

[11] P. Martins, A.C. Lopes, S. Lanceros-Mendez, Electroactive phases of poly(vinylidene fluoride): Determination, processing and applications, Prog. Polym. Sci. 39 (2014) 683–706. doi:10.1016/j.progpolymsci.2013.07.006.

[12] V.K. Tiwari, P.K. Kulriya, D.K. Avasthi, P. Maiti, Radiation-resistant behavior of poly(vinylidene fluoride)/layered silicate nanocomposites., ACS Appl. Mater. Interfaces. 1 (2009) 311–8. doi:10.1021/am800040q.

[13] C.J. Tavares, S.M. Marques, L. Rebouta, S. Lanceros-Mendez, V. Sencadas, C.M. Costa, et al., PVD-Grown photocatalytic TiO2 thin films on PVDF substrates for sensors and actuators applications, Thin Solid Films. 517 (2008) 1161–1166. doi:10.1016/j.tsf.2008.06.024.

[14] S.M. Marques, C.J. Tavares, S. Lanceros-Mendez, Z. Denchev, X-ray Scattering Experiments on Sputtered Titanium Dioxide Coatings onto PVDF Polymers for Self-Cleaning Applications, J. Appl. Polym. Sci. 119 (2011) 726–731. doi:10.1002/app.

[15] C. Lopes, C. Gonçalves, P. Pedrosa, F. Macedo, E. Alves, N.P. Barradas, et al., TiAgx thin films for lower limb prosthesis pressure sensors: Effect of composition and structural changes on the electrical and thermal response of the films, Appl. Surf. Sci. 285 (2013) 10–18. doi:10.1016/j.apsusc.2013.07.021.

[16] S.M. Marques, N.K. Manninen, S. Ferdov, S. Lanceros-Mendez, S. Carvalho, Ti1− xAgx electrodes deposited on polymer based sensors, Appl. Surf. Sci. 317 (2014) 490–495. doi:10.1016/j.apsusc.2014.08.142.

[17] R.X. Wang, X.M. Tao, Y. Wang, G.F. Wang, S.M. Shang, Microstructures and electrical conductance of silver nanocrystalline thin films on flexible polymer substrates, Surf. Coatings Technol. 204 (2010) 1206–1210. doi:10.1016/j.surfcoat.2009.10.030.

[18] R.C. Adochite, D. Munteanu, M. Torrell, L. Cunha, E. Alves, N.P. Barradas, et al., The influence of annealing treatments on the properties of Ag:TiO2 nanocomposite films prepared by magnetron sputtering, Appl. Surf. Sci. 258 (2012) 4028–4034. doi:10.1016/j.apsusc.2011.12.095.

[19] P. Pedrosa, E. Alves, N.P. Barradas, N. Martin, P. Fiedler, J. Haueisen, et al., Electrochemical behaviour of nanocomposite Agx:TiN thin films for dry biopotential electrodes, Electrochim. Acta. 125 (2014) 48–57. doi:10.1016/j.electacta.2014.01.082.

[20] P. Pedrosa, D. Machado, C. Lopes, E. Alves, N.P. Barradas, N. Martin, et al., Nanocomposite Ag:TiN thin films for dry biopotential electrodes, Appl. Surf. Sci. 285 (2013) 40–48. doi:10.1016/j.apsusc.2013.07.154.

[21] H. Cao, X. Liu, F. Meng, P.K. Chu, Biological actions of silver nanoparticles embedded in titanium controlled by micro-galvanic effects, Biomaterials. 32 (2011) 693–705. doi:10.1016/j.biomaterials.2010.09.066.

[22] P.J. Kelly, H. Li, K. a. Whitehead, J. Verran, R.D. Arnell, I. Iordanova, A study of the antimicrobial and tribological properties of TiN/Ag nanocomposite coatings, Surf. Coatings Technol. 204 (2009) 1137–1140. doi:10.1016/j.surfcoat.2009.05.012.

[23] C.F.A. Alves, F. Oliveira, I. Carvalho, a. P. Piedade, S. Carvalho, Influence of albumin on the tribological behavior of Ag–Ti (C, N) thin films for orthopedic implants, Mater. Sci. Eng. C. 34 (2014) 22–28. doi:10.1016/j.msec.2013.09.031.

[24] D.M. Eby, H.R. Luckarift, G.R. Johnson, Hybrid Antimicrobial Enzyme and Silver Nanoparticle Coatings for Medical Instruments, ACS Appl. Mater. Interfaces. 1 (2009) 1553–1560. doi:10.1021/am9002155.

[25] P.J. Kelly, H. Li, P.S. Benson, K.A. Whitehead, J. Verran, R.D. Arnell, et al., Comparison of the tribological and antimicrobial properties of CrN/Ag, ZrN/Ag, TiN/Ag, and TiN/Cu nanocomposite coatings, Surf. Coatings Technol. 205 (2010) 1606–1610. doi:10.1016/j.surfcoat.2010.07.029.

[26] I. Safi, Recent aspects concerning d.c. reactive magnetron sputtering of thin films: a review, Surf. Coatings Technol. 127 (2000) 203–218. doi:10.1016/S0257-8972(00)00566-1.

[27] D. Depla, S. Mahieu, R. De Gryse, Magnetron sputter deposition: Linking discharge voltage with target properties, Thin Solid Films. 517 (2009) 2825–2839. doi:10.1016/j.tsf.2008.11.108.

[28] S. Konstantinidis, RF amplified magnetron source for efficient titanium nitride deposition, Surf. Coatings Technol. 174-175 (2003) 100–106. doi:10.1016/S0257-8972(03)00528-0.

[29] N.K. Manninen, R.E. Galindo, N. Benito, N.M. Figueiredo, a Cavaleiro, C. Palacio, et al., Ag–Ti(C, N)-based coatings for biomedical applications: influence of silver content on the structural properties, J. Phys. D. Appl. Phys. 44 (2011) 375501. doi:10.1088/0022-3727/44/37/375501.

[30] A.G. Spencer, R.P. Howson, R.W. Lewin, Pressure stability in reactive magnetron sputtering, Thin Solid Films. 158 (1988) 141–149. doi:10.1016/0040-6090(88)90310-0.

[31] S.V. Meschel, O.J. Kleppa, Thermochemistry of some binary alloys of noble metals (Cu, Ag, Au) and transition metals by high temperature direct synthesis calorimetry, J. Alloys Compd. 350 (2003) 205–212. doi:10.1016/S0925-8388(02)00983-0.

[32] M. Li, C. Li, F. Wang, W. Zhang, Experimental study and thermodynamic assessment of the Ag–Ti system, Comput. Coupling Phase Thermochem. 29 (2005) 269–275. doi:10.1016/j.calphad.2005.09.002.

[33] K. Zeng, R. Schimid-Fetzer, Critical assessment and thermodynamic modeling of the Ti-N system, Zeitschrift Für Met. 87 (n.d.) 540–554.

[34] L. Tan, T.R. Allen, P. Demkowicz, High temperature interfacial reactions of TiC, ZrC, TiN, and ZrN with palladium, Solid State Ionics. 181 (2010) 1156–1163. doi:10.1016/j.ssi.2010.06.054.

[35] T. de los Arcos, P. Oelhafen, U. Aebi, a Hefti, M. Düggelin, D. Mathys, et al., Preparation and characterization of TiN–Ag nanocomposite films, Vacuum. 67 (2002) 463–470. doi:10.1016/S0042-207X(02)00232-4.

[36] R. Escobar Galindo, N.K. Manninen, C. Palacio, S. Carvalho, Advanced surface characterization of silver nanocluster segregation in Ag-TiCN bioactive coatings by RBS, GDOES, and ARXPS., Anal. Bioanal. Chem. 405 (2013) 6259–69. doi:10.1007/s00216-013-7058-z.

[37] V.S.K. Chakravadhanula, C. Kübel, T. Hrkac, V. Zaporojtchenko, T. Strunskus, F. Faupel, et al., Surface segregation in TiO2-based nanocomposite thin films. Nanotechnology. 23 (2012) 495701 (7 pp). doi:10.1088/0957-4484/23/49/495701.

[38] M.P. Silva, C.M. Costa, V. Sencadas, A.J. Paleo, S. Lanceros-Méndez, Degradation of the dielectric and piezoelectric response of β-poly(vinylidene fluoride) after temperature annealing, J. Polym. Res. 18 (2011) 1451–1457. doi:10.1007/s10965-010-9550-x.

[39] J. Gomes, J. Serrado Nunes, V. Sencadas, S. Lanceros-Mendez, Influence of the β-phase content and degree of crystallinity on the piezo- and ferroelectric properties of poly(vinylidene fluoride), Smart Mater. Struct. 19 (2010) 065010 (7pp). doi:10.1088/0964-1726/19/6/065010.

5. Strain analysis on $Ti_{1-x}Ag_x$ and Ag-TiN_x electrodes deposited on polymer based sensors

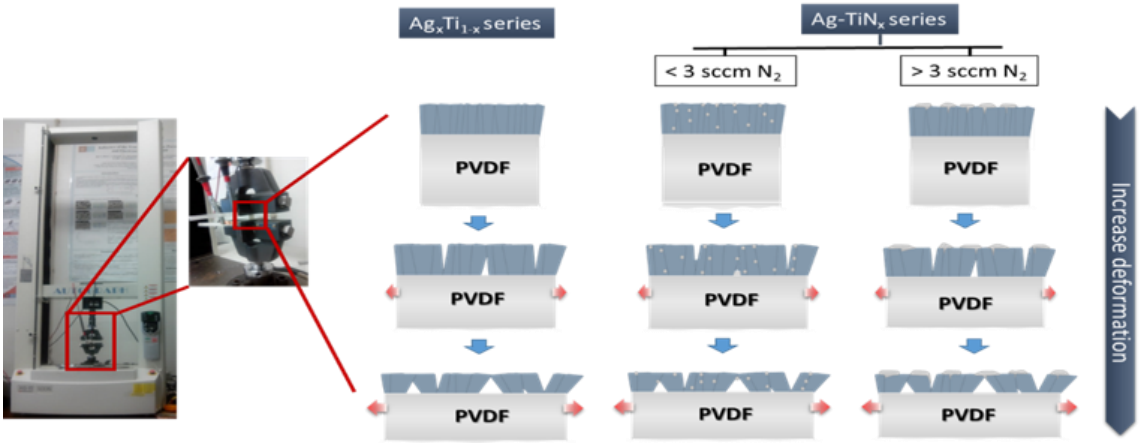

This chapter is based on the publication: S. M. Marques, P. Costa, S. Lanceros-Mendez, S. Carvalho. *Strain analysis on $Ti_{1-x}Agx$ and Ag-TiN_x electrodes deposited on polymer based sensors* re-submitted to Thin Solid Films, Oct 2015, Q2, Impact factor: 1.922

This chapter focuses on the mechanical properties of both $Ti_{1-x}Ag_x$ and Ag-TiN_x electrode's series characterized in chapters 3 and 4. The uniaxial stretching of piezoelectric polymer (PVDF) coated with different thin films, as well as the electrical resistance variation during mechanical stimulation were analyzed since the sensors will be subjected to mechanical and electrical solicitations. In addition physical contact with the human body can also cause degradation of the electrodes and therefore affect its functional performance.

The main conclusion is that all films showed piezoresitive properties, which increase with increasing applied strain and reaching gauge factors (GF) up to 700. All thin films deposited on β-PVDF exhibited a similar behavior with respect to the electro-mechanical properties, the GF increasing with increasing strain being higher in the plastic zone than in the elastic one.

Samples from Ag-TiN_x series showed higher GF values when compared with the samples from $Ti_{1-x}Ag_x$ series, which can be explained by the presence of Ag nanoparticles/clusters imbedded in the TiN matrix. Higher GF values are desired for more sensitive sensors.

Keywords: *Sensors, piezoelectric polymers, sputtering, gauge factor.*

5.1 Introduction

The future of prosthetic implants relies in the incorporation of prevention mechanisms based on the integration of sensor systems, which allow to obtain valuable information about a wide range of biomechanical signals [1,2]. In this scope, piezoresistive [3,4] and piezoelectric [5] materials allow the incorporation of strain and force sensors in numerous applications. Particularly interesting are piezoelectric materials as they do not need external power supply, being even able to provide energy to a circuit, upon mechanical solicitation, keeping the system operational for longer periods of time [6,7].

Due to its important piezoelectric and piezoresistive properties, poly(vinylidene fluoride) (PVDF) has been widely investigated [8] and it is being used for an extensive variety of applications as sensor and actuators. For the different polymorphs of PVDF, the β phase is the one with the largest piezoelectric response [9,10], being the one used as substrate material in this work.

That phase can be obtained in different ways [9], the uniaxial stretching of α-phase (non-electroactive) being the most common one [11,12]. Further, for improving the piezoelectric response, the material need be poled, i.e. the randomly organized dipolar moments must be aligned against an applied electric field [11,12].

Together with the particular nature and properties of the base polymer for sensor applications, PVDF in the present case, there is still the need for its surface functionalization in terms of electrical contacts. The present approach consists in using a magnetron sputtered conductive thin layer to detect the pressure or strain-induced electric charge, produced by a solicitation in the polymer [13]. Taking into account the main requirements of the targeted application, the selected films must show good electrical conductivity and since they will be used within the human body they must be biocompatible. Furthermore, the layered composite will be subjected to mechanical and electrical solicitations and physical contact with the human interfaces that can cause degradation of the coating, and therefore can affect its functional performance [13]. In this scope, the good electrical conductivity of Ag and Ti, $Ti_{1-x}Ag_x$ as well as Ag-TiN_x coatings represents a good candidate for conductive materials. In addition, Ti is biocompatible, TiN is an electrically conductive coating, with an excellent chemical stability in most media and suitable mechanical properties, leading to a wide scope of applications, including those in the biomedical area [14,15]. TiN is also biocompatible, but it is relatively hard and with high Young's Modulus [14–17].

Silver shows interesting intrinsic characteristics, such as low Young's Modulus, high electrical conductivity [18] and effective antibacterial performance [19–22], in particular in its nanocrystalline form [17,20]. It is also an excellent biosensor material [15]. Thus, the inclusion allows to improve the lifetime of biodevices and within the TiN films may offer the possibility to tailor the Young's Modulus of the electrode [23] since Ag increases the plasticity of TiN (a brittle material) [15].

Nevertheless, there are two major obstacles to the direct use of metal and ceramic thin film as conductive films for mechanical polymer based sensors.

First, the Young's Modulus of metal is several order of magnitude higher than that of polymers (50–100 GPa compared to 0.2–1 MPa) [24,25] and for ceramic materials, the Young´s Modulus tends to be higher than for metals (generally in the range of 100-800 GPa for dense polycrystalline ceramics) [26]; secondly, the limit of elasticity for metals is very low, typically 2–3 % and if a metal or ceramic is strained above this limit, it will crack and reduce the electrical conductivity of the sensor [24,25]. It has been reported that metallic TiO_2 thin films also deposited on PVDF substrates withstand large deformations up to 10% without evidencing, in optical microscopy, submicron cracking features [11]. TiAg electrodes with Ag content of about 8 at. % show a very poor resistance to stretching, with the electrical resistance increasing sharply after the application of deformation, with a limit of ε = 3% [25]. At 1 % strain, cracks start to appear perpendicular to the stretch direction, and the cracks turned out to be sufficiently wide to totally hinder the conducting path for strains of 3% [25]. Also, for ITO (indium tin oxide) thin films deposited onto β-PVDF the electrical resistance increases sharply for strains between 2 and 2.5%, due to the formation of cracks [27]. Regarding this results, the main goal of this work is to manipulate the silver contents in $Ti_{1-x}Ag_x$ system and the nitrogen content in the Ag-TiN_x system to achieve larger deformations with suitable electrical conductivity their use as electrodes as well as to evaluate the performance of the films as piezoresistive sensors by measuring the electrical resistance variation under mechanical solicitation.

Thus, $Ti_{1-x}Ag_x$ and Ag-TiN_x coatings, were deposited by magnetron sputtering in piezoelectric PVDF substrates and the mechanical and piezoresistive responses of these thin films correlated with the developed morphology.

5.2 Experimental details

5.2.1 $Ti_{1-x}Ag_x$ and Ag-TiN_x thin films

Ti_{1-x}Agx and Ag-TiN_x coatings were deposited by d.c./pulsed d.c. magnetron sputtering onto β-PVDF thin films with a thickness of approximately 28 μm (Precision Acoustics Ltd). One pure Ti target (99.99 %) and one Ag target (99.99%)) (both with 200x100 mm^2) were used in argon atmosphere for the $Ti_{1-x}Ag_x$ coatings and in Ar + N_2 mixtures for the Ag-TiN_x films and with the substrates rotating at 70 mm from the targets at a constant speed of 7 rpm.

The depositions were performed without any external heating of the substrate and no bias polarization was applied on the substrate holder. Further details concerning these depositions can be found elsewhere [28,29].

Chemical composition estimation was performed with an EDAX - Pegasus X4M – Energy dispersive spectrometer (EDS/EBSD) apparatus coupled with a Scanning Electron Microscope (SEM). The surface morphology and thickness of the deposited films were examined by SEM through a NanoSEM – FEI Nova 200 (FEG/SEM). Since the depth of analysis at 10 kV is about 300 nm for pure Ag and 700 nm for pure Ti, $Ti_{1-x}Ag_x$ and Ag-TiN_x coatings with a thickness of 1 μm were deposited onto Silicon (Si) substrates for EDS analysis [28,29]. The structure and phase distribution of the coatings were analyzed by powder X-ray diffraction (XRD) using a Bruker D8 Discover diffractometer (CuKα radiation – λ =1.5406 Å, step 0.04°, time per step 1s and 6-60 2θ interval).

5.2.2 Mechanical tests

Mechanical stress-strain measurements were performed using an universal testing machine Shimadzu model AG-IS with a load cell of 50 N. Measurements were performed, up to sample mechanical breaking, at room temperature in the tensile mode on rectangular samples with dimensions of approximately ≈20 mm × 10 mm × 28 μm at a test velocity of 0.2 mm/min.. In the elastic zone the Young's Modulus of the composite samples was calculated using Equation 2:

$$E = \frac{\sigma}{\varepsilon} = \frac{F/A_0}{\Delta L/L_0} \qquad \text{Equation 2}$$

Where E refers to the Young's Modulus, σ to the stress and ε to the strain. F is the force, A_0, the original cross-sectional area through which the force is applied, ΔL the amount by which the original length (L_0) of the sample changes.

5.2.3 Piezoresistive characterization

Mechanical measurements were performed considering the whole system: PVDF polymer coated with thin films.

The electrical resistance of the samples (approximate dimensions: rectangular samples with an area of 20 × 10 mm^2 and a thickness of 28 μm) was measured in the $Ti_{1-x}Ag_x$ and Ag-TiN_x electrodes with an Agilent 34401A multimeter synchronized with the mechanical deformation of the sample, applied in the tensile mode at a test velocity of 2 mm/min with an AG-IS universal testing machine from Shimadzu with a load cell of 50 N.

5.3 Results and discussion

The samples from the two different series show different chemical composition and therefore different mechanical and piezoresistive properties.

5.3.1 Chemical composition and phase composition

The $Ti_{1-x}Ag_x$ and Ag-TiN_x series deposition conditions together with the coating´s chemical composition, deposition rate and Young´s Modulus of the piezoresistive films deposited on in the β-PVDF polymer substrate are summarized in Table 5.1.

Table 5.1– Chemical composition, Young's Modulus of $Ti_{1-x}Ag_x$ and Ag-TiN_x coatings and some experimental details

Series	Coating (Sample reference)	N_2 flow (sccm)	Film thickness (nm)	Chemical Composition (at. %)			N/Ti ratio	Ag/Ti ratio	Young's Modulus (GPa)
				Ti	Ag	N			
	PVDF-β								1.8
$Ti_{1-x}Ag_x$ series	Ti	0	218.6	100	0	0	-	0	1.8
	Ag/Ti (0.11)	0	223.0	89.8	10.2	0	-	0.11	2.1
	Ag/Ti (0.69)	0	84.2	59.2	40.8	0	-	0.69	2.2
	Ag/Ti (3.71)	0	157.4	21.2	78.8	0	-	3.71	1.4
	Ag	0	164.7	0	100	0	-	-	2.1
Ag-TiN_x series	TiN1Ag	1	211.7	68	7	25	0.4	0.10	1.9
	TiN2Ag	2	227.5	57	6	37	0.7	0.11	1.7
	TiN3Ag	3	141.7	44	18	38	0.9	0.41	2.3
	TiN8Ag	8	75.8	42	18	40	1	0.43	1.8
	TiN15Ag	15	86.7	42	18	40	1	0.43	2.1

The $Ti_{1-x}Ag_x$ coatings were labeled according to the Ag/Ti atomic ratio, while the coatings of pure titanium and pure silver are labeled as Ti and Ag, respectively. The Ag-TiN_x series was labeled according to the N_2 flow applied e.g. TiN2Ag was deposited with a nitrogen flow of 2 sccm. For this series, the sample without nitrogen corresponds to the same deposition conditions of the sample Ag/Ti(0.11). The selection of these deposition conditions is related with results concerning its structural characteristics and sheet resistivity, as discussed in [28].

The XRD patterns of the coatings are depicted in figure 5.1.

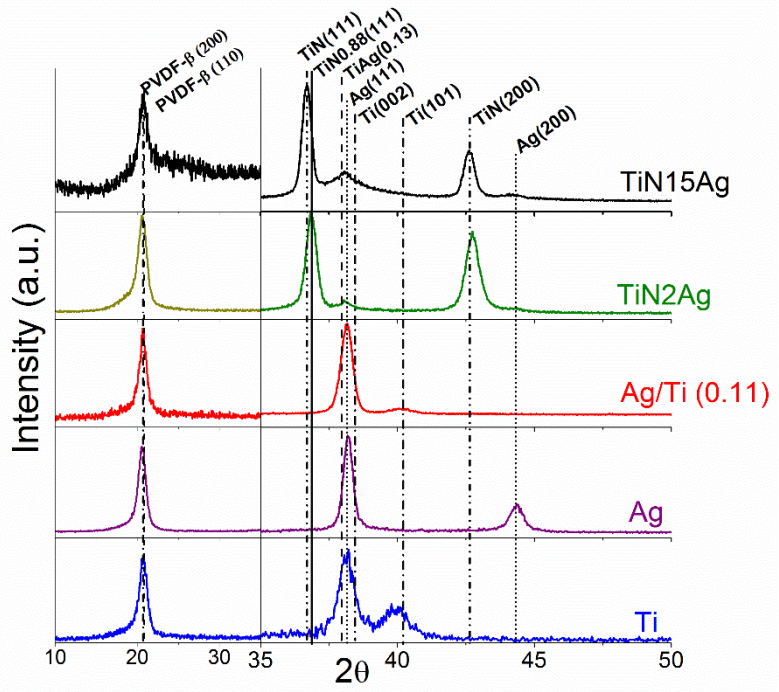

Figure 5.1 – XRD patterns of $Ti_{1-x}Ag_x$ and Ag-TiN_x coatings deposited onto PVDF substrates.

XRD peaks corresponding to the atomic planes (200) and (110) of β-PVDF indicate that the deposition conditions do not induce any phase change in the polymer. Pure Ti coating crystallizes in a hexagonal closed packed structure and in the Ag coating, it is possible to identify a crystalline fcc-Ag. The XRD patterns of Ag/Ti (0.11) indicate that the most intense peak is located at about 37.8°. Previous studies in TiAg coatings [28] suggest the formation of an TiAg phase in addition to the Ti (002) and Ag (111) phases, indicating that this coating is composed by a mixture of crystalline phases. TiN2Ag coating, present a sub-stoichiometric TiN phase and a second crystalline phase, which is attributed to an fcc-Ag phase. In the TiN15Ag sample, two crystalline fcc phases can be clearly identified: TiN and Ag phases.

The Young´s modulus for the different samples does not change significantly. These similarities are related with the difference between the thickness of the polymer and the coating. In fact, taking into account the value of the Young's modulus for β-PVDF, it seems that the mechanical response is mainly regulated by the polymer, since it is much thicker than the metallic or ceramic thin film. However, the nature of the thin film, more metallic or ceramic, will affect the conducting and piezoresistive behavior of the different samples which will be discussed later.

5.3.2 Morphology

SEM analysis of the two series was performed in order to evaluate the thin films morphology and the presence of Ag nanoclusters on the surface. The cross section and surface SEM micrographs of the coatings are depicted in Figure 5.2 for the $Ti_{1-x}Ag_x$ series and in Figure 5.3 for the Ag-TiN_x series.

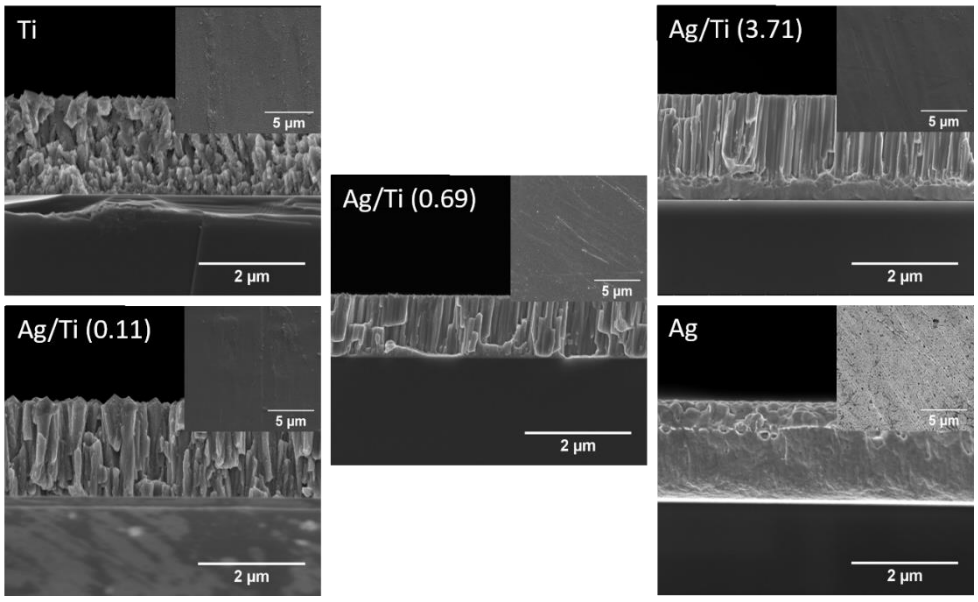

Figure 5.2 – Cross-section SEM micrographs on SE mode of different $Ti_{1-x}Ag_x$ thin films. The insets are micrographs in SE mode of the surface of the different coatings.

A cross-section SEM images of the coatings in both series exhibit a columnar structure for the different films. Silver nanoparticles are only observed for the Ag-TiN_x series. In the samples TiN8Ag and TiN15Ag, it is no longer possible to observe silver bulk as in TiN1Ag, TiN2Ag and TiN3Ag, being just visible at the surface of the coating.

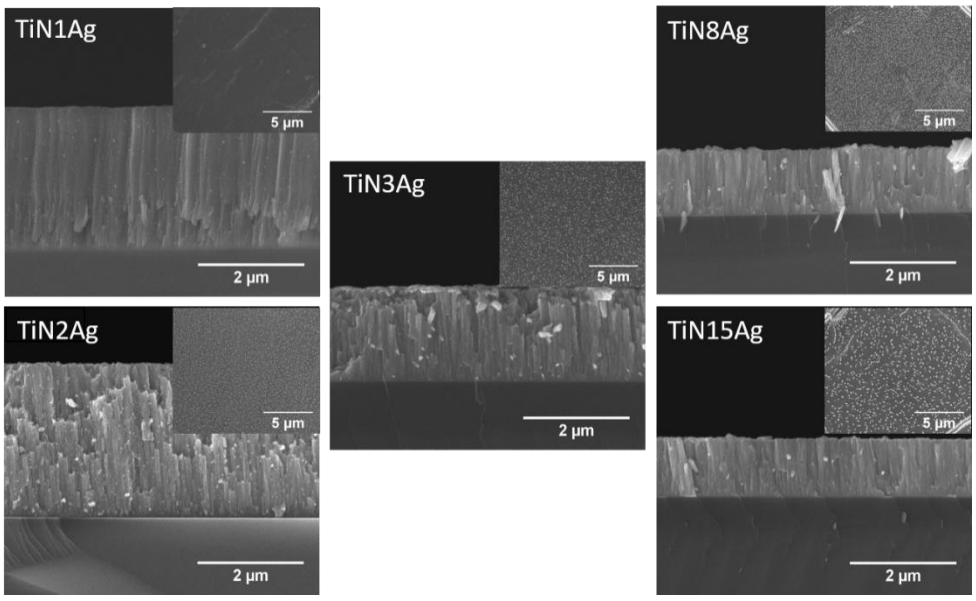

Figure 5.3 - Cross-section SEM micrographs on SE mode of different Ag-TiN_x thin films. The inceptions are micrographs in SE mode of the surface of the different coatings.

5.3.3 Mechanical behavior of $Ti_{1-x}Ag_x$ and Ag-TiN_x coated samples under uniaxial stretching

The mechanical properties of different samples (β-PVDF as substrate and thin films deposited on PVDF for both series) were evaluated by stress-strain uniaxial stress experiments up to 10% of strain (Figure 5.4). The electrode films influence the mechanical behavior of the samples, mainly after yielding.

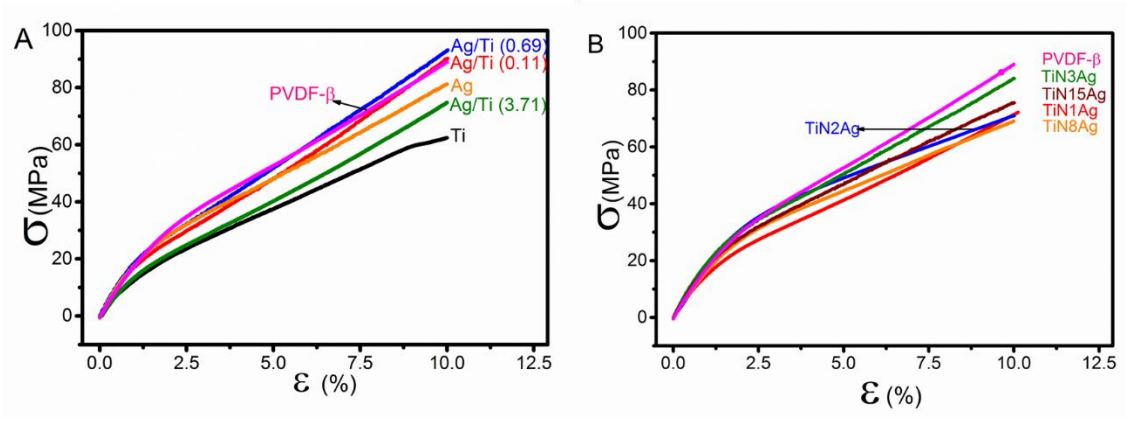

Figure 5.4 – Mechanical stress-strain curves of both series of samples up to 10% of strain: A) for the $Ti_{1-x}Ag_x$ series and B) for the Ag-TiN_x series.

The mechanical properties of both series, $Ti_{1-x}Ag_x$ and Ag-TiN_x, show similar behavior for all films deposited on β-PVDF substrates.

The linear mechanical region is lower than 1% of strain for all samples, showing a slight decrease with increasing Ti on the $Ti_{1-x}Ag_x$ samples. Comparing the two series, $Ti_{1-x}Ag_x$ and Ag-TiN_x, the mechanical properties of the composite samples are mainly determined by the β-PVDF substrates, as observed in in Figure 5.4.

5.3.4 Piezoresistive properties

The piezoresistive properties are analyzed in both sample series up to 5% deformation (Figure 5.5).

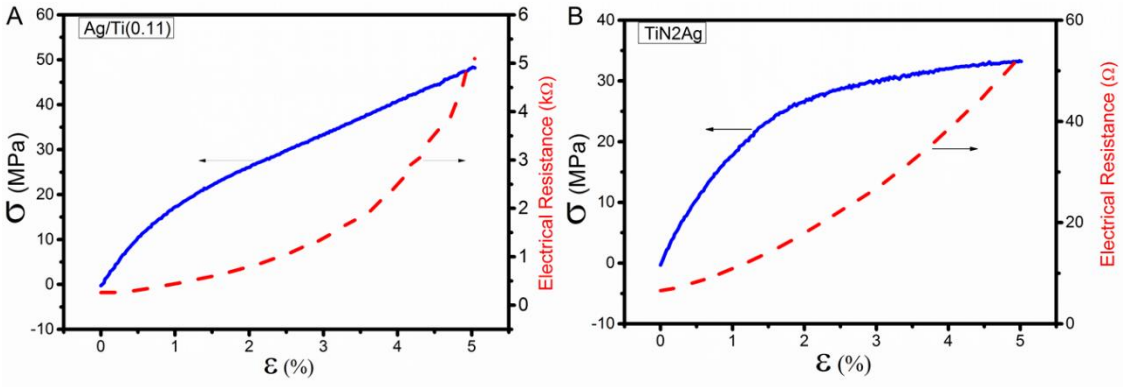

Figure 5.5 – Representative mechanical and electrical properties for both series up to 5% of strain: Ag/Ti(0.11) (A) and or TiN2Ag (B). The electrical resistance variation is measured during mechanical deformation.

The electrical resistance of the films in each sample was measured during mechanical strain up to 5% for all samples and its variation follows the mechanical deformation, as can be seen, in an example for each series, in Figure 5.5. Comparing to the results from the literature for related films [25,27,30], a better piezoresistive behavior is obtained, as $Ti_{1-x}Ag_x$ and Ag-TiN_x samples still present a thin film conducting path for strains up to 5%, instead the maximum 2 or 3% strain previously reported for TiO_2 thin films as a base layer for flexible electronics [30], indium tin oxide (ITO) thin films for transparent electrodes for optoelectronic and electro-optic devices [27] and Ti-Ag electrodes for large deformation sensors applications [25].

The $Ti_{1-x}Ag_x$ and Ag-TiN_x films show an increase of the electrical resistance with increasing mechanical strain applied to the composites, as presented for Ti/Ag (0.11) and TiN2Ag samples (Figure 5.5). The correlation of the electrical and mechanical properties of the samples shows their piezoresistive behavior.

The piezoresistivity can be quantified by the Gauge Factor (GF) (Equation 1):

$$GF = (\Delta R/R)/\varepsilon = (d\rho/\rho)/\varepsilon + 1 + 2\vartheta \qquad \textit{Equation 1}$$

where ε is the strain, ρ the electrical resistivity, R is the steady-state material electrical resistance before deformation, ΔR, the variation of the electrical resistance with strain and ν is the Poisson ratio.

This equation included the intrinsic piezoresistive effect ($(d\rho/\rho)/\varepsilon$) and the geometrical effect contributions ($1+2\vartheta$) [31]. The geometrical effect is lower than 2 ($0<\vartheta<0.5$), and piezoresistive values above the geometrical factor are due to intrinsic piezoresistive effect. The commercial strain gages show GF≈2 and low deformations [32].

The piezoresistive response of the samples can be analyzed for the three different zones of the thermoplastic characteristic mechanical response of the polymer substrate: elastic, yielding and plastic zones. These piezoresistive behavior, presented in Figure 5.6 as a representative example for the TiN2Ag sample, shows that the gauge factor values increase with increasing mechanical strain.

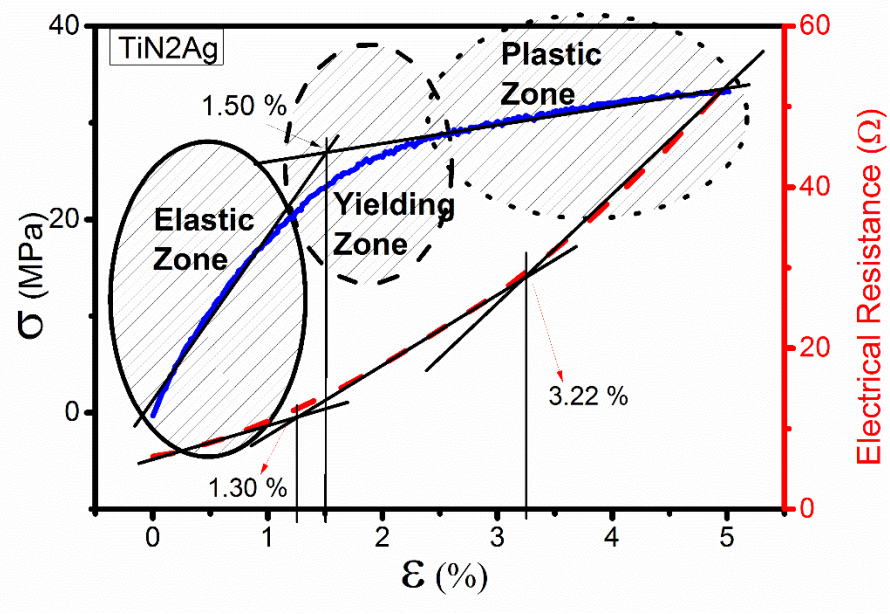

Figure 5.6 – Effect of the mechanical deformation of the composites on the electrical properties of the deposited films.

The electrical resistance depends on the mechanical solicitation to the composite films. The electrical resistance variation with the strain applied to the different samples is presented in Figure 5.7 and Table 5.2 summarizes the piezoresistive properties for all samples as a function of the mechanical behavior.

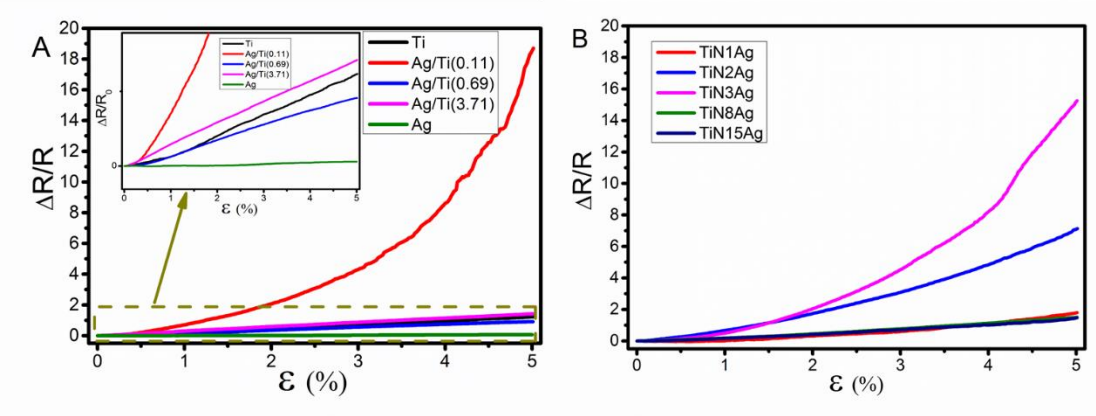

Figure 5.7 – Electrical resistance variation with mechanical strain for: A) $Ti_{1-x}Ag_x$ and B) Ag-TiN_x sample series.

Figure 5.7 shows that the piezoresistive response increases with applied strain for samples. Ag/Ti (0.11) and TiN3Ag are the samples with the larger GF for each series. In Table 5.2 are identified the different mechanical regions (elastic, yielding and plastic zones) and the corresponding average GF for each sample in the different zones of the stress-strain curves. The electrical behavior of Ag/Ti (0.69), Ag/Ti (3.71) and TiN8Ag do not show three different zones as the mechanical properties of the samples.

Table 5.2 – Piezoresistive properties for samples as a function of the mechanical behavior of the PVDF composites.

Series	Coating (Sample reference)	Mechanical zones (%) vs Gauge Factor	Yielding Point (%)	$R_{initial}$ / R_{final} (Ω)
$Ti_{1-x}Ag_x$ series	Ti	0 → 1.04 → 3 → 5 vs 13.5→ 29.3 → 27.4	2.24	88.4/197.4
	Ag/Ti (0.11)	0 → 1.5 → 3 → 5 vs 92.9 → 202.6 → 670	0.97	259.0 / 5113.1
	Ag/Ti (0.69)	0 → 0.54 → 5 vs 6.6 → 20.1	1.04	108.5/207.5
	Ag/Ti (3.71)	0 → 5 vs 28.5	1.64	17.5/42.5
	Ag	0 → 0.65 → 2.41 → 5 vs 0.7 → 0.5 → 1.9	1.28	0.84/0.89
Ag-TiN_x series	TiN1Ag	0 → 0.73 → 2.53 → 5 vs 62.1 → 242 → 515.8	2.24	6.4/116.1
	TiN2Ag	0 →1.3 → 3.2 → 5 vs 74.6 → 130.5 → 202.9	1.5	6.6 / 53.4
	TiN3Ag	0 → 1.50 → 3.88 → 5 vs 74.6 → 272.2 → 709.0	1.12	8.0/130.3
	TiN8Ag	0 → 1.30 → 5 vs 19.3 → 34.1	1.08	6.0/14.9
	TiN15Ag	0 → 0.68 → 3.12 → 5 vs 14.3 → 27.3 → 34.3	1.44	40.8/101.0

Table 5.2 and Figure 5.8 show that the piezoresistive properties of the $Ti_{1-x}Ag_x$ series is distinct for samples with only Ti or Ag.

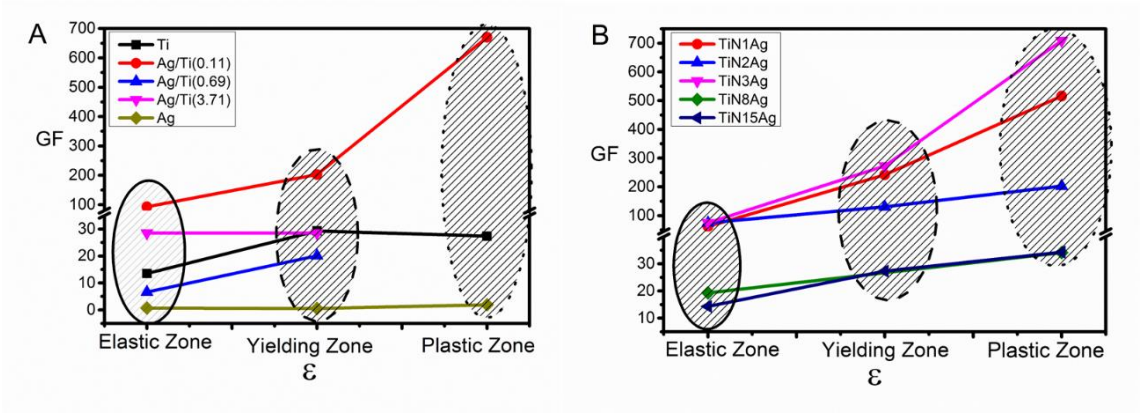

Figure 5.8 – Piezoresistive sensibility for both series as a function of the mechanical zone - elastic, yielding and plastic- for both series of samples. Gauge factor for A) $Ti_{1-x}Ag_x$ and B) Ag-TiN_x samples.

Thin films with Ag show one extrinsic behavior until 5% of strain, with a GF of 0.5 and 1.9. On the other hand, Ti films show intrinsic piezoresistive effect with GF increasing from 13 up to near 30 with increasing mechanical strain in the sample. The sheet resistivity for the $Ti_{1-x}Ag_x$ series presents a typical behavior of a binary alloy (Table 5.2). They present the lower value of resistivity and GF for the Ag and the Ti samples. When there is a mixture of silver and titanium, the sheet resistivity increases, as discussed in previous published results [28]. This sample also shows the largest piezoresistive response, with GF from near 100 to 600 with applied strain. So, the Ag/Ti ratio of 0.11 presents an interesting piezoresistive behavior for strain sensor applications. Thus, the mixture of phases observed by XRD demonstrate that Ag atoms could assume the part of solute impurities in the Ti solvent structure, leading to an increase of the electrical resistivity and the electrical resistivity variation under applied strains, i.e. of the GF, relatively to the Ti and Ag thin films.

The Ag-TiN_x sample series show, in general, larger GF values for samples with lower nitrogen flow until 3 sccm. The GF varies between 14 and 700, increasing with increasing strain. These samples show larger GF values up to larger strains (5%). Increasing nitrogen flow the GF values decrease between 10 and 30. The lower electromechanical sensibility in of the Ag-TiN_x series for higher nitrogen flow is identified with the immiscibility of Ag and TiN particles and the placement of Ag particles on the surface of the coating, as indicated by the SEM images (Figure 5.3). P. Pedrosa et al. [14] also reported the development of Ag clusters/aggregates that widely and consistently cover the thin film surface, results agreeing with the work of T. de los Arcos et al. [33]. The same behavior is observed in the TiN8Ag and TiN15Ag samples.

The piezoresistive response strongly changes from a ceramic to a metallic behavior, by the existence of Ag clusters on the surface of the coatings.

For samples with low nitrogen flow (< 3 sccm), the piezoresistive response can be ascribed to the ceramic characteristic of a TiN-like coatings with low Ag content, prompting to a non-uniform, rough and porous surface which reduce the conductivity of the films [14].

The piezoresistive properties up to larger strain presented for both series can be explained by the electrically conductive path maintained by the columnar structure of the films deposited on the PVDF substrate (Figure 5.9).

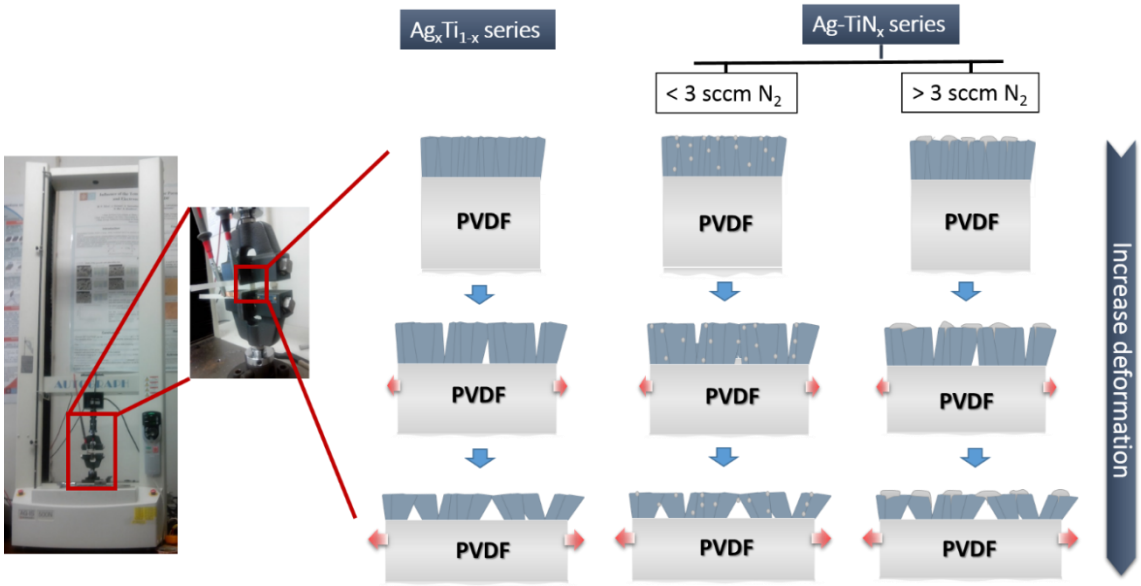

Figure 5.9 – Schematic representation of the thin films morphological variations during mechanical deformation leading to the observed electrical response.

Figure 9 shows a schematic representation of the proposed mechanism explaining the obtained results. The coatings deposited on the PVDF polymer films are very thin when compared with the polymer thickness (28 μm). So, the mechanical response is mainly determined by the polymer response. As shown in figure 5.7 and Table 5.2, the electrical resistance does not increase significantly even for deformation up to 5%, indicating that the percolation paths within the coating do not completely break while keeping the contact between columns in certain areas, allowing the electrical conductivity, though with increased resistivity, as it can be confirmed by Figure 5.10. Before stress-strain uniaxial stress experiment, samples presented a more defined columnar structure and less dense induced by the strain applied during stress experiment.

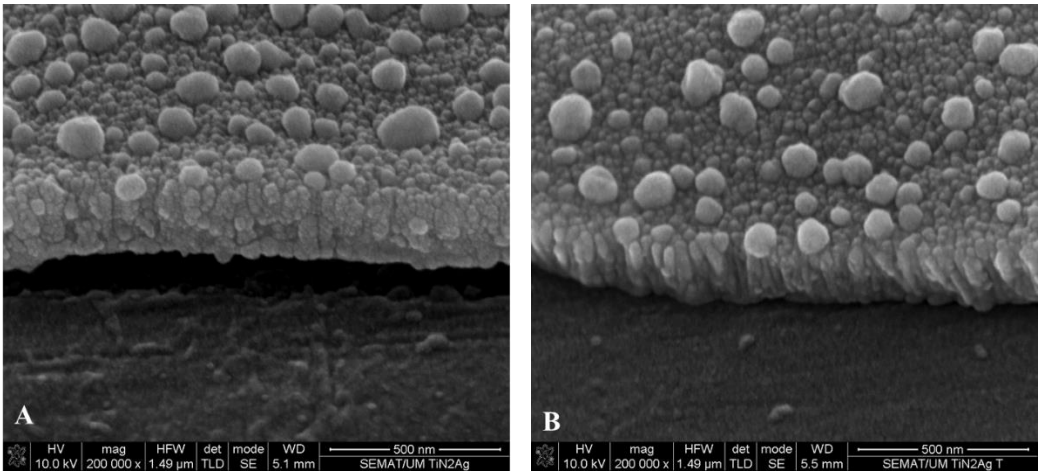

Figure 5.10 - SEM micrographs on SE mode of TiN2Ag sample before (A) and after (B) stress-strain uniaxial stress experiment.

5.4 Conclusions

$Ti_{1-x}Ag_x$ and Ag-TiN_x thin films prepared with different Ag/Ti ratios and nitrogen flow can be used as piezoresistive films deposited on polymers, with piezoresistive response up to 5% of strain. SEM images shows a columnar growth in all samples and the nitrogen influences the morphology of Ag-TiN_x films, with the nitrogen flow leading to Ag particles segregation. These characteristic decreases the piezoresistive response of the samples. On the other hand, mechanical properties such as maximum strain, are similar for all composite samples and mainly determined by the polymer substrate. The samples show suitable piezoresistive properties up to 5% of strain.

The piezoresistive behavior of metallic thin films deposited on β-PVDF polymer shows gauge factor values ranging from pure geometrical response up to 700 for the plastic mechanical zone of the samples. In general, the GF increases with increasing strain in the samples, being larger in the plastic zone than in the elastic one. The samples of the Ag-TiN_x series show highest GF values.

5.5 References

[1] R. Branemark, P.-I. Branemark, B. Rydevik, R.R. Myers, Osseointegration in skeletal reconstruction and rehabilitation, J. Rehabil. Res. Dev. 38 (2001) 1–8.

[2] S.P.S.P. Mohanty, E. Kougianos, Biosensors: a tutorial review, Potentials, IEEE. 25 (2006) 35–40.

[3] V. Correia, V. Sencadas, M.S. Martins, C. Ribeiro, P. Alpuim, J.G. Rocha, et al., Piezoresistive sensors for force mapping of hip-prostheses, Sensors Actuators A Phys. 195 (2013) 133–138. doi:10.1016/j.sna.2013.03.013.

[4] P. Alpuim, V. Correia, E.S. Marins, J.G. Rocha, I.G. Trindade, S. Lanceros-Mendez, Piezoresistive silicon thin film sensor array for biomedical applications, Thin Solid Films. 519 (2011) 4574–4577. doi:10.1016/j.tsf.2011.01.300.

[5] V. Correia, C. Caparros, C. Casellas, L. Francesch, J.G. Rocha, S. Lanceros-Mendez, Development of inkjet printed strain sensors, Smart Mater. Struct. 22 (2013) 105028. doi:10.1088/0964-1726/22/10/105028.

[6] J. Nunes-Pereira, V. Sencadas, V. Correia, J.G. Rocha, S. Lanceros-Méndez, Energy harvesting performance of piezoelectric electrospun polymer fibers and polymer/ceramic composites, Sensors Actuators A Phys. 196 (2013) 55–62. doi:10.1016/j.sna.2013.03.023.

[7] J.G. Rocha, L.M. Gonçalves, P.F. Rocha, M.P. Silva, S. Lanceros-Mendez, Energy Harvesting From Piezoelectric Materials Fully Integrated in Footwear, Ind. Electron. IEEE Trans. 57 (2010) 813–819. doi:10.1109/TIE.2009.2028360.

[8] R. Gregorio Jr., R.C. Capitão, Morphology and phase transition of high melt temperature crystallized poly (vinylidene fluoride), J. Mater. Sci. 35 (2000) 299–306.

[9] P. Martins, A.C. Lopes, S. Lanceros-Mendez, Electroactive phases of poly(vinylidene fluoride): Determination, processing and applications, Prog. Polym. Sci. 39 (2014) 683–706. doi:10.1016/j.progpolymsci.2013.07.006.

[10] V.K. Tiwari, P.K. Kulriya, D.K. Avasthi, P. Maiti, Radiation-resistant behavior of poly(vinylidene fluoride)/layered silicate nanocomposites., ACS Appl. Mater. Interfaces. 1 (2009) 311–8. doi:10.1021/am800040q.

[11] C.J. Tavares, S.M. Marques, L. Rebouta, S. Lanceros-Mendez, V. Sencadas, C.M. Costa, et al., PVD-Grown photocatalytic TiO2 thin films on PVDF substrates for sensors and actuators applications, Thin Solid Films. 517 (2008) 1161–1166. doi:10.1016/j.tsf.2008.06.024.

[12] S.M. Marques, C.J. Tavares, S. Lanceros-Mendez, Z. Denchev, X-ray Scattering Experiments on Sputtered Titanium Dioxide Coatings onto PVDF Polymers for Self-Cleaning Applications, J. Appl. Polym. Sci. 119 (2011) 726–731. doi:10.1002/app.

[13] C. Lopes, C. Gonçalves, P. Pedrosa, F. Macedo, E. Alves, N.P. Barradas, et al., TiAgx thin films for lower limb prosthesis pressure sensors: Effect of composition and structural changes on the electrical and thermal response of the films, Appl. Surf. Sci. 285 (2013) 10–18. doi:10.1016/j.apsusc.2013.07.021.

[14] P. Pedrosa, D. Machado, C. Lopes, E. Alves, N.P. Barradas, N. Martin, et al., Nanocomposite Ag:TiN thin films for dry biopotential electrodes, Appl. Surf. Sci. 285 (2013) 40–48. doi:10.1016/j.apsusc.2013.07.154.

[15] P. Pedrosa, E. Alves, N.P. Barradas, N. Martin, P. Fiedler, J. Haueisen, et al., Electrochemical behaviour of nanocomposite Agx:TiN thin films for dry biopotential electrodes, Electrochim. Acta. 125 (2014) 48–57. doi:10.1016/j.electacta.2014.01.082.

[16] S. Piscanec, L. Ciacchi, E. Vesselli, G. Comelli, O. Sbaizero, S. Meriani, et al., Bioactivity of TiN-coated titanium implants, Acta Mater. 52 (2004) 1237–1245. doi:10.1016/j.actamat.2003.11.020.

[17] P.J. Kelly, H. Li, P.S. Benson, K.A. Whitehead, J. Verran, R.D. Arnell, et al., Comparison of the tribological and antimicrobial properties of CrN/Ag, ZrN/Ag, TiN/Ag, and TiN/Cu nanocomposite coatings, Surf. Coatings Technol. 205 (2010) 1606–1610. doi:10.1016/j.surfcoat.2010.07.029.

[18] R.X. Wang, X.M. Tao, Y. Wang, G.F. Wang, S.M. Shang, Microstructures and electrical conductance of silver nanocrystalline thin films on flexible polymer substrates, Surf. Coatings Technol. 204 (2010) 1206–1210. doi:10.1016/j.surfcoat.2009.10.030.

[19] H. Cao, X. Liu, F. Meng, P.K. Chu, Biological actions of silver nanoparticles embedded in titanium controlled by micro-galvanic effects, Biomaterials. 32 (2011) 693–705. doi:10.1016/j.biomaterials.2010.09.066.

[20] P.J. Kelly, H. Li, K. a. Whitehead, J. Verran, R.D. Arnell, I. Iordanova, A study of the antimicrobial and tribological properties of TiN/Ag nanocomposite coatings, Surf. Coatings Technol. 204 (2009) 1137–1140. doi:10.1016/j.surfcoat.2009.05.012.

[21] C.F.A. Alves, F. Oliveira, I. Carvalho, a. P. Piedade, S. Carvalho, Influence of albumin on the tribological behavior of Ag–Ti (C, N) thin films for orthopedic implants, Mater. Sci. Eng. C. 34 (2014) 22–28. doi:10.1016/j.msec.2013.09.031.

[22] D.M. Eby, H.R. Luckarift, G.R. Johnson, Hybrid Antimicrobial Enzyme and Silver Nanoparticle Coatings for Medical Instruments, ACS Appl. Mater. Interfaces. 1 (2009) 1553–1560. doi:10.1021/am9002155.

[23] R.C. Adochite, D. Munteanu, M. Torrell, L. Cunha, E. Alves, N.P. Barradas, et al., The influence of annealing treatments on the properties of Ag:TiO2 nanocomposite films prepared by magnetron sputtering, Appl. Surf. Sci. 258 (2012) 4028–4034. doi:10.1016/j.apsusc.2011.12.095.

[24] S. Rosset, H.R. Shea, Flexible and stretchable electrodes for dielectric elastomer actuators, Appl. Phys. A Mater. Sci. Process. 110 (2013) 281–307. doi:10.1007/s00339-012-7402-8.

[25] A. Ferreira, C. Lopes, N. Martin, S. Lanceros-Méndez, F. Vaz, Nanostructured functional Ti-Ag electrodes for large deformation sensor applications, Sensors Actuators A Phys. (2014). doi:10.1016/j.sna.2014.09.031.

[26] D.J. Green, An Introduction to the Mechanical Properties of Ceramics, Cambridge University Press, 1998.

[27] L. Rebouta, L. Rubio-Peña, C. Oliveira, S. Lanceros-Mendez, C.J. Tavares, E. Alves, Strain dependence electrical resistance and cohesive strength of ITO thin films deposited on electroactive polymer, Thin Solid Films. 518 (2010) 4525–4528. doi:10.1016/j.tsf.2009.12.022.

[28] S.M. Marques, N.K. Manninen, S. Ferdov, S. Lanceros-Mendez, S. Carvalho, Ti1−xAgx electrodes deposited on polymer based sensors, Appl. Surf. Sci. 317 (2014) 490–495. doi:10.1016/j.apsusc.2014.08.142.

[29] S.M. Marques, N.K. Manninen, S. Lanceros-Mendez, S. Carvalho, Ag-TiNx electrodes deposited on piezoelectric poly(vinylidene fluoride) for biomedical sensor applications, Sensors Actuators A Phys. 234 (2015) 1–8. doi:10.1016/j.sna.2015.08.016.

[30] C.J. Tavares, S.M. Marques, S. Lanceros-Méndez, V. Sencadas, V. Teixeira, J.O. Carneiro, et al., Strain analysis of photocatalytic TiO2 thin films on polymer substrates, Thin Solid Films. 516 (2008) 1434–1438. doi:10.1016/j.tsf.2007.03.134.

[31] P. Costa, C. Silvia, J.C. Viana, S. Lanceros Mendez, Extruded thermoplastic elastomers styrene–butadiene–styrene/carbon nanotubes composites for strain sensor applications, Compos. Part B Eng. 57 (2014) 242–249. doi:10.1016/j.compositesb.2013.10.006.

[32] M. Cremona, L.. Gazola, L.. Scavarda do Carmo, J.T.. Castro, C.. Achete, In situ hard coatings strain measurement using a commercial strain-gage device, Thin Solid Films. 377-378 (2000) 436–440. doi:10.1016/S0040-6090(00)01271-2.

[33] T. de los Arcos, P. Oelhafen, U. Aebi, a Hefti, M. Düggelin, D. Mathys, et al., Preparation and characterization of TiN–Ag nanocomposite films, Vacuum. 67 (2002) 463–470. doi:10.1016/S0042-207X(02)00232-4.

6. PVD-grown antibacterial Ag-TiN thin films on piezoelectric PVDF substrates for sensors applications

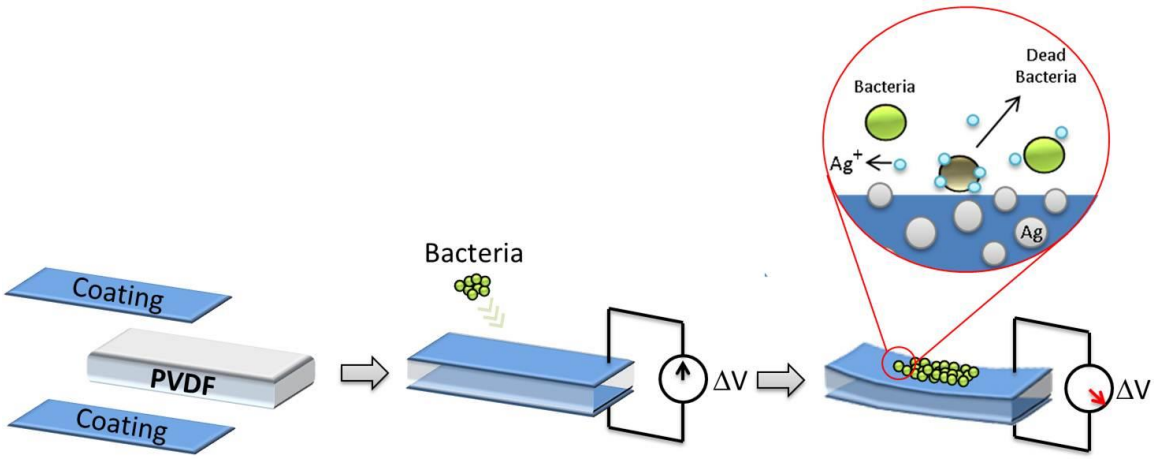

This chapter is based on the publication: S.M. Marques, I. Carvalho, M. Henriques, T. Polcar, S. Carvalho, PVD-grown antibacterial Ag-TiN films on piezoelectric PVDF substrates for sensor applications, Surf. Coatings Technol. 281 (2015) 117–124, doi:10.1016/j.surfcoat.2015.09.057, Q1, Impact factor: 1.998

This chapter is focused in the evaluations of the antibacterial activity of the developed electrodes, assessed by agar diffusion method.

For $Ti_{1-x}Ag_x$ series, Ti, Ag and Ag/Ti(0.11) samples (in this chapter denominated as Ag/Ti(0.11)R because is a replication of the previous sample) were selected. This specific sample was selected since it showed the highest piezoresistive response and a specific phase composition: TiAg and Ti, (and maybe Ag). Ti sample was used as negative control.

From Ag-TiN_x series, it was selected the TiN2Ag sample (here called TiN2AgR). This sample, not only exhibited an Ag amount close to the Ag/Ti(0.11)R sample, but also presented a very different structure (compared with Ag/Ti(0.11)R sample). It showed a remarkable mechanical performance with similarly high GF. In fact if the piezoresistive behavior, is taken in account, the sample that should be selected, would be TiN3Ag, however this sample has 18 at.% as silver content. This sample was discarded, due to the team previous studies which found that those high values could promote cytotoxicity problems.

Two additional samples were deposited in order to be used as controls for Ag-TiN_x series sample: TiN, as negative control, and a stoichiometric TiN sample with 10 at.% of silver – sample TiN6Ag(new), as positive control. The TiN6Ag(new) sample was deposited in order to achieve a stoichiometric sample with clear silver segregation (without free Ti) as the samples with high nitrogen content but without high silver content.

The main conclusion of this chapter is that only the samples from Ag-TiN_x series presented antibacterial activity. XPS results showed that the as-deposited samples from the Ag-TiN_x series exhibited silver clusters smaller than 4 nm. In order to deepen the results obtained, samples were analyzed after the Halo test (antibacterial test). XPS analyses showed the disappearance of these Ag nanoparticles clusters in agreement with the SEM results, which displayed a visible aggregation and a significant decrease in the number of Ag nanoparticles. This suggest that silver nanoparticles aggregated and diffused through the agar killing bacteria or inhibiting their grown in the vicinity. All results show that Ag-TiN_x electrodes are more promising candidates to be used in PVDF sensor protection than $Ti_{1-x}Ag_x$ electrodes.

Keywords: *Piezoelectric PVDF; Ag coatings; Sputtering; Sensors protection; Antibacterial activity.*

6.1 Introduction

The use of biomaterials is becoming increasingly common, in most cases as total or partial replacement of organs and tissues. Although there are some biomaterials presenting suitable mechanical properties and low cytotoxicity, they are often prone to microbial colonization [1,2]. This colonization is frequently associated to *Staphylococcus epidermidis*, being one of the most common bacteria found in orthopedics prostheses [3,4]. In addition, infections caused by this microorganism are often associated to implant failure [5]. Hence, this strengthens the urgent need for the development of new coatings with improved antimicrobial properties.

On the other hand, the future of prosthetic implants lays in the implementation of prevention mechanisms based on sensor systems, which allow to obtain valuable information about a wide range of biomechanical signals [6,7].

Piezoelectric materials are interesting for the development of such sensors because this material transforms mechanical loads into electrical signals, however, conductive electrodes are necessary for signal acquisition. Such electrodes must show good electrical conductivity and, since they are used in the human body, they must be biocompatible. Suitable electrodes may be produced with Ti-based coatings with multifunctional properties, such as electrical conductivity and antibacterial characteristics. Titanium and its alloys have been widely used as materials for artificial implants due to their biocompatibility and good corrosion resistance [8], and Ti shows electrical conductivity around 43 μΩ.cm [9]. TiN is an electrically conductive coating, with excellent chemical stability and outstanding mechanical properties, leading to a broad range of applications, including those in the biomedical area [10,11]. TiN is also biocompatible, but it is relatively hard [10–13]. The silver addition (good antimicrobial agent) to the TiN films may lead to a softer electrode, since silver presents a low Young's Modulus [21] increasing the plasticity of TiN [11]. So, these surfaces open a wide range of possible applications, especially those related to coatings on polymers to develop flexible devices [10]. As referred above, silver is also known as an antibacterial agent [14–17], in particular in its nanocrystalline form [13,15], and an excellent material for biosensor applications [11].

Akhavan et al.[18,19] reported two studies about the antibacterial effect of silver, one in which an electric field was applied in the direction of silver nanorods grown on a Ti interlayer deposited by d.c. magnetron sputtering, and another which reported compact Ag nanorods capped by sol-gel mesoporous TiO_2 layer, both deposited onto silicon substrates. The two studies showed a strong, fast and lasting antibacterial activity against *Escherichia coli* (*E. coli*).

Different coatings produced by magnetron sputtering have been considered as potential candidates for functional conductive electrodes for polymeric sensors. Regarding biomedical applications, Ag-TiN_x [10,11,20] and $Ti_{1-x}Ag_x$ [9,21] coatings have been proposed for prosthesis pressure sensors and dry biopotential electrodes, respectively, due to their specific electrical and biological properties. However, in those studies the coatings were deposited on silicon and glass substrates. In fact, the high temperatures associated with the sputtering process represent the major limitation in the development of functional electrode coatings on piezoelectric PVDF substrates, due to the inevitable structural changes promoted by temperature as well as eventual depolarization of the sample, which leads to the loss of the piezoelectric response. Two recent studies [22,23], show the successful deposition of $Ti_{1-x}Ag_x$ and Ag-TiN_x coatings by sputtering on PVDF substrates, maintaining the piezoelectric response of the polymer.

The aim of the present work is to assess the antibacterial properties of $Ti_{1-x}Ag_x$ and Ag-TiN_x electrodes produced by d.c. magnetron sputtering on PVDF substrate, in order to extend their application potential.

6.2 Materials and methods

6.2.1 Coatings preparation

$Ti_{1-x}Ag_x$ and Ag-TiN_x coatings were deposited by d.c./pulsed magnetron sputtering onto PVDF thin sheets with a thickness of approximately 28 μm (Precision Acoustics Ltd). One pure Ti target (99.99 %) and one Ag target (99.99 %) (both with 200 x 100 mm^2) were used in an argon atmosphere for the $Ti_{1-x}Ag_x$ coatings and an Ar + N_2 mixture for Ag-TiN_x coatings, with the substrates rotating at 70 mm from the target at a constant speed of 7 rpm. For both series, the working pressure in the was about 0.17 Pa and the argon flow was kept constant at 60 sccm while the N_2 reactive gas flux was changed in the range of 0-6 sccm for Ag-TiN_x coatings.

In order not to vary significantly the Ag content in the Ag-TiN_x films, the current density (J) applied to each target was kept constant. The Ti target was connected to a pulsed d.c. power supply, while the Ag target was connected to a d.c. power supply. The frequency and reverse time were fixed at 200 kHz and 1536 ns, respectively, corresponding to a duty cycle of 69 %. The deposition time was varied in order to obtain a thickness ranging between 120 to 230 nm. In order to avoid the structural damage of the polymer substrate, the substrate temperature must be ideally kept below ~100 °C, far from the melt transition temperature of PVDF [24].

In this sense, the depositions were performed without any external heating of the substrate and no bias polarization was applied on the substrate holder.

6.2.2 Chemical and physical analysis

Chemical composition was obtained with an EDAX - Pegasus X4M – Energy dispersive spectroscopy (EDS/EBSD) apparatus coupled with a scanning electron microscopy (SEM). Since the depth of analysis at 10 kV is about 300 nm for pure Ag and 700 nm for pure titanium, $Ti_{1-x}Ag_x$ and Ag-TiN_x coatings with a thickness of 1 μm were deposited onto Si substrate for EDS analysis.

The structure and phase distribution of the coatings were analyzed by powder X-ray diffraction (XRD) using a Bruker D8 Discover diffractometer (Cu Kα radiation – λ =1.5406 Å, step 0.04°, time per step 1s and 6-60 2θ interval).

X-ray photoelectron spectroscopy (XPS) was carried out to analyze the chemical bonds of the compounds on the coating surface, before and after biological tests. The XPS analysis was performed using a Kratos AXIS Ultra HSA, with VISION software for data acquisition and CasaXPS software for data analysis. The analysis was carried out with a monochromatic Al Kα X-ray source (1486.7 eV), operating at 15 kV (90 W), in FAT mode (Fixed Analyzer Transmission), with a pass energy of 40 eV for regions ROI and 80 eV for survey. Data acquisition was performed with a pressure lower than 1 $x10^{-6}$ Pa, and a charge neutralization system was used. The effect of the electric charge was corrected by the reference of the carbon peak (285 eV). The deconvolution of spectra was carried out using the CasaXPS program, in which a peak fitting was performed using Gaussian-Lorentzian peak shape after a Shirley type background subtraction.

The surface morphology was examined by SEM through a NanoSEM – FEI Nova 200 (FEG/SEM) equipped with a field emission gun (FEG), operated in high vacuum mode with a chamber pressure of 0.003 Pa. The micrographs were obtained with secondary (SE) and backscattered (BSE) electron detectors in “through-the-lens” (TLD) mode at acceleration voltage between 5 and 10 kV and working distance of around 5 mm. Measurements were performed in three areas randomly chosen in all samples before and after the biological tests. Magnifications of 40 000x (40 Kx) and 150 000x (150 Kx) were used. The particle size and distribution were analyzed using the ImageJ software and a descriptive statistical analysis was performed.

6.2.3 Antibacterial properties

The antibacterial activity of $Ti_{1-x}Ag_x$ and Ag-TiN_x coatings was tested against *Staphylococcus epidermidis* (*S. epidermidis*, IE186 strain, a clinical isolate belonging to the CEB Biofilm Group collection). Zone of inhibition (ZoI) tests, adapted from Kirby-Bauer test [25], were carried out to determine the diffusion of silver from the coatings surface. The Halo size was used as a qualitative measure of the sample activity.

S. epidermidis was cultivated in liquid medium, by inoculation of a single colony on 20 mL of Tryptic Soy Broth (TSB, Merck) and incubated for 18 h at 37°C, and 120 rpm. Afterwards, the resultant cell suspension was adjusted to an optical density (OD) of 1.0 at 640 nm and properly diluted in TSB to $1x10^7$ CFU.mL^{-1}.

The incubation of the bacteria in the agar was performed in two different ways: in the first one, 1 ml of cells suspension was added to 14 ml of cooled (< 50°C) Tryptic Soy Agar (TSA, Merck) and placed into sterile plastic petri dishes; in the second, an aliquot of cells suspension (100 µL), containing approximately $1x10^5$ CFU.mL^{-1} (this concentration is required in order to maintain the same order of magnitude as the first procedure) was spread in TSA Petri dishes.

After medium solidification, the samples (previously sterilized by exposure of ± 1 h to UV light) were placed separately on the top of an agar plate, with the coated side in contact with the agar, and incubated for 24 h, at 37°C. PVDF substrate, Ti and TiN coatings (without silver) were used as negative controls. After the incubation period, the Halo (zone of transparent medium, which means that there is no bacteria growth) formed around the sample was measured and photographed to record the results (images captured with Image Lab™ software). All experiments were carried out in duplicate per samples and repeated at least in three independent assays.

6.3 Results and discussion

6.3.1 Chemical composition

Table 6.1 shows some results about deposition conditions, chemical composition together with the thicknesses of the deposited coatings obtained by SEM analysis. The deposition rate was determined from the deposition time and coatings thickness.

Table 6.1 - Chemical composition of $Ti_{1-x}Ag_x$ and Ag-TiN_x coatings and some experimental details

Series	Coating	J_{Ti} (mA/cm^2)	J_{Ag} (mA/cm^2)	N_2 flow (sccm)	Thickness on polymers (nm)	Deposition rate (nm/h)	Chemical Composition (at. %)			N/Ti
							Ti	Ag	N	
$Ti_{1-x}Ag_x$ series	Ti	5	0	0	219	437	100	0	0	0
	Ag/Ti (0.11)R	7.5	0.05	0	201	803	93	7	0	0
	Ag	0	2.5	0	165	659	0	100	0	0
Ag-TiN_x series	TiN2AgR	7.5	0.05	2	227	910	61	5	34	0.56
	TiN6Ag (new)	10	0.05	6	129	663	52	10	38	0.73
	TiN	10	0	6	122	630	57	0	43	0.75

The $Ti_{1-x}Ag_x$ coatings were labelled according to the Ag/Ti atomic ratio, while pure titanium and pure silver coatings are labelled as Ti and Ag, respectively. The Ag-TiN_x series are labelled according to the N_2 flow applied e.g. TiN2AgR was deposited with a nitrogen flow of 2 sccm while the titanium nitride is labelled as TiN. Further details concerning the chemical composition versus deposition parameters, of the similar samples, can be found elsewhere [22,23].

6.3.2 Structural analysis

Figure 6.1 shows the XRD diffraction patterns of $Ti_{1-x}Ag_x$ and Ag-TiN_x systems. The reference peaks, obtained from the International Centre for Diffraction Data (ICDD) database, of the main crystalline phases are identified namely hcp-Ti (ICDD 00-044-1294), fcc-Ag (ICDD 00-004-0783), fcc-TiN (ICDD 00-038-1420) and tetragonal TiAg (ICDD 00-006-0560), together with the crystalline peaks of PVDF (ICDD 00-042-1649) [24].

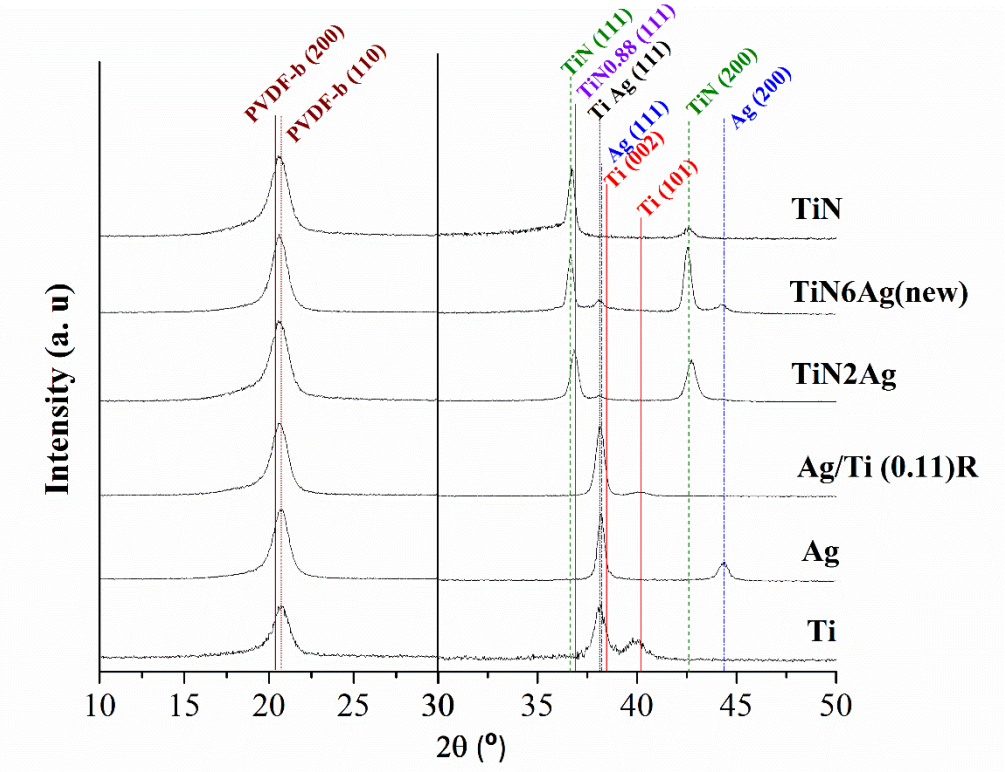

Figure 6.1 - XRD patterns of both $Ti_{1-x}Ag_x$ and Ag-TiN_x coatings deposited (Cu Kα radiation).

XRD peaks corresponding to atomic planes (200) and (110) of β-PVDF (Figure 6.1a) indicate that the deposition conditions do not induce any phase change in the polymer. This means that the piezoelectric phase of PVDF is still present.

These results were in fact already discussed in previous works reported by the authors [22,23]. The previous published results stated that for $Ti_{1-x}Ag_x$ series, the values of the piezoelectric response vary from 19.6 to 27.6 $pC.N^{-1}$, allow for maintaining the functional piezoelectric response of the polymer.

For the Ag-TiN_x series, with increasing nitrogen flow, the piezoelectricity response tends to decrease. However, this slight variation does not compromise the piezoelectric response for the required application. Further discussion and details can be seen elsewhere [22,23]. The XRD pattern of Ag/Ti (0.11)R coating indicates that the most intense peak is located at ≈38.1°, which is very close to the TiAg(111) and Ag(111) peaks (see Figure 6.1b). Previous studies of $Ti_{1-x}Ag_x$ coatings deposited by magnetron sputtering suggested the formation of the TiAg crystalline phase, although it is difficult to identify Ag, Ti and TiAg phases since they show very similar diffraction patterns [9,22,23].

Together with the TiAg phase, the presence of the Ti (002) peak can also be identified, which suggests that the coating is composed by a mixture of crystalline TiAg and Ti phases. Since the amount of Ti present in the coating is high (93 at. %), TiAg phase is formed until the Ag is consumed and the remaining titanium forms a crystalline Ti phase [22,23].

TiN6Ag(new) and TiN coatings display a diffraction peak located at ≈36.7° which is attributed to fcc-TiN phase and TiN2AgR coating exhibits a diffraction peak at ≈36.9° ascribed to sub-stoichiometric TiN phase that can be related to lower N/Ti atomic ratio in this film than in the standards. These samples show another peak located at ≈42.5° which has been assigned to TiN (200). A previous study with similar coatings also detected such peak; however, it was observed in coatings with higher Ag contents [10]. To minimize the surface energy, the atoms tend to have planes with the maximum compactness parallel to the surface, in the case of fcc-phase the plan is (111) but due to the new phase growth (Ag phase), these conditions can be changed. Furthermore, this new phase is detected in samples with silver (TiN2AgR and TiN6Ag(new)) showing two diffraction peaks at ≈38° and ≈44.4° which represent (111) and (200) planes of fcc-Ag, respectively.

6.3.3 Morphology

SEM analyses were performed in order to evaluate surface characteristics of the films, such as the presence of Ag nanoparticles on the surface before and after biological tests. Figure 6.2 show the SEM micrograph of the coatings of both $Ti_{1-x}Ag_x$ and Ag-TiN_x systems, before Halo test.

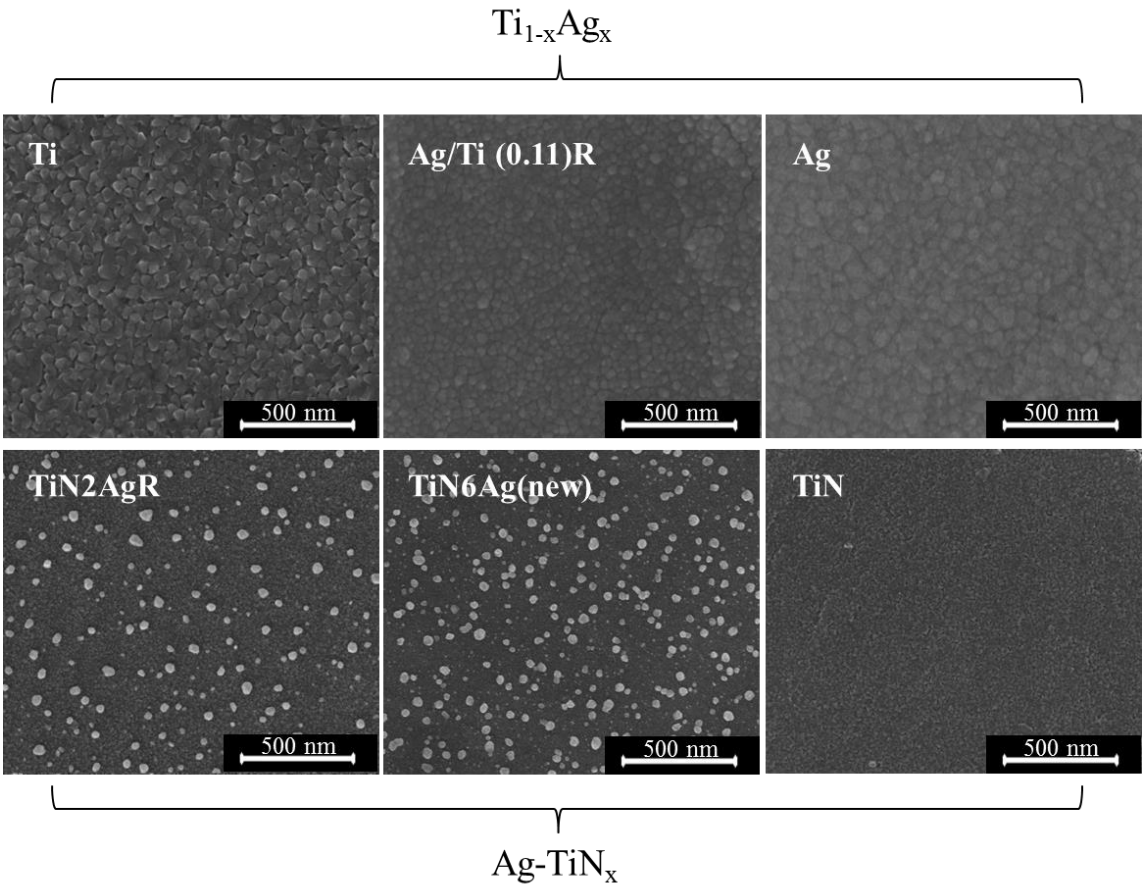

Figure 6.2 - SEM micrograph of the $Ti_{1-x}Ag_x$ and Ag-TiN_x coating systems.

The SEM micrographs of similar coatings of $Ti_{1-x}Ag_x$ systems were discussed in a previous paper [22], where it was verified that the coatings were homogeneous and no clusters were found on the surface. The present films also do not show any Ag nanoparticles, which corroborates XRD analysis (Figure 6.1), suggesting the formation of crystalline TiAg phases. On the other hand, the surface of the Ag-TiN_x coating system exhibited Ag nanoparticles like the authors discussed in a previous paper [23]. Several studies reported that the co-deposition of Ag and titanium nitride (TiN) [26], carbonitride (TiCN) [27] and oxide (TiO_2) [28] results in the formation of nanocomposites with Ag nanoparticles embedded in the matrix coating, and the size of these nanoparticles strongly depends on the amount of silver incorporated in the coating.

The formation of Ag nanoparticles is related to the immiscibility of Ag in these matrices. Lopes et al [9] and also the authors [23] reported that Ag-TiN_x coatings were composed by Ag nanoparticles and/or clusters segregated from the TiN cubic grain boundaries.

6.3.4 Antimicrobial properties

Figure 6.3 shows an example of the Halo tests carried out on $Ti_{1-x}Ag_x$, Ag-TiN_x systems and PVDF substrate. Figure 6.3a depicts the PVDF substrate, and Figure 6.3c, 6.3d and 6.3f show Ti, Ag/Ti (0.11)R and Ag samples from $Ti_{1-x}Ag_x$ system, respectively. Figure 6.3b, 6.3e and 6.3g display respectively TiN, TiN2AgR and TiN6Ag(new) samples from Ag-TiN_x system. The Ag coating (Figure 6.3f) shows a weak Halo around (≈0.5±0.08 mm), which maybe too small to prove antibacterial properties.In contrast, in samples from the Ag-TiN_x system, (TiN2AgR and TiN6Ag(new) - Figures 3e and 3g, respectively), a clear Halo surrounding the samples is observed, with dimensions between ≈1.8±0.3 mm and ≈1.4±0.1 mm for TiN2AgR and TiN6Ag(new), respectively, enhancing the antibacterial activity. This result is ascribed to the silver diffusion through the agar.

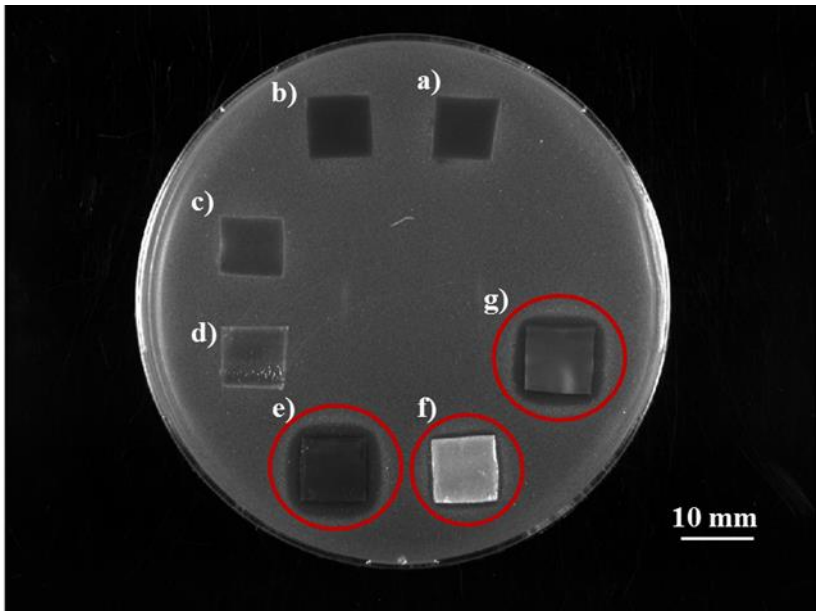

Figure 6.3 – Zone of inhibition assays of different samples: a) PVDF, b) TiN, c) Ti, d) Ag/Ti (0.11)R, e) TiN2AgR, f) Ag and g) TiN6Ag(new) against S. epidermidis. The red circles highlight samples with the Halo inhibition.

Interestingly, in spite of the fact that Ag/Ti (0.11)R sample (Figure 6.3d) possess silver content values comparable to the other samples, it does not have any inhibition zone.

This apparent absence of antibacterial activity may be explained by the bonding between Ag and Ti preventing silver segregation and hence its diffusion (the chemical bonds will be discussed later in section 6.4.5). This assumption is consistent with previous XRD results, which showed the possible formation of crystalline TiAg phases.

Figure 6.4 presents the SEM images of coatings surface, after microbiological tests from TiN6Ag(new) and Ag/Ti (0.11)R. Despite having similar amounts of silver, these two samples possess different matrices (TiN or Ti, respectively), and thus, it is expected that silver to behave differently.

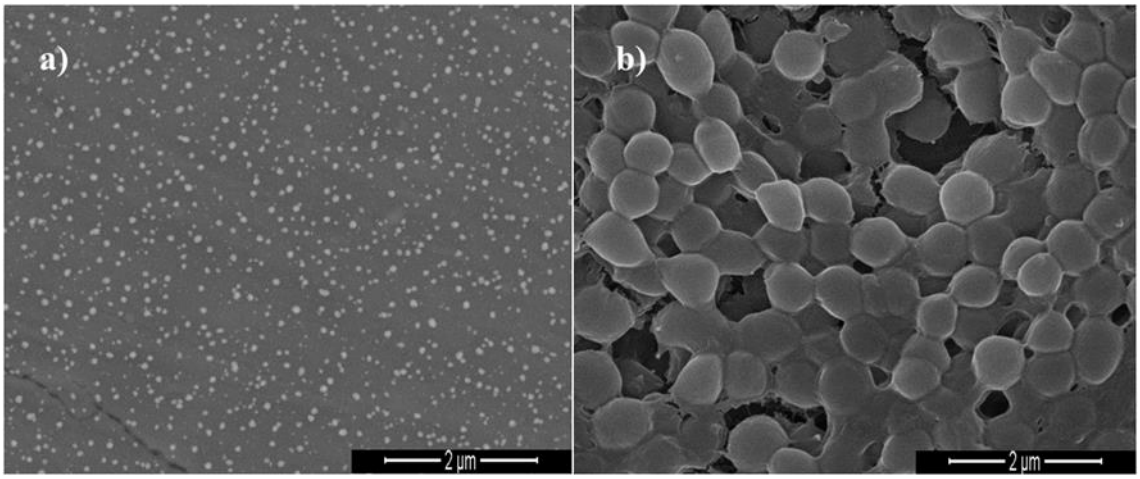

Figure 6.4 - SEM micrographs of (a) TiN6Ag(new) and (b) Ag/Ti (0.11)R coatings surface, after Halo test on a S. epidermidis agar layer. SEM images from the samples surface show in (a) Ag nanoparticles (BSE image) and in (b) a microbial colonies.

From the observation of the surface of samples from the Ag-TiN_x system (Figure 6.4a), no bacteria on the surface are noticed, corroborating its antibacterial effect observed in the Halo test (Figure 6.3). Figure 6.4a was obtained using the BSE mode and clearly shows Ag nanoparticles dispersed all over the film surface. Ag/Ti (0.11)R coating (Figure 6.4b) of $Ti_{1-x}Ag_x$ systems shows some microbial colonies. These results confirm that silver in the $Ti_{1-x}Ag_x$ coating system has no antibacterial effect, allowing bacterial colonization, in contrast with the antibacterial activity of the Ag-TiN_x coating system, which presents a reduction in the number Ag nanoparticles at the surface after biological test (discussed below) certainly due to their diffusion through the agar which induce inhibition of bacteria growth.

Figure 6.5 shows the TiN6Ag(new) coating surface before (a) and after (b) the Halo test. Figures 6.5c and 6.5d correspond to Figures 6.5a and 6.5b, respectively, treated by ImageJ software.

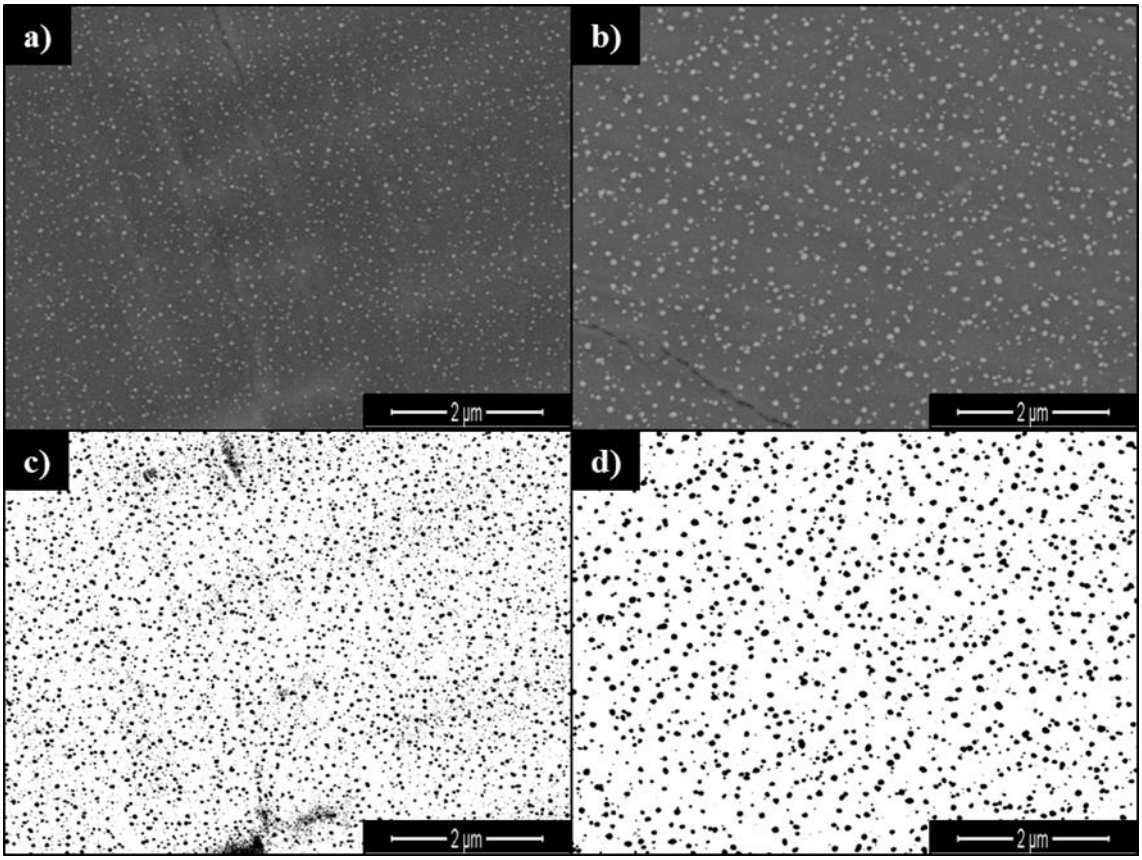

Figure 6.5 - SEM micrograph of TiN6Ag(new) coating surface, obtained in BSE mode, before (a) and after (b) Halo test (c) and (d) are the same images that (a) and (b) respectively, treated by imageJ software.

The SEM micrographs clearly show a modification on the coatings surface after the Halo test, where i) an increase in the Ag particles size and ii) a decrease in the number of Ag nanoparticles is observed. In order to quantify this trends, i) the covering area of the particles in relation to the total area was calculated and reported as a percentage and ii) the number of particles (independently of the size) was counted being the results shown in table 6.2.

Table 6.2 - Percentage of Ag area covered and number of Ag particles in the TiN6Ag(new) sample surface

TiN6Ag(new)	Ag Area (%)	Number of particles
As deposited	14	9012
After Halo test	8	1517

In addition, the corresponding particle size distribution of the silver particles before and after the Halo test are shown in Figure 6.6. After Halo test, there is a 6% reduction in the area occupied by the Ag nanoparticles, which is accompanied by a reduction in the total number of Ag particles. Simultaneously, the histograms clearly suggest an increase in the particles size.

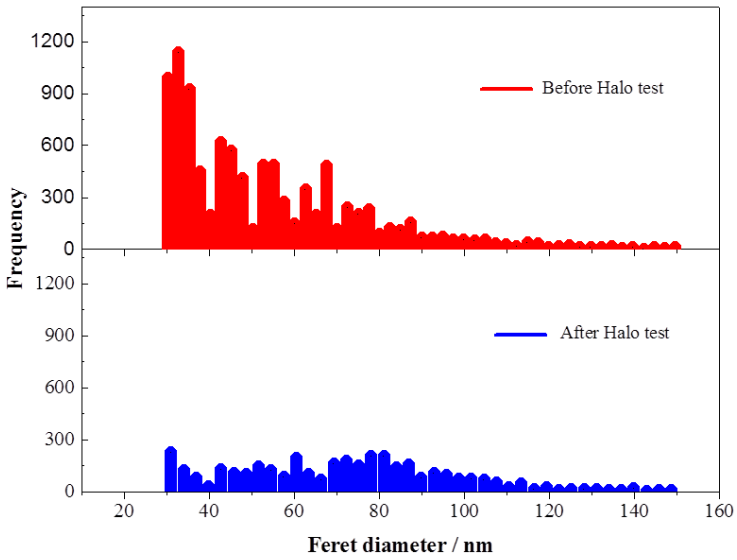

Figure 6.6 - Particle size distribution histogram of the silver nanoparticles, evaluated from the corresponding SEM micrograph of TiN6Ag(new) coating surface.

Thus, it might be concluded that during the Halo tests a phenomena of particles agglomeration or coalescence is occurring, which combined with some diffusion of Ag through the agar, which probably contributes to the reduction in the number of Ag particles. The Ag nanoparticles agglomeration in different fluids has been reported by Li et al. [29] and this agglomeration was attributed to the occurrence of Ag dissolution. In fact, dissolution-precipitation is a well-established coalescence process that occurs in liquid media. This process is also known as Ostwald ripening and involves the dissolution (in this case ionization of Ag) of small Ag nanoparticles, which aftermost grow on the surface of bigger Ag nanoparticles [30].

Possibly, this mechanism explains the increase in Ag particle size during the Halo test and plays a fundamental role in the antibacterial performance, since it is accepted that the Ag biocidal activity is mostly promoted by the presence of Ag ions.

Other studies assessed the release behavior of silver ions of composites as Ag/TiO_2, $Ag–SiO_2$, and attributed to water diffusion characteristics on the matrix [31,32].

6.3.5 Chemical bonding analysis by XPS

XPS analyses were performed on as deposited samples of both $Ti_{1-x}Ag_x$ and Ag-TiN_x systems and on samples with antibacterial activity after performing the Halo test in order to relate the chemical changes in the sample surface.

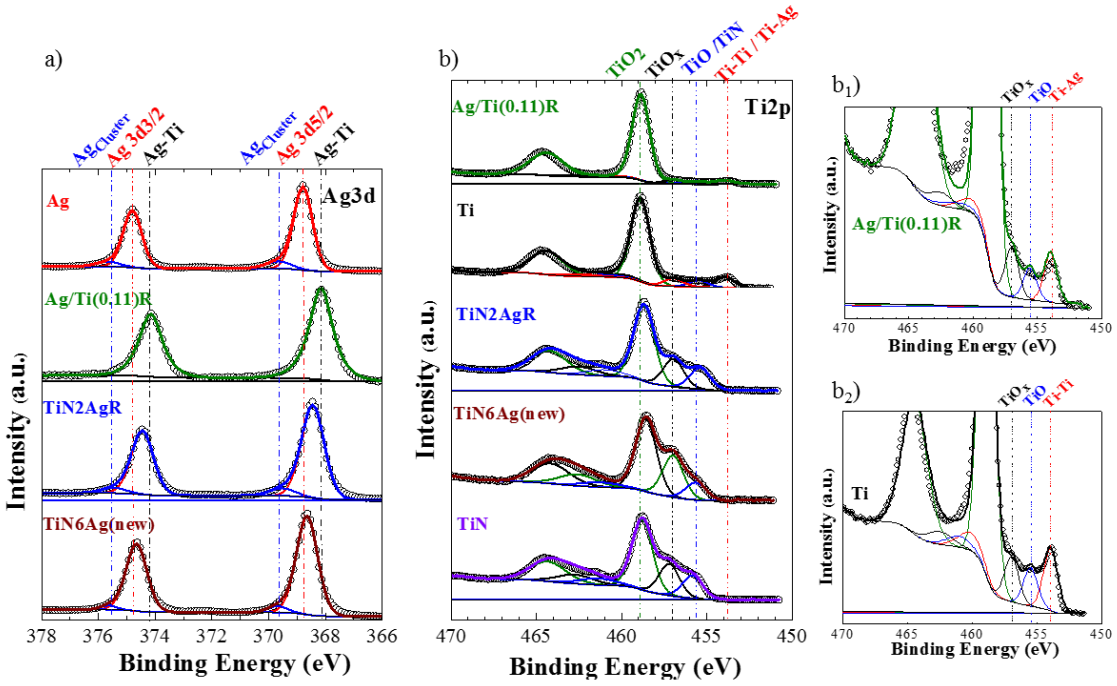

Figure 6.7 - XPS spectra of Ag 3d (a) and Ti 2p (b) core levels of $Ti_{1-x}Ag_x$ and Ag-TiN_x systems before the Halo test. (b_1) and (b_2) represent the amplification of Ti 2p core level for Ag/Ti (0.11)R and Ti coatings, respectively.

Figure 6.7a shows the Ag 3d photoelectron spectra of Ag, Ag/Ti (0.11)R, TiN2AgR and TiN6Ag(new) coatings before performing the Halo test. The Ag/Ti (0.11)R coating shows an Ag 3d doublet with the Ag 3d5/2 peak at ≈368.1 eV (separated of Ag 3d3/2 peak by 6.0 eV) with full width at half maximum (FWHM) of ≈1.0 eV which is attributed to Ag-Ti bond, in accordance with Moulder et al. [33] which identified this bond as Ag alloys.

The counterpart is also observed in Figure 6.7b in the Ti 2p3/2 band at ≈453.9 eV (separated of Ti 2p1/2 by ≈6.2 eV) with FWHM of ≈1.2 eV which is assigned to Ag-Ti and Ti-Ti bond for Ag/Ti (0.11)R and Ti coating, respectively. These bands can be observed in the amplified Figures 6.7b1 and 6.7b2. These results corroborate the resistivity results for $Ti_{1-x}Ag_x$ series, showing a typical behavior of a binary alloy system, already published by the authors in another paper [22], and confirm the aforementioned antibacterial inactivity since silver is not available to diffuse through the agar.

Ag, TiN2AgR and TiN6Ag(new) coatings show the deconvolution of Ag 3d doublet into two Gaussian components (each Gaussian component of Ag $3d_{5/2}$ and Ag $3d_{3/2}$ separated by 6.0 eV). The binding energy of the one of Ag $3d_{5/2}$ peak component is ≈368.8 eV with FWHM of ≈0.9 eV which is attributed to Ag-Ag metallic bonds [25]. The binding energy of the other component appears approximately to 369.5 eV (≈1.1 eV FWHM), which is ascribed to metallic sub-nanoparticles associated with clusters smaller than 4 nm [34]. Calderon et al. [35] also detected this band in ZrCN-Ag samples. After performing the Halo test, this contribution (metallic sub-nanoparticles) disappears as observed in Figure 6.8.

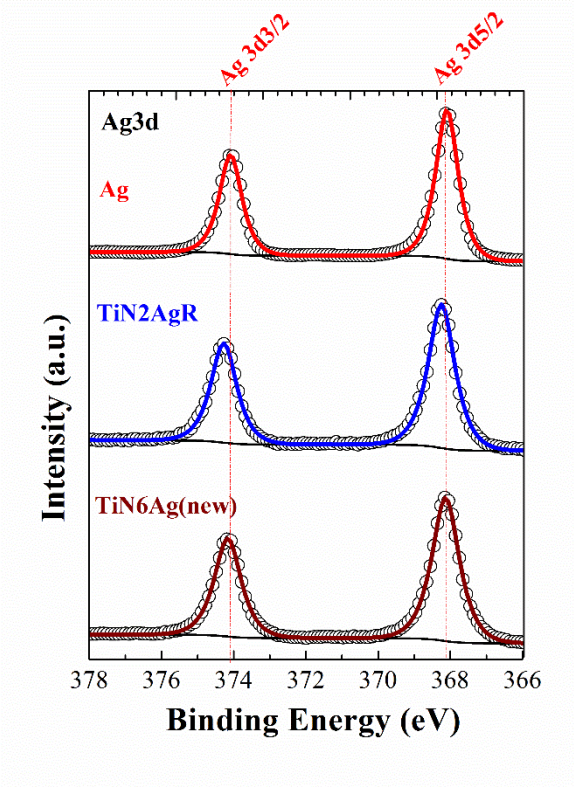

Figure 6.8 - XPS spectra of Ag 3d core level of $Ti_{1-x}Ag_x$ and Ag-TiN_x systems after the Halo test.

These outcomes are in agreement with the SEM results that showed the existence of nanoparticles on TiN2AgR and TiN6Ag(new) coatings surface before the biological tests, whereas a perceptible aggregation (increase on the particle size) and a significant decrease in the nanoparticles number (small particles) is observed after the biological tests.

6.4 Conclusions

The aim of this study was the evaluation of the antibacterial properties of $Ti_{1-x}Ag_x$ and Ag-TiN_x systems. In both systems, the presence of β-PVDF phase diffraction peaks was observed, indicating that the deposition conditions did not damage the polymeric substrate, being possible to conclude that piezoelectric properties were kept. This is useful for the development of sensors for biomedical application. In this sense it is essential to establish whether the materials show antibacterial properties.

It has been demonstrated that only the Ag-TiN_x coatings show antibacterial activity. In this case, Ag clusters are formed on the coating surface and silver can diffuse through the agar inducing inhibition of bacterial growth. In the case of $Ti_{1-x}Ag_x$ system, silver is chemically bonded (Ti-Ag bond), and hence it does not show any antibacterial activity. Although pure Ag coating produces a Halo during bacterial tests, the ZoI measure is too small to conclude whether this coating has antibacterial properties.

Further studies should be carried out in order to clarify the effect of silver and/or silver ion released.

This work highlighted the potential of silver nanoparticles, especially in the Ag-TiN_x series, and it was an essential step towards the assessment of the ideal system for used as sensor protection.

6.5 References

[1] F. Guimarães, C. Oliveira, E. Sequeiros, M. Torres, M. Susano, Structural and Mechanical properties of Ti – Si – C – ON for biomedical applications, Technology. 202 (2008) 2403 – 2407. doi:10.1016/j.surfcoat.2007.08.056.

[2] C. Oliveira, L. Gonçalves, B.G. Almeida, C.J. Tavares, S. Carvalho, F. Vaz, et al., XRD and FTIR analysis of Ti–Si–C–ON coatings for biomedical applications, Surf. Coatings Technol. 203 (2008) 490–494. doi:10.1016/j.surfcoat.2008.06.121.

[3] L. Montanaro, P. Speziale, D. Campoccia, S. Ravaioli, I. Cangini, G. Pietrocola, et al., Scenery of Staphylococcus implant infections in orthopedics, Future Microbiol. 6 (2011) 1329–49. doi:10.2217/fmb.11.117.

[4] J.P. O'Gara, H. Humphreys, Staphylococcus epidermidis biofilms: importance and implications, J. Med. Microbiol. 50 (2001) 582–7. http://www.ncbi.nlm.nih.gov/pubmed/11444767.

[5] P.F. Sharkey, W.J. Hozack, R.H. Rothman, S. Shastri, S.M. Jacoby, Insall Award paper. Why are total knee arthroplasties failing today?, Clin. Orthop. Relat. Res. (2002) 7–13. http://www.ncbi.nlm.nih.gov/pubmed/12439231 (accessed May 30, 2014).

[6] R. Brånemark, P.I. Brånemark, B. Rydevik, R.R. Myers, Osseointegration in skeletal reconstruction and rehabilitation: a review, J. Rehabil. Res. Dev. 38 (2001) 175–181.

[7] S.P. Mohanty, E. Kougianos, Biosensors : A Tutorial Review, (n.d.) 1–12.

[8] C.F.A.F.A. Alves, F. Oliveira, I. Carvalho, a. P.P. Piedade, S. Carvalho, Influence of albumin on the tribological behavior of Ag–Ti (C, N) thin films for orthopedic implants, Mater. Sci. Eng. C. Mater. Biol. Appl. 34 (2014) 22–28. doi:10.1016/j.msec.2013.09.031.

[9] C. Lopes, C. Gonçalves, P. Pedrosa, F. Macedo, E. Alves, N.P. Barradas, et al., TiAgx thin films for lower limb prosthesis pressure sensors: Effect of composition and structural changes on the electrical and thermal response of the films, Appl. Surf. Sci. 285 (2013) 10–18. doi:10.1016/j.apsusc.2013.07.021.

[10] P. Pedrosa, D. Machado, C. Lopes, E. Alves, N.P. Barradas, N. Martin, et al., Applied Surface Science Nanocomposite Ag : TiN thin films for dry biopotential electrodes, Appl. Surf. Sci. 285 (2013) 40–48. doi:10.1016/j.apsusc.2013.07.154.

[11] P. Pedrosa, E. Alves, N.P. Barradas, N. Martin, P. Fiedler, J. Haueisen, et al., Electrochemical behaviour of nanocomposite Agx:TiN thin films for dry biopotential electrodes, Electrochim. Acta. 125 (2014) 48–57. doi:10.1016/j.electacta.2014.01.082.

[12] S. Piscanec, L. Colombi, E. Vesselli, G. Comelli, O. Sbaizero, S. Meriani, et al., Bioactivity of TiN-coated titanium implants, Acta Mater. 52 (2004) 1237–1245. doi:10.1016/j.actamat.2003.11.020.

[13] P.J.J. Kelly, H. Li, P.S.S. Benson, K.A.A. Whitehead, J. Verran, R.D.D. Arnell, et al., Comparison of the tribological and antimicrobial properties of CrN/Ag, ZrN/Ag, TiN/Ag, and TiN/Cu nanocomposite coatings, Surf. Coatings Technol. 205 (2010) 1606–1610. doi:10.1016/j.surfcoat.2010.07.029.

[14] H. Cao, X. Liu, F. Meng, P.K. Chu, Biological actions of silver nanoparticles embedded in titanium controlled by micro-galvanic effects, Biomaterials. 32 (2011) 693–705. doi:10.1016/j.biomaterials.2010.09.066.

[15] P.J.J. Kelly, H. Li, K.A.A. Whitehead, J. Verran, R.D.D. Arnell, I. Iordanova, A study of the antimicrobial and tribological properties of TiN / Ag nanocomposite coatings, Surf. Coat. Technol. 204 (2009) 1137–1140. doi:10.1016/j.surfcoat.2009.05.012.

[16] D.R. Monteiro, L.F. Gorup, A.S. Takamiya, A.C. Ruvollo-Filho, E.R. de Camargo, D.B. Barbosa, The growing importance of materials that prevent microbial adhesion: antimicrobial effect of medical devices containing silver., Int. J. Antimicrob. Agents. 34 (2009) 103–10. doi:10.1016/j.ijantimicag.2009.01.017.

[17] M. Rai, A. Yadav, A. Gade, Silver nanoparticles as a new generation of antimicrobials, Biotechnol. Adv. 27 (2009) 76–83. doi:10.1016/j.biotechadv.2008.09.002.

[18] O. Akhavan, E. Ghaderi, Capping antibacterial Ag nanorods aligned on Ti interlayer by mesoporous TiO2 layer, Surf. Coatings Technol. 203 (2009) 3123–3128. doi:10.1016/j.surfcoat.2009.03.033.

[19] O. Akhavan, E. Ghaderi, Enhancement of antibacterial properties of Ag nanorods by electric field, Sci. Technol. Adv. Mater. 10 (2009) 015003. doi:10.1088/1468-6996/10/1/015003.

[20] P. Pedrosa, C. Lopes, N. Martin, C. Fonseca, F. Vaz, Electrical characterization of Ag:TiN thin films produced by glancing angle deposition, Mater. Lett. 115 (2014) 136–139. doi:10.1016/j.matlet.2013.10.044.

[21] D. Machado, P. Pedrosa, C. Fonseca, N. Martin, F. Vaz, Structural and Morphological Changes in Ag:TiN Nanocomposite Films Promoted by In-Vacuum Annealing, J. Nano Res. 25 (2013) 67–76. doi:10.4028/www.scientific.net/JNanoR.25.67.

[22] S.M. Marques, N.K. Manninen, S. Ferdov, S. Lanceros-Mendez, S. Carvalho, Ti1− xAgx electrodes deposited on polymer based sensors, Appl. Surf. Sci. 317 (2014) 490–495. doi:10.1016/j.apsusc.2014.08.142.

[23] S.M. Marques, N.K. Manninen, S. Lanceros-Mendez, S. Carvalho, Ag-TiNx electrodes deposited on piezoelectric poly(vinylidene fluoride) for biomedical sensor applications, Sensors Actuators A Phys. (2015). doi:10.1016/j.sna.2015.08.016.

[24] P. Martins, A.C.C. Lopes, S. Lanceros-Mendez, Electroactive phases of poly(vinylidene fluoride): Determination, processing and applications, Prog. Polym. Sci. 39 (2014) 683–706. doi:10.1016/j.progpolymsci.2013.07.006.

[25] A. Bauer, W. Kirby, J. Sherris, M. Turk, Antibiotic susceptibility testing by standard single disk method, Am. J. Clin. Pathol. 45 (1966) 493–496.

[26] T. de los Arcos, P. Oelhafen, U. Aebi, A. Hefti, M. Düggelin, D. Mathys, et al., Preparation and characterization of TiN–Ag nanocomposite films, Vacuum. 67 (2002) 463–470. doi:10.1016/S0042-207X(02)00232-4.

[27] R. Escobar Galindo, N.K. Manninen, C. Palacio, S. Carvalho, Advanced surface characterization of silver nanocluster segregation in Ag-TiCN bioactive coatings by RBS, GDOES, and ARXPS., Anal. Bioanal. Chem. 405 (2013) 6259–69. doi:10.1007/s00216-013-7058-z.

[28] V.S.K. Chakravadhanula, T. Hrkac, V. Zaporojtchenko, R. Podschun, V.G. Kotnur, a Kulkarni, et al., Nanostructural and functional properties of Ag-TiO2 coatings prepared by co-sputtering deposition technique., J. Nanosci. Nanotechnol. 11 (2011) 4893–4899. doi:10.1140/epjd/e2007-00186-5.

[29] X. Li, J.J. Lenhart, H.W. Walker, Dissolution-Accompanied Aggregation Kinetics of Silver Nanoparticles, Langmuir. 26 (2010) 16690–16698. doi:10.1021/la101768n.

[30] G. Cao, NANOSTRUCTURES AND NANOMATERIALS - Synthesis, Properties and Applications, Imperial College Press, London, 2004. doi:10.1142/9781860945960.

[31] Y. Liu, X. Wang, F. Yang, X. Yang, Excellent antimicrobial properties of mesoporous anatase TiO2 and Ag/TiO2 composite films, Microporous Mesoporous Mater. 114 (2008) 431–439. doi:10.1016/j.micromeso.2008.01.032.

[32] O. Akhavan, E. Ghaderi, Bactericidal effects of Ag nanoparticles immobilized on surface of SiO2 thin film with high concentration, Curr. Appl. Phys. 9 (2009) 1381–1385. doi:10.1016/j.cap.2009.03.003.

[33] J.F. Moulder, W.F. Stickle, P.E. Sobol, K.D. Bomben, Handbook of X-ray Photoelectron Spectroscopy, Perkin-Elmer Corporation, 1979. doi:10.1002/sia.740030412.

[34] A. Siozios, H. Zoubos, N. Pliatsikas, D.C. Koutsogeorgis, G. Vourlias, E. Pavlidou, et al., Growth and annealing strategies to control the microstructure of AlN:Ag nanocomposite films for plasmonic applications, Surf. Coatings Technol. 255 (2014) 28–36. doi:10.1016/j.surfcoat.2013.11.025.

[35] S.C. Velasco, V. Lopez, C.F.A. Alves, a Cavaleiro, S. Carvalho, Structural and electrochemical characterization of Zr – C – N – Ag coatings deposited by d.c. dual magnetron sputtering, Corros. Sci. 80 (2014) 229–236. doi:10.1016/j.corsci.2013.11.036.

7. MC3T3-E1 cell response to $Ti_{1-x}Ag_x$ and Ag-TiN_x electrodes deposited on piezoelectric PVDF substrates for sensor applications

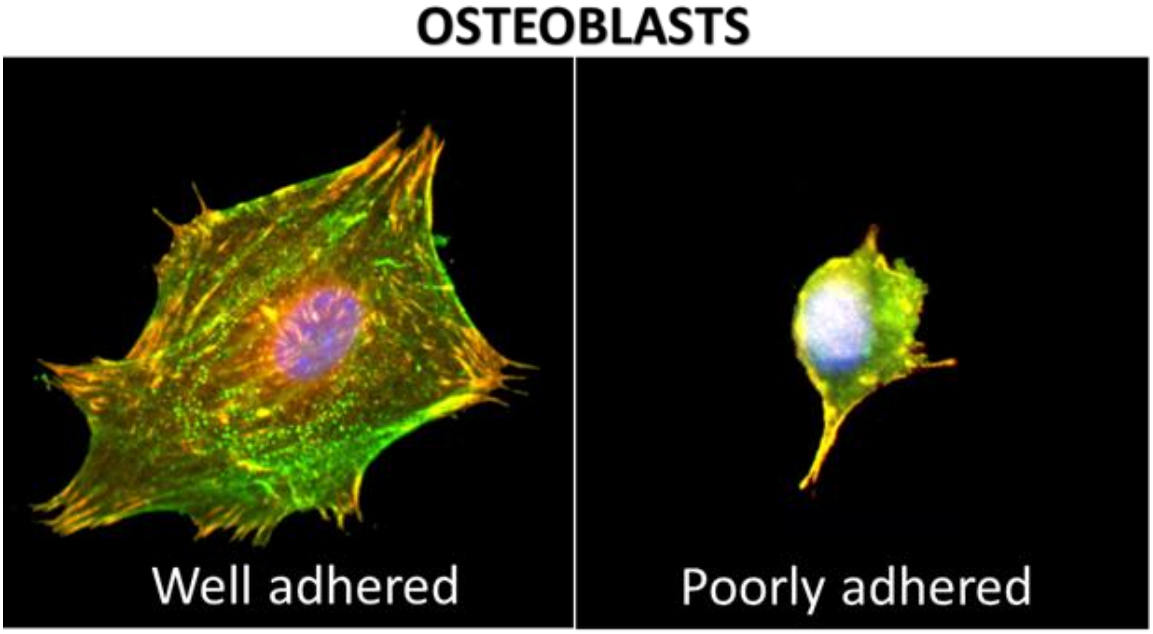

This chapter is based on the publication: S.M. Marques, P. Rico, J. L. Gómes Ribelles, S. Lanceros-Mendez, M. Henriques, S. Carvalho, *MC3T3-E1 cell response to $Ti_{1-x}Ag_x$ and Ag-TiN_x electrodes deposited on piezoelectric PVDF substrates for sensor applications*, ready-for-submission.

Taking into account the results discussed in previous chapters, good piezoelectric and piezoresistive properties and antibacterial activity, three samples were selected to evaluate their behavior with osteoblastic cells. The Ag/Ti(0.11)R sample was selected from $Ti_{1-x}Ag_x$ series, the TiN2AgR sample from Ag-TiN_x series and TiN sample discussed in Chapter 6. As a result, this chapter is focused on the evaluation of osteoblast MC3T3-E1 cells behaviors in terms of proliferation, adhesion and differentiation of two different systems used as electrodes for this sensor: $Ti_{1-x}Ag_x$ and Ag-TiN_x were deposited by d.c. and pulsed magnetron sputtering at room temperature on poli(vinylidene fluoride) (PVDF), given the different features of each sample in terms of surface characteristics, topography and chemistry. The different performances of these samples will influence the cells capacity to adhere, proliferate and differentiate. Since this kind of sensors has the function of detect dynamic mechanical loads at an early stage of problems associated with implantation of prostheses, they cannot be covered by osteoblastic cells at the beginning. Otherwise, the sensor will also detect mechanical loads performed by the cells.

The results indicated a better effect, at an initial stages of cell cultures, of Ag-TiN_x electrodes compared with $Ti_{1-x}Ag_x$ and TiN, in terms of diminished cell adhesion and proliferation. Nevertheless, when cell culture time was longer, cells grown onto Ag-TiN_x electrodes were capable to proliferate and also differentiate at desirable rates, indicating the suitability of this coating for sensor application in prostheses devices. So, it was possible to conclude that the silver nanoparticles on the top of TiN2AgR sample, has a significant effect on cells response and Ag-TiN_x electrodes are promising electrodes for tissue engineering applications in the design of sensors for prostheses application to detect dynamic mechanical loads.

Keywords: *Sensors, Ag nanoparticles, piezoelectric polymers, sputtering, MC3T3 osteoblastic cells.*

7.1 Introduction

Innovative materials are increasingly being designed in order to identify novel strategies to improve the current therapeutic treatments for biomedical applications. Synthetic and natural polymers are compounds of large interest in many fields, especially in the biomedical area [1,2]. They have been extensively used in the past as materials for smart prostheses and sensors, among others, since they are particularly suited to interface with cells, characteristic that allows their use in a broad range of tissue engineering applications [3,4].

An illustration of that advancement relays on the use of piezoresistive [5,6] and piezoelectric materials as strain and force sensor [7] for diverse applications. These sensors are adequate for the design of prostheses, especially because piezoelectric materials do not require external power supply [8], providing energy to the circuit and maintaining the system active for longer periods of time [9,10].

Poly(vinylidene fluoride) (PVDF) has been extensively studied since 1970 [11] for applications in the field of sensors and actuators , and more specifically, for biomedical applications [12], including implantable devices [13]. PVDF is a chemically stable thermoplastic fluoropolymer synthesized by the polymerization of vinylidene difluoride. PVDF β phase is the one that possesses the largest effective dipole moment and is being used for pressure sensing applications [3,13–17], energy generation and storage and, due to its biocompatibility, also for biomedical applications and tissue engineering [12,18]. However, despite of the excellent properties of piezoelectric PVDF for sensor and actuator applications, there is still a need to improve its properties by surface functionalization for acquiring or applying the electrical signal from/to the piezoelectric material.

Taking into account the properties of the individual elements, titanium nitride (TiN), titanium doped with silver ($Ti_{1-x}Ag_x$) and titanium nitride doped with silver (Ag-TiN_x) systems were selected for this study. These systems [17,19,20] have been successful deposited by sputtering on PVDF substrates, maintaining the piezoelectric response of the polymer. TiN, produced by either chemical vapour deposition (CVD) or physical vapour deposition (PVD) methods, shows excellent biocompatibility, supporting cell adhesion and proliferation and being suited for orthopaedic implants or blood contacting materials [21]. Regarding biomedical applications, Ag-TiN_x [22–24] and $Ti_{1-x}Ag_x$ [25,26] coatings have been proposed for prosthesis pressure sensors and dry biopotential electrodes, respectively, due to their specific electrical and biological properties.

When sensors are designed for being used inside the human body, their constituted materials should not be simply passively tolerated by the cells, but should actively provide an appropriate environment to facilitate cellular contacts [27], be biocompatible, bioactive and ideally possess antibacterial properties. Titanium and its alloys have been used for many years as component of dental, orthopaedic and cardiovascular prostheses due to its mechanical stability and biocompatibility [28,29]. Further, silver is a well-known antibacterial agent [30–33] and also allows tuning the electrical response [3]. A recent study [20], showed comparison of $Ti_{1-x}Ag_x$ and Ag-TiN_x series, reporting that only Ag-TiN_x series presented antibacterial activity.

In this work the biological activity of titanium nitride (TiN), titanium doped with silver ($Ti_{1-x}Ag_x$) and titanium nitride doped with silver (Ag-TiN_x) electrodes deposited by magnetron sputtering on PVDF substrates was analyzed by examining cell behavior of mouse MC3T3-E1 osteoblastic cell line. Multiple phenotypic features including initial adhesion, morphology, long term growth and functional differentiation were examined.

7.2 Materials and methods

7.2.1 Electrodes preparation

$Ti_{1-x}Ag_x$, Ag-TiN_x and TiN coatings were deposited by dc/pulsed dc magnetron sputtering onto PVDF thin films with a thickness of approximately 28 μm (28 micron PVDF uniaxial stretched and poled unmetallized, Precision Acoustics Ltd). One pure Ti target (99.99 %) and one Ag target (99.99 %) (both with 200 nm x 100 mm) were used in Ar + N_2 mixtures, with the substrates rotating at 70 mm from the target at a constant speed of 7 rpm. During deposition, the argon flow was kept constant at 60 sccm while the reactive gas flow, N_2, was 2 and 6 sccm for Ag-TiN_x sample and TiN, respectively. The current density (J) applied to each target was maintained constant, 7.5 mA/cm^2 for Ti target and 0.05 mA/cm^2 for Ag target, for $Ti_{1-x}Ag_x$ and Ag-TiN_x, respectively. Further details concerning these depositions can be found elsewhere [17,19,20]. For TiN sample the current density applied to Ti target was 10 mA/cm^2. The Ti target was connected to the pulsed dc power supply, while the Ag target was connected to a dc power supply. The frequency and reverse time were fixed at 200 kHz and 1536 ns, respectively, corresponding to a duty cycle of 69 %. The deposition time was varied in order to obtain a final thickness between 122 and 227 nm.

In order to avoid the structural damage of the polymer substrate, the substrate temperature must be ideally kept below ≈100 °C (far from the melting temperature of PVDF) [14]. In this sense, the depositions were performed without any external heating of the substrate and no bias polarization was applied on the substrate holder.

7.2.2 Electrodes characterization

The surface thickness and morphology were examined by scanning electron microscopy (SEM) through a NanoSEM – FEI Nova 200 (FEG/SEM) and chemical composition estimation was performed with an EDAX - Pegasus X4M - Energy dispersive spectrometer (EDS) apparatus coupled to SEM. Since the depth of analysis at 10 kV is about 300 nm for pure Ag and 700 nm for Ti, coatings with 1 μm of thickness were deposited onto silicon (Si) substrates for EDS analysis [17,19].

In order to study the topography of the surfaces, roughness of Ti based coatings were measured from Atomic force microscopy (AFM) images (size 5 μm × 5 μm). The root-mean-square average of height deviations taken from the mean image data plane (Rq) was calculated using the roughness subroutine in the NanoScope III apparatus (Digital Instruments) operating in tapping mode. The roughness values are an average of three measurements. AFM analyses were performed on silicon and PVDF substrates.

The wettability of the different electrodes was determined using a contact angle meter apparatus (OCA 15 Plus, Dataphysics). All measurements were performed at room temperature and two microliters drops of pure water (polar liquid); formamide (polar liquid, Sigma) and α-bromonaphthalene (apolar liquid, Sigma), with known surface energy components [34,35], were used as reference liquids. The surface free energy was determine using the van Oss approach [36].

7.2.3 Fibronectin adsorption

To analyze fibronectin, FN adsorption on material surfaces, samples were covered with FN from human plasma (Sigma Aldrich) from a solution of concentration 20 μg/mL in DPBS for 10 minutes. After adsorption samples were rinsed in PBS to eliminate the non-adsorbed protein. Atomic force microscopy (AFM) was performed in a Multimode AFM equipped with NanoScope III apparatus (Digital Instruments) operating in tapping mode in air on PVDF substrates without and with FN coating.

For the cell culture experiments, die-cast circular samples were obtained of different materials evaluated composed by PVDF coated with different coatings acting as electrodes. Sample disks (12 mm diameter) were coated with FN 20 µg/ml (1 h at room temperature to complete saturation).

7.2.4 Biological evaluation of the electrodes

7.2.4.1 Cell culture

Prior to seeding on FN-coated substrates the samples were exposed to ultraviolet (UV) light for 1 h in order to sterilize samples. Murine MC3T3-E1 osteoblast cells (RIKEN cell bank, Japan) were maintained in a Dulbecco's Modified Eagle Medium (DMEM, Invitrogen) supplemented with 10 % fetal bovine serum (FBS, Invitrogen) and 1 % penicillin–streptomycin (P/S, Lonza) in a humidified atmosphere at 37 °C and 5 % CO2, and passaged twice a week using standard techniques before cells reached confluence.

In all experiments performed, density of seeding was 10.000 cells/cm2, for cell adhesion and differentiation experiments, and 50.000 cells/cm2 for proliferation assays. Cells were initially cultured for 3 h in the absence of serum in culture medium in order to direct initial cell attachment only with deposited FN onto materials. Each experiment was performed in triplicate. Glass coverslips of 12 mm diameter were used as control substrates in all experiments performed.

7.2.4.2 Cell adhesion

To examine initial cell adhesion, cells were washed after 3 h of culture in Dulbecco's phosphate buffered saline (DPBS, Invitrogen) and fixed in 10 % formalin solution (Sigma) at 4 °C for 30 min. Samples were then rinsed with DPBS and incubate with permeabilization buffer (10.3 g sucrose, 0.292 g NaCl, 0.06 g MgCl2, 0.476 g Hepes buffer, 0.5 ml Triton X-100, in 100 ml water, pH 7.2) at room temperature for 5 min. To reduce the background signal, samples were incubated in 5 % Goat Serum (GS, Invitrogen)/DPBS/TritonX-100 0.1 %, 5 minutes at room temperature and subsequently incubated with the primary antibody anti-vinculin (Sigma, dilution 1:400) for 1 h at 37 °C. Then, they were washed with DPBS/Triton X-100 0.1 % and then incubated with a secondary antibody anti-mouse-Cy3 (Santa Cruz Technologies, dilution 1:200) and with BODIPY® FL phallacidin (1:400, molecular probes) for 1 h at 37 °C. Finally samples were rinsed in DPBS four times for 5 min each before being mounted in Vectashield containing DAPI staining (Vector Laboratories). A

Leica DM6000B fluorescent microscope was used. The image system was equipped with a Leica DFC350FX camera.

7.2.4.3 Cell proliferation

MTS quantitative assay (The CellTiter 96 Aqueous One Solution Cell Proliferation Assay, Promega) was performed in order to assess proliferation of MC3T3-E1 cells onto PVDF coated with TiN, $Ti_{1-x}Ag_x$ and Ag-TiN_x coatings. Cells in a concentration of 50.000 cells/cm^2 were seeded onto different substrates and metabolic activity was measured after 24 h. After, cells were incubated 3 h with MTS (tetrazolium salt) at 37 °C and the formation of formazan product was followed by measuring absorbance at 490 nm. All measurements were performed in triplicate. The percentage of cellular viability was calculated using the Equation 3:

$$\%\ Prolif. = \frac{OD_{490S}}{OD_{490C}} \times 100 \qquad \text{Equation 3}$$

Where OD_{490S} means the measured optical density of the sample (cells growth in the presence of sample) and OD_{490C} means the measured optical density of the control (medium without cells).

7.2.4.4 Cell differentiation

After 3 h of culture, the basal medium was changed to DMEM medium supplemented with 10% FBS and 1 % P/S for 48 h until MC3T3-E1 cells reached confluence to favor differentiation conditions. After that, cells were stimulated to differentiate with osteogenic differentiation medium (1 % P/S + 10 % FBS + Ascorbic acid, 50 μg/ml + β-Glycerophosphate, 10 mM + Dexamethasone, 0.1 μM). Osteogenic markers were evaluated after 15 days of culture except Runt-related transcription factor 2 (Runx2) that was analyzed after 3 days. Immunostaining procedures were performed as explained above (see 7.2.4.2-cell adhesion) but using different antibodies indicated in Table 7.1.

Table 7.1 – Primary and secondary antibody used for the differentiation experiments

Osteogenic differentiation	Primary antibody	Secondary antibody
Runx2	Anti-runx2 rabbit anti-mouse (0.9 mg/ml) (Sigma, dilution 1:200)	Alexa fluor 488 Goat anti rabbit (Life Technologies, dilution 1:100)
OPN (Osteopontin)	OPN mouse monoclonal IgG1 (200 µg/ml) (Santa Cruz biotechnology, dilution 1:200)	Alexa fluor 488 goat anti mouse (2 mg/ml)(Life Technologies, dilution 1:200)
OCN (Osteocalcin)	Rb pAb to osteocalcin (1 mg/ml)(Santa Cruz biotechnology) (dilution 1:200)	Alexa fluor 488 Goat anti rabbit (Life Technologies, dilution 1:200)

7.2.5 Image analysis

Images from the fluorescence microscope (DAPI channel - nuclei, and FTIC channel - OCN or OPN detection) of the MC3T3 culture were acquired at 10x magnification (n = 10), transformed to an 8-bit grayscale bitmap (Fiji-ImageJ software) and segmented using the Trainable Weka Segmentation plugin to create a binary mask, for both DAPI and FTIC channels. Total nuclei per image or total expression of OCN/OPN were counted using the particle analysis command.

7.2.6 Statistical analysis

Results are shown as mean ± standard deviation (SD). Differentiated cell quantification was analyzed by ordinary one-way ANOVA test using a Tukey's multiple comparisons test. $p < 0.05$ was considered significant and indicated with an asterisk on each figure. All experiments were performed at least per triplicate.

7.3 Results and discussion

7.3.1 Electrodes characterization

Table 7.2 represents synthesis conditions, coating´s chemical composition and thickness of the deposited electrodes.

Table 7.2 – Chemical composition, current density applied to titanium (J_{Ti}) and silver (J_{Ag}) targets, thickness, roughness (coating performed on silicon substrates) and some experimental details on thin film electrode deposition

Coatings	N_2 flow (sccm)	J_{Ti} (mA/cm²)	J_{Ag} (mA/cm²)	Thickness on polymers (nm)	Chemical Composition (at. %)			N/Ti	Roughness (nm)
					Ti	*Ag*	*N*		
TiN	6	10	0	122.5	57	0	43	0.75	3.24
Ag/Ti (0.11)R	0	7.5	0.05	200.8	93	7	0	-	3.55
TiN2AgR	2	7.5	0.05	227.5	61	5	34	0.56	21.00

Using these deposition conditions it was possible to obtain a sub-stoichiometric TiN coating. The characterization of similar coatings of $Ti_{1-x}Ag_x$ systems, like Ag/Ti (0.11)R electrodes and for Ag-TiN_x systems, like TiN2AgR electrodes, were already discussed [17,19]. Further details concerning the chemical composition versus deposition parameters, of similar samples, can be found elsewhere [17,19].

In fact, the differences between Ag/Ti (0.11)R and TiN2AgR samples, are originated from the type of bond that silver promotes. Ag/Ti (0.11)R sample presents higher amount of Ti (93%), so Ti bonds with Ag until the latter is consumed and the remaining Ti stays in a crystalline metallic form. For the TiN2AgR sample, since silver presents a very low affinity to bind with nitrogen [19,24,37], Ti bonds to nitrogen forming a sub-stoichiometric TiN matrix with incorporated silver nanoparticles, as it is possible to observe in SEM micrographs in Figure 7.1.

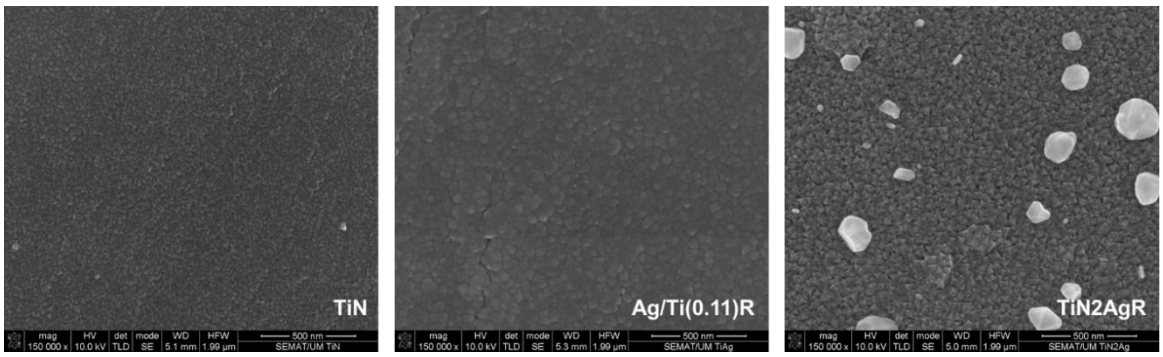

Figure 7.1 - SEM micrographs on SE mode of the different electrodes. Scale bar is 500 nm.

Similar behaviour has been observed before, showing that co-deposition of Ag and TiN [38], TiO2 [39] and TiCN [40] leads to the formation of Ag nanoparticles incorporated in a matrix coating.

Figure 7.1 shows representative SEM micrographs of the characterized coatings on which it is possible to observe that TiN and Ag/Ti(0.11)R samples are homogenous without Ag clusters.

These results are in line with previous works [17,19], suggesting the formation of a crystalline TiAg phase, combined with crystalline hcp-Ti and cannot be excluded a fcc-Ag phase. In TiN2AgR, it is possible to detect Ag clusters on the top of the TiN matrix. This phenomenon [19] is correlated with the immiscibility of Ag in a matrix like TiN. Also the suppression of the TiAg intermetallic phase is explained by the higher enthalpy of formation of TiAg in comparison with TiN phase (-1.6 kJ/mol and -330 kJ/mol, respectively). So, Ti will favorably bind to N atoms and Ag will grow as a second phase [19].

Figure 7.2 shows tapping-mode AFM images (height images) of the different electrodes deposited on silicon substrates.

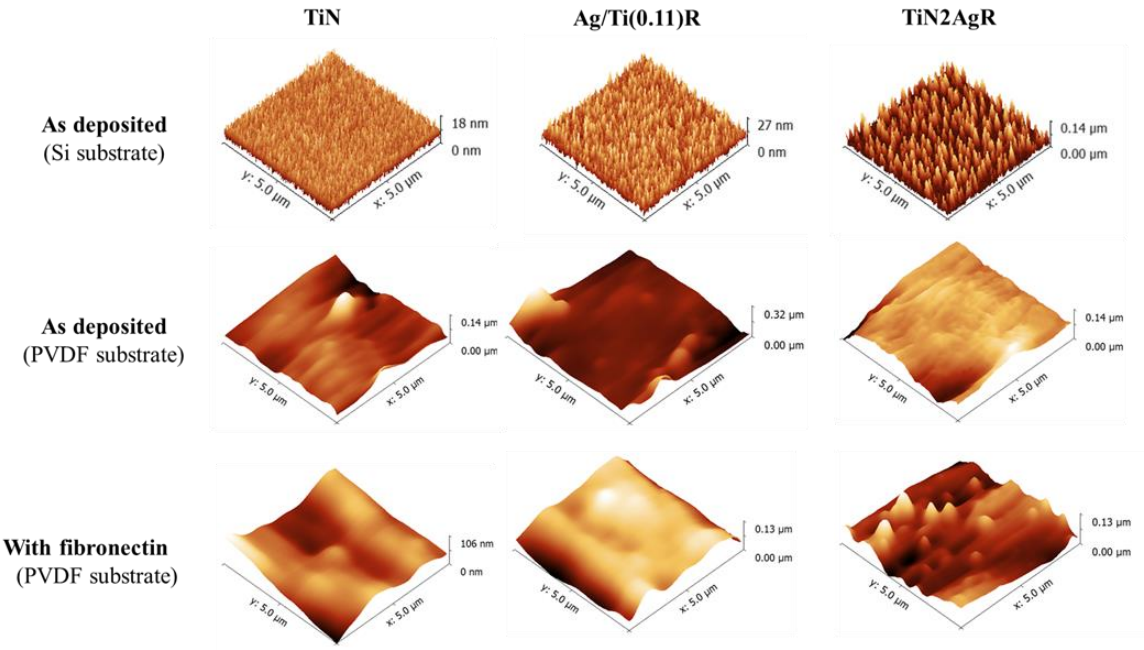

Figure 7.2 - Tapping-mode AFM images (height) of different electrode coatings deposited by magnetron sputtering on silicon and poled PVDF-β substrates as deposited and after coating with FN (20 µg/ml) with a scan range of 5 µm x 5 µm.

The results show that while TiN and Ag/Ti(0.11)R coatings present similar roughness values between 3.24 and 3.55 nm, respectively, AgTiN2R sample show a roughness of 21.00 nm due to the presence of silver nanoparticles on the top of the surface of the thin film in agreement with the SEM micrographs presented on Figure 7.1.

As for all biological experimental conditions tested on this work samples were coated with FN, a component of ECM that enhances initial cell attachment and subsequent cell behavior, the topography of the different electrode coatings was analyzed and compared after FN adsorption.

Figure 7.2 shows the surface topography of different electrodes as deposited on PVDF and after adsorption of FN (20 μg/mL).

AFM images showed that the characteristic roughnesses of the coatings were not altered by the presence of FN.

The surface hydrophobicity of the different electrodes was assessed by contact angle measurements and the results are summarized in Table 7.3. According to the van Oss approach [36], the hydrophobicity of a given material is defined by the variation of the free energy (ΔG) of interaction between the materials surfaces immersed in water (w). When ΔG is negative, the free energy of interaction between molecules is attractive, revealing a superior interaction molecule-molecule then with water, so the material surface is hydrophobic.

Table 7.3 - Water (θ_W), formamide (θ_F) and bromonaphtalene (θ_B) contact angles, surface energy components (apolar Lifshitz-van der Walls free energy component (γ^{LW}), electron acceptor surface energy component (γ^+) and electron donor surface free energy component (γ^-) and degree of hydrophobicity (ΔG) of the different electrodes deposited onto PVDF substrates

Electrodes	*Contact angle ± SD[a] (deg)*			*Surface energy components (mJ m^{-2})*			*ΔG (mJ m^{-2})*
	θ_W	θ_F	θ_B	γ^{LW}	γ^+	γ^-	
TiN	*108.6±4.1*	*73.1±4.1*	*28.0±8.5*	*39*	*0*	*0*	*-107.2*
Ag/Ti(0.11)R	*99.5±2.9*	*80.8±3.4*	*24.5±3.1*	*41*	*0*	*2*	*-81.0*
TiN2AgR	*118.5±2.1*	*94.9±7.0*	*15.5±1.4*	*43*	*0*	*0*	*-109.0*

The water contact angles obtained for the different coatings (Figure 7.3) are higher than 90°, suggesting a hydrophobic character [41,42], also confirmed by the negative values of ΔG.

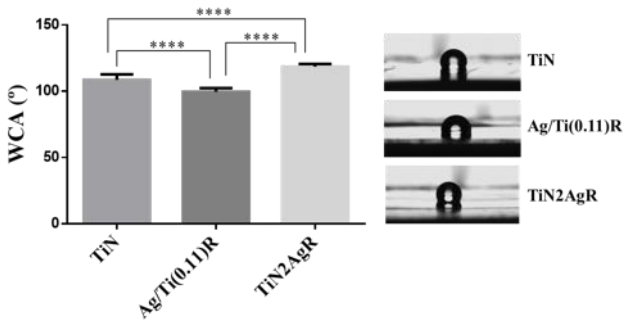

*Figure 7.3 - Water contact angle of different samples expressed as a mean ± standard deviation. Significant values as ****p < 0.0001.*

7.3.2 Cell behavior on the deposited electrodes

7.3.2.1 Cell adhesion

Cells were cultured without serum for 3 h in order to avoid adsorption of other proteins from the serum in competition with FN previously adsorbed on the substrate. Then, the development of F-actin fibers and vinculin detection as a marker of focal adhesion protein was investigated as a function of the different electrodes deposited onto PVDF (Figure 7.4).

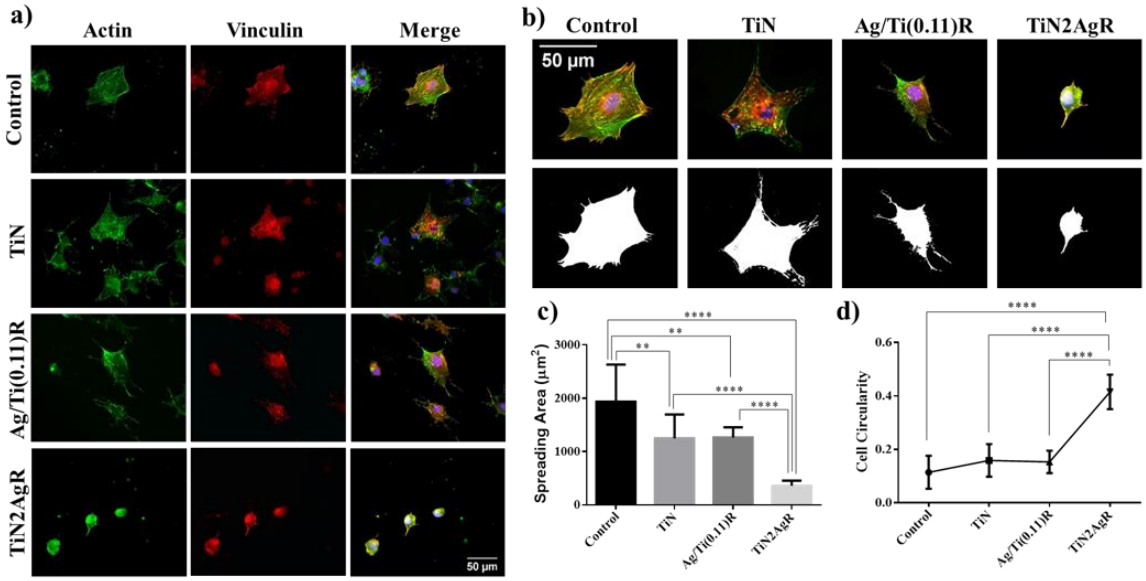

*Figure 7.4 - a) Adhesion of MC3T3-E1 cells after 3 hours of culture on FN coated substrates and control (glass). The first column shows F-actin cytoskeleton (green) and the second one vinculin (red). Nuclei were counterstained with DAPI. b) Magnification of images as an example of sequential process followed for binary mask creation for analysis of spreading area (c)) and circularity (d)) parameters. Data was represented as mean ± standard deviation. Significant values as ****p < 0.0001, **p = 0.003. Scale bar is 50 µm.*

It is interesting to note that the state of the actin cytoskeleton strongly depends on the presence of Ag particles in contact with cells. F-actin cytoskeleton was well developed in cells cultured on TiN and Ag/Ti(0.11)R electrodes, similarly to the control glass. In contrast, no actin fibers were found in cells cultured on the TiN2AgR electrode, although the ring around the cell periphery, characteristic of the initial stages of F-actin polymerization [43] is clearly visible (Figure 7.4b).

The organization into focal adhesions and integrin clustering, comes from the ability to form stable links between the extracellular matrix and the actin cytoskeleton [44]. Well-defined focal adhesions were found on the control glass, TiN and Ag/Ti(0.11)R samples, consequent with the development of the actin cytoskeleton. In contrast, vinculin is not organized into focal adhesions on the TiN2AgR sample, but randomly distributed throughout the cell.

Moreover, cell morphology depends strongly on the presence of Ag particles on TiN2AgR coating: cells tend to be more rounded and lacking defined focal contacts. The morphologic parameter circularity was calculated by image analysis and it is shown in Figure 7.4.

The results are in line with those obtained in previous works such as reported by Huang et al. [45] describing that cell adhesion of TiN coated titanium for dental applications was higher when compared to bare Ti surfaces, the gold standard biocompatible metal used in clinical applications [46]. The results obtained in Ag/Ti(0.11)R electrodes were similar to those observed on TiN.

One could argue that it should be expected differences due to the Ag content of the coating, but as silver in the Ag/Ti(0.11)R electrodes is bonded to Ti, the Ag particles appear hidden and do not interact directly with cells (no silver on the top of the surface can be observed (Figure 7.1). On the contrary, in TiN2AgR electrodes, Ag nanoparticles are on the surface (Figure 7.1), a fact that seems to reduce initial cell adhesion in terms of cytoskeleton development, diffuses focal adhesion contacts and consequently leads to severe changes in cell morphology.

Moreover, it could also be argued that adhesion results seem to correlate with surface roughness. For Ag/Ti(0.11)R electrode, the results are very similar to those observed on TiN, The topography of these two samples are quite similar (Table 7.2 and Figure 7.2) due to the fact that silver in the Ag/Ti(0.11)R electrode is bonded to Ti, the surface becomes smoother, which do not interfere negatively onto cells adhesion. Nevertheless, TiN2AgR electrodes present two main differences with respect to the other two coatings: the chemical structure of the surface showing Ag nanoparticles and the consequent rough topography. Nanoscale structure of the material surface has been found to have positive effects on osteoblast cell response, including initial cell adhesion and subsequent proliferation and expression of differentiation markers. A common theme of cellular adhesion on nanoscale protrusions is the observation of a decrease in cellular adhesion with increasing nanoprotrusion height >70 nm [47] while reducing the height of nanoprotrusion to less than 50 nm has been shown for numerous cell types to return the frequency of focal-adhesion formation to that of cells cultured on planar controls [48]. Therefore, as the sputtered coatings are in range lower than 50 nm (3 nm to 21 nm), the topography is not considered as the main material property influencing the observed cell behavior, but the chemical structure of the coatings in terms of presence of Ag nanoparticles is acting instead.

Ag nanoparticles act as antibacterial agent [20] and also affect cell adhesion. Indeed, the results are consistent with those obtained in the work of Cao et al. [30] that showed the influence of silver nanoparticles in cell adhesion and proliferation, reporting round morphology of cells and diminished F-actin and vinculin expression.

In order to investigate possible long term effects of Ag particles in cell adhesion, MC3T3-E1 cells were cultured for 15 days. Figure 7.5 shows results of actin staining and vinculin detection.

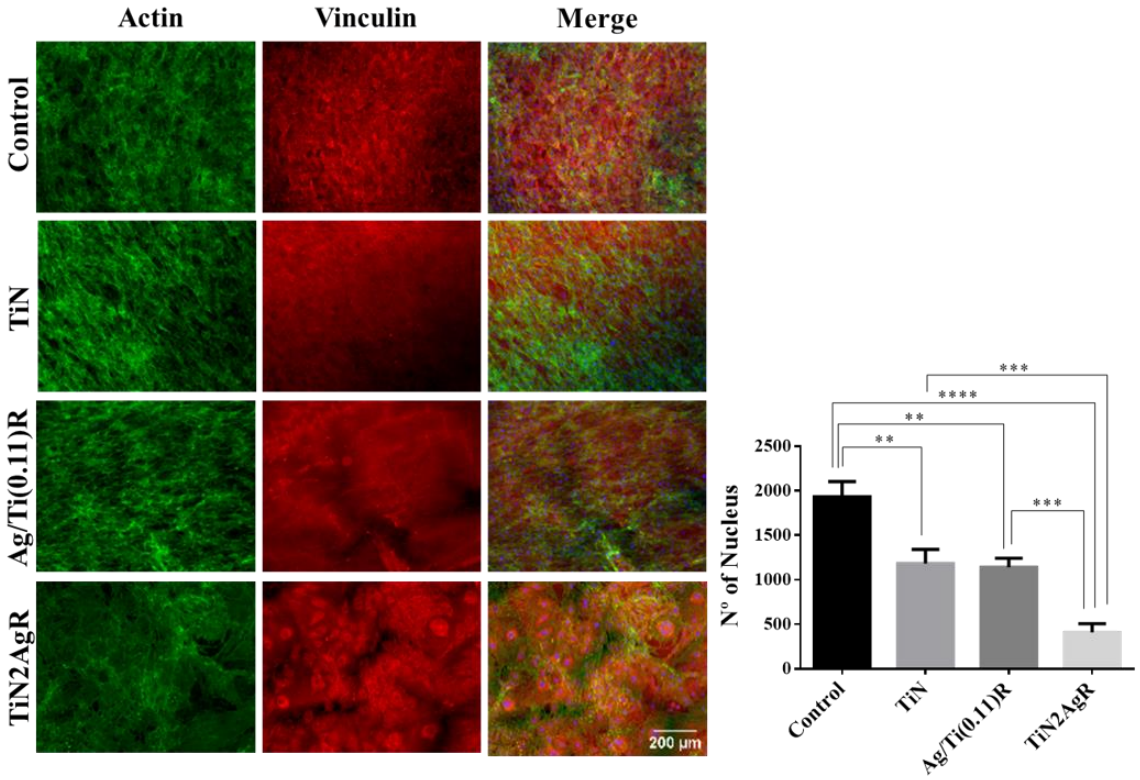

*Figure 7.5 - Adhesion of MC3T3-E1 cells after 15 days of culture on FN coated substrates. The first column shows F-actin cytoskeleton (green) and the second one vinculin (red). Nuclei were counterstained with DAPI. Scale bar is 200 µm. Graph shows quantification of number of nuclei for each substrate represented as mean ± standard deviation. Significant values as ****p < 0.0001, ***p < 0.001, **p < 0.01, *p < 0.05.*

Although the number of cells on TiN2AgR coating were lower when compared to TiN and Ag/Ti(0.11)R coatings, it is considered that the quantity observed is enough for re-population of the affected area when prostheses implantation occurs. The fact that TiN2AgR coatings could maintain low rates of cell adhesion at the beginning of the implantation and at the same time possesses antimicrobial activity [20] confers to this coating an evident advantage: avoid side infections due to clinical intervention while sensors allow measuring mechanical signals maintaining minimal number of cell attachment at the beginning, and at the same time, maintaining the capability of recovering cell population necessary for tissue regeneration and healing after initial intervention.

7.3.2.2 Cell proliferation

MTS assay was used to assess possible cytotoxic effect of surfaces and proliferation rates (Figure 7.6). Comparing the different sputtered coatings, the highest proliferation rates occur in the TiN electrode with similar levels to the control glass. Further, the percentage of proliferation decreases with increasing Ag content in the samples, in particular in the TiN2AgR sample, which presents silver nanoparticles at the surface of the film.

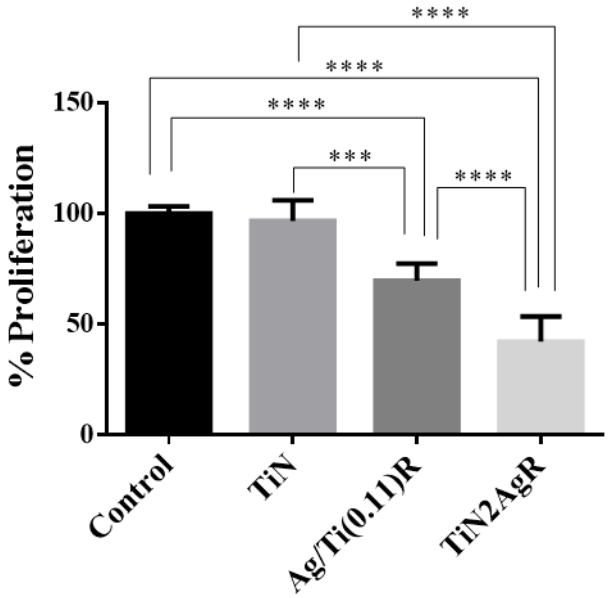

*Figure 7.6 - Proliferation rates of the MC3T3-E1 cells on the different surfaces after 24 h of cell culture represented as mean ± standard deviation. Significant values as ****p < 0.0001, ***p = 0.0001.*

The proliferation results are in line with those obtained by Cao et al.[30] wherein proliferation rates tend to decrease with the presence of Ag nanoparticles. Although the proliferation trend of the cells seems to be affected by Ag presence, the capability of cellular division is not altered at all, indicating that the coatings are not cytotoxic and the TiN2AgR electrode is capable to support regeneration of the cell population. Also in this case, topography does not seem to affect proliferation, as the proliferation rates observed for the Ag/Ti(0.11)R coating diminished in comparison to TiN and the control glass substrates. The results seem again to be correlated with the presence of Ag on the samples with an increased effect observed on the samples with Ag nanoparticles at the surface.

7.3.2.3 Cell differentiation

The evaluation of different transcription factors and specific gene expression as markers for osteoblast differentiated cells is a valuable method to assess the biologic activity of biomaterials and their potential ability to stimulate the growth of bone tissue in the process of implant osteointegration.

Runx2 is a specific transcription factor [49] that controls expression of a wide range of genes within the osteoblast phenotype (Osteocalcin, Osteopontin among others). Numerous studies have indicated its importance in the skeletal development of numerous mammalian organisms [50].

OCN (Osteocalcin) and OPN (Osteopontin) are osteoblast genes that promote osteoblast phenotype. OCN is one of the few osteoblast specific genes and is one of the most abundant proteins present in bone. It is thought to play an important role in the differentiation of osteoblast progenitor cells, with significant up-regulation observed in both matrix synthesis and mineralization. OPN is a secreted adhesive glycophosphoprotein that has been detected within bone, teeth, kidneys, epithelial lining tissues, blood plasma and breast milk. As a consequence, osteopontin cannot be considered bone specific, although it does perform important bone related functions. Within bone tissue it plays key functions in cell: adhesion, migration and survival [49,50].

Thus, to further evaluate the biological activity of different sputtered coatings onto PVDF, different osteoblast specific markers were analysed. Protein detection was realized by immunofluorescence after 15 days of culture for OPN and OCN, while Runx2 was detected after 3 days of culture due to its role as an early expression transcription factor in osteogenesis. Intensity of staining of Runx2 expression is represented on Figure 7.7.

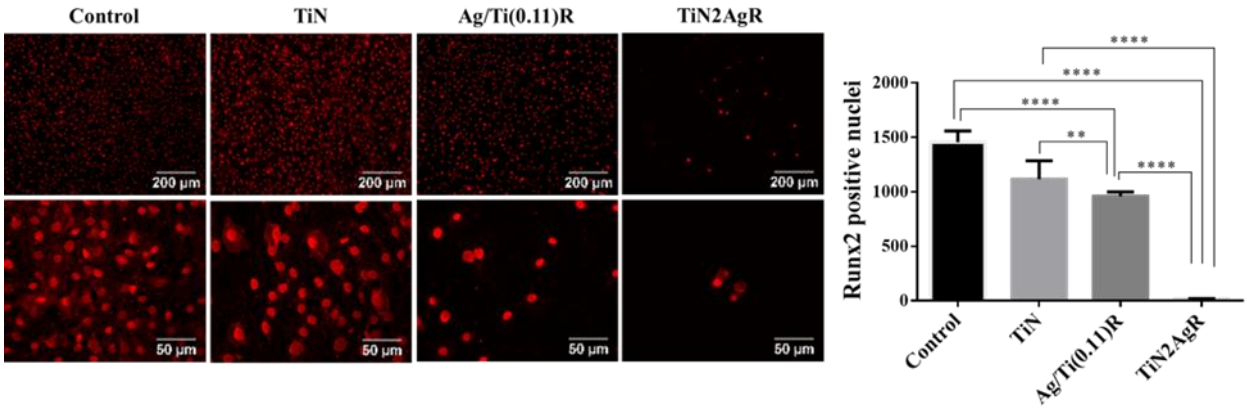

*Figure 7.7 - Fluorescence microscopy images showing expression of Runt-related transcription factor 2 (Runx2) as red inside the nucleus. Scale bar on the top row is 200 µm and bottom row represents a magnification with a scale bar of 50 µm. Graph shows quantification of number of nuclei expressing Runx2 represented as mean ± standard deviation. Significant values as ****p < 0.0001, **p < 0.01.*

Both Ag/Ti(0.11)R and TiN2AgR FN-coated electrodes showed lower levels of Runx2 staining when compared with the positive control (glass) and the TiN electrode, indicating again a strong effect directly dependent on the presence of Ag nanoparticles, being more pronounced on TiN2AgR electrode. In contrast Runx2 levels were similar between glass control and TiN electrode showing no significant differences.

Other osteogenic markers such as OCN and OPN were also analyzed, leading to similar results. Ag/Ti(0.11)R and TiN2AgR electrodes showed lower levels of staining, although in these cases the expression of these osteogenic markers become less affected by the effect of Ag particles, resulting in similar levels of staining between silver-containing coatings (Figure 7.8).

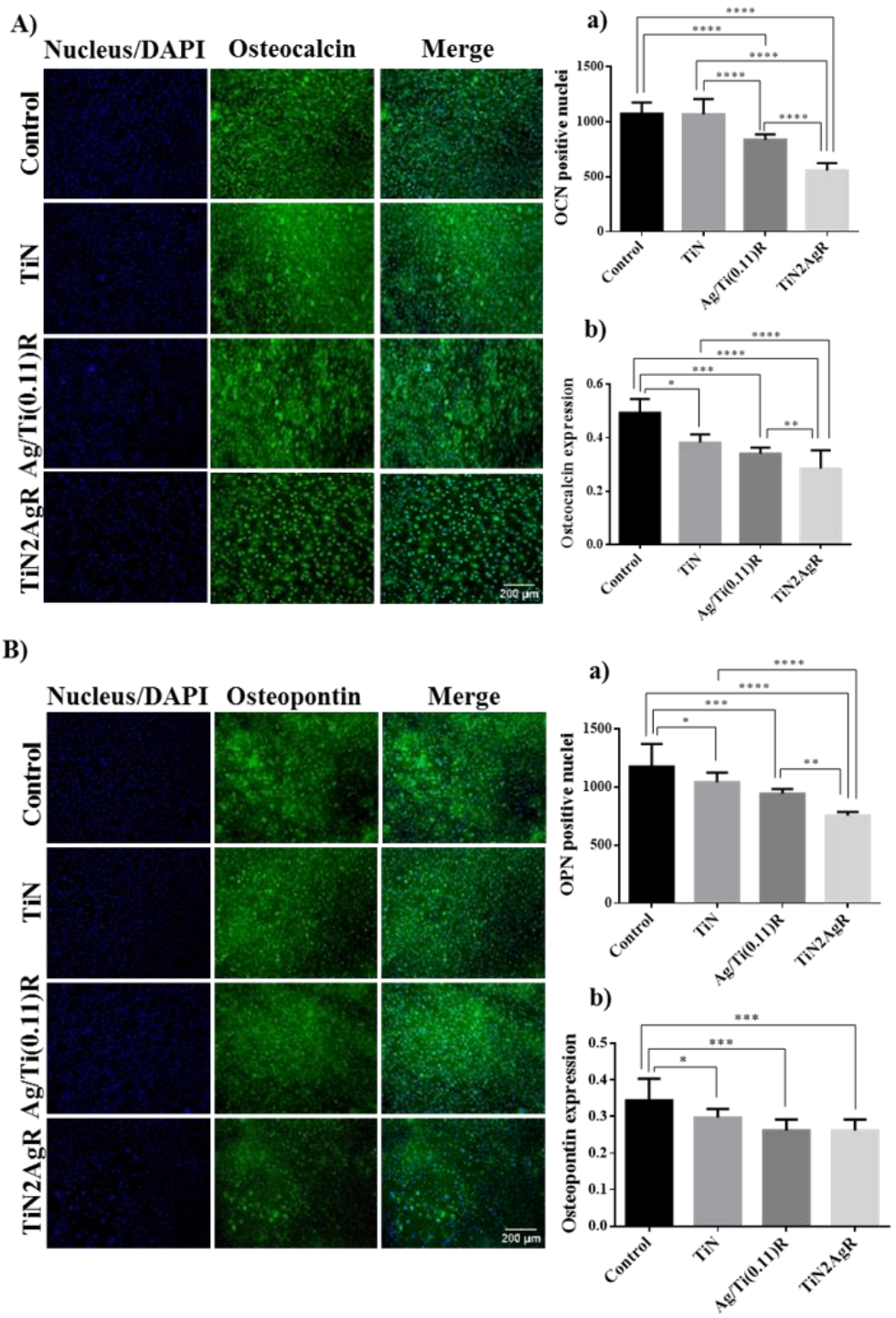

*Figure 7.8 - Fluorescence microscopy images showing expression of Osteocalcin (A) and Osteopontin (B) as green. Nucleus are showed as blue. Scale bar on the bottom is 200 µm. Graph shows number of nuclei (a) and OCN and OPN quantification (b) represented as mean ± standard deviation. Significant values as ****p < 0.0001, ***p < 0.001, **p < 0.01, *p > 0.05.*

The fact that we found in all the quantified experiments lower cell levels on TiN2AgR electrodes, probably due to a delay on initial cell adhesion and spreading, consequently originates lower levels of osteogenic markers analyzed.

Differences obtained between Runx2 expression and other osteogenic markers used in this work could be explained if we consider other transcription factors controlling gene expression of OCN and OPN such as Osterix (Osx). Osx regulates numerous osteoblast genes including OCN and OPN, and it may also act in conjunction with other regulators such as Runx2 although Osx may act downstream or independently of Runx2 [39].

Overall, it was observed that after two weeks of induction under osteogenic conditions, significant OCN and OPN expression levels, though presence of silver nanoparticles at the surface of the film (TiN2Ag sample) results in a significant decrease of osteoblast differentiation markers. Similar results have been reported by Shtansky at al. [51], in a study of TiCaPCON films doped with Ag and Cu in which cells adhere, proliferate and differentiate onto films with 0.4 and 1.2 at.% of Ag. When Ag contents were above 4 at.%, attachment of the cells became lower, even with death of some cells and a significant reduction of osteoblastic differentiation markers was observed [51].

7.4 Conclusions

The main objective of this work was to evaluate the biological activity, in terms of osteogenic induction, of $Ti_{1-x}Ag_x$ and Ag-TiN_x electrodes, deposited by d.c. and pulsed magnetron sputtering on poly(vinylidene fluoride), PVDF, using MC3T3 osteoblastic cells.

The results indicate that the electrode which presented lower initial adhesion is the Ag-TiN_x system. Similar behavior was observed concerning proliferation and differentiation, where the Ag-TiN_x system presented the lower levels compared with TiN and control glass samples.

We can conclude that the presence of silver nanoparticles in the surface of Ag-TiN_x electrodes affects initial cell response in a significant way.

Taking into account the function of these electrodes for the development of sensors to detect mechanical loads on prostheses in an early stage, the Ag-TiN_x system showed the most promising behavior to use as electrode for this specific sensor application.

7.5 References

[1] J. Jagur-Grodzinski, Polymers for tissue engineering, medical devices, and regenerative medicine. Concise general review of recent studies, Polym. Adv. Technol. 17 (2006) 395–418. doi:10.1002/pat.729.

[2] K.S. Katti, Biomaterials in total joint replacement, Colloids and Surfaces. 39 (2004) 133–142. doi:10.1016/j.colsurfb.2003.12.002.

[3] R. Costa, C. Ribeiro, A.C. Lopes, P. Martins, V. Sencadas, R. Soares, et al., Osteoblast, fibroblast and in vivo biological response to poly(vinylidene fluoride) based composite materials, J. Mater. Sci. Mater. Med. 24 (2013) 395–403. doi:10.1007/s10856-012-4808-y.

[4] R. Ravichandran, S. Sundarrajan, J.R. Venugopal, S. Mukherjee, S. Ramakrishna, Advances in polymeric systems for tissue engineering and biomedical applications., Macromol. Biosci. 12 (2012) 286–311. doi:10.1002/mabi.201100325.

[5] V. Correia, V. Sencadas, M.S. Martins, C. Ribeiro, P. Alpuim, J.G. Rocha, et al., Piezoresistive sensors for force mapping of hip-prostheses, Sensors Actuators A Phys. 195 (2013) 133–138. doi:10.1016/j.sna.2013.03.013.

[6] P. Alpuim, V. Correia, E.S. Marins, J.G. Rocha, I.G. Trindade, S. Lanceros-Mendez, Piezoresistive silicon thin film sensor array for biomedical applications, Thin Solid Films. 519 (2011) 4574–4577. doi:10.1016/j.tsf.2011.01.300.

[7] V. Correia, C. Caparros, C. Casellas, L. Francesch, J.G. Rocha, S. Lanceros-Mendez, Development of inkjet printed strain sensors, Smart Mater. Struct. 22 (2013) 1–10. doi:10.1088/0964-1726/22/10/105028.

[8] A.H. Rajabi, M. Jaffe, T.L. Arinzeh, Piezoelectric Materials for Tissue Regeneration: A Review, Acta Biomater. 24 (2015) 12–23. doi:10.1016/j.actbio.2015.07.010.

[9] J. Nunes-Pereira, V. Sencadas, V. Correia, J.G. Rocha, S. Lanceros-Méndez, Energy harvesting performance of piezoelectric electrospun polymer fibers and Polymer/Ceramic composites, Sensors Actuators A Phys. 196 (2013) 55–62. doi:10.1016/j.sna.2013.03.023.

[10] J.G. Rocha, L.M. Gonçalves, P.F. Rocha, M.P. Silva, S. Lanceros-Mendez, Energy Harvesting From Piezoelectric Materials Fully Integrated in Footwear, Ind. Electron. IEEE Trans. 57 (2010) 813–819. doi:10.1109/TIE.2009.2028360.

[11] R. Gregorio Jr., R.C. Capitão, Morphology and phase transition of high melt temperature crystallized poly (vinylidene fluoride), J. Mater. Sci. 35 (2000) 299–306.

[12] C. Ribeiro, V. Sencadas, D.M. Correia, S. Lanceros-Méndez, Piezoelectric polymers as biomaterials for tissue engineering applications, Colloids Surfaces B Biointerfaces. 136 (2015) 46–55. doi:10.1016/j.colsurfb.2015.08.043.

[13] Y. Qin, M.M.R. Howlader, M.J. Deen, Y.M. Haddara, P.R. Selvaganapathy, Polymer integration for packaging of implantable sensors, Sensors Actuators, B Chem. 202 (2014) 758–778. doi:10.1016/j.snb.2014.05.063.

[14] P. Martins, A.C. Lopes, S. Lanceros-Mendez, Electroactive phases of poly(vinylidene fluoride): Determination, processing and applications, Prog. Polym. Sci. 39 (2014) 683–706. doi:10.1016/j.progpolymsci.2013.07.006.

[15] V.K. Tiwari, P.K. Kulriya, D.K. Avasthi, P. Maiti, Radiation-resistant behavior of poly(vinylidene fluoride)/layered silicate nanocomposites., ACS Appl. Mater. Interfaces. 1 (2009) 311–8. doi:10.1021/am800040q.

[16] S.M. Marques, C.J. Tavares, S. Lanceros-Mendez, Z. Denchev, X-ray Scattering Experiments on Sputtered Titanium Dioxide Coatings onto PVDF Polymers for Self-Cleaning Applications, J. Appl. Polym. Sci. 119 (2011) 726–731. doi:10.1002/app.

[17] S.M. Marques, N.K. Manninen, S. Ferdov, S. Lanceros-Mendez, S. Carvalho, Ti1−xAgx electrodes deposited on polymer based sensors, Appl. Surf. Sci. 317 (2014) 490–495. doi:10.1016/j.apsusc.2014.08.142.

[18] D.M. Correia, R. Gonçalves, C. Ribeiro, V. Sencadas, G. Botelho, J.L.G. Ribelles, et al., Electrosprayed poly(vinylidene fluoride) microparticles for tissue engineering applications, RSC Adv. 4 (2014) 33013–33021. doi:10.1039/C4RA04581E.

[19] S.M. Marques, N.K. Manninen, S. Lanceros-Mendez, S. Carvalho, Ag-TiNx electrodes deposited on piezoelectric poly(vinylidene fluoride) for biomedical sensor applications, Sensors Actuators A Phys. 234 (2015) 1–8. doi:10.1016/j.sna.2015.08.016.

[20] S.M. Marques, I. Carvalho, M. Henriques, T. Polcar, S. Carvalho, PVD-grown antibacterial Ag-TiN films on piezoelectric PVDF substrates for sensor applications, Surf. Coatings Technol. 281 (2015) 117–124. doi:10.1016/j.surfcoat.2015.09.057.

[21] S. Mandl, B. Rauschenbach, Improving the biocompatibility of medical implants with plasma immersion ion implantation, Surf. Coatings Technol. 156 (2002) 276–283.

[22] P. Pedrosa, C. Lopes, N. Martin, C. Fonseca, F. Vaz, Electrical characterization of Ag:TiN thin films produced by glancing angle deposition, Mater. Lett. 115 (2014) 136–139. doi:10.1016/j.matlet.2013.10.044.

[23] P. Pedrosa, D. Machado, C. Lopes, E. Alves, N.P. Barradas, N. Martin, et al., Nanocomposite Ag:TiN thin films for dry biopotential electrodes, Appl. Surf. Sci. 285 (2013) 40–48. doi:10.1016/j.apsusc.2013.07.154.

[24] P. Pedrosa, E. Alves, N.P. Barradas, N. Martin, P. Fiedler, J. Haueisen, et al., Electrochemical behaviour of nanocomposite Agx:TiN thin films for dry biopotential electrodes, Electrochim. Acta. 125 (2014) 48–57. doi:10.1016/j.electacta.2014.01.082.

[25] D. Machado, P. Pedrosa, C. Fonseca, N. Martin, F. Vaz, Structural and Morphological Changes in Ag:TiN Nanocomposite Films Promoted by In-Vacuum Annealing, J. Nano Res. 25 (2013) 67–76. doi:10.4028/www.scientific.net/JNanoR.25.67.

[26] C. Lopes, C. Gonçalves, P. Pedrosa, F. Macedo, E. Alves, N.P. Barradas, et al., TiAgx thin films for lower limb prosthesis pressure sensors: Effect of composition and structural changes on the electrical and thermal response of the films, Appl. Surf. Sci. 285 (2013) 10–18. doi:10.1016/j.apsusc.2013.07.021.

[27] J. Pärssinen, H. Hammarén, R. Rahikainen, V. Sencadas, C. Ribeiro, S. Vanhatupa, et al., Enhancement of adhesion and promotion of osteogenic differentiation of human adipose stem cells by poled electroactive poly(vinylidene fluoride), J. Biomed. Mater. Res. - Part A. 103A (2015) 919–928. doi:10.1002/jbm.a.35234.

[28] Y.-Y. Chang, H.-L. Huang, C.-H. Lai, J.-T. Hsu, T.-M. Shieh, A.Y.-J. Wu, et al., Analyses of Antibacterial Activity and Cell Compatibility of Titanium Coated with a Zr–C–N Film, PLoS One. 8 (2013) 1–8. doi:10.1371/journal.pone.0056771.

[29] M. Niinomi, Metallic biomaterials, J. Artif. Organs. 11 (2008) 105–110. doi:10.1007/s10047-008-0422-7.

[30] H. Cao, X. Liu, F. Meng, P.K. Chu, Biological actions of silver nanoparticles embedded in titanium controlled by micro-galvanic effects, Biomaterials. 32 (2011) 693–705. doi:10.1016/j.biomaterials.2010.09.066.

[31] P.J. Kelly, H. Li, K. a. Whitehead, J. Verran, R.D. Arnell, I. Iordanova, A study of the antimicrobial and tribological properties of TiN/Ag nanocomposite coatings, Surf. Coatings Technol. 204 (2009) 1137–1140. doi:10.1016/j.surfcoat.2009.05.012.

[32] C.F.A. Alves, F. Oliveira, I. Carvalho, a. P. Piedade, S. Carvalho, Influence of albumin on the tribological behavior of Ag–Ti (C, N) thin films for orthopedic implants, Mater. Sci. Eng. C. 34 (2014) 22–28. doi:10.1016/j.msec.2013.09.031.

[33] D.M. Eby, H.R. Luckarift, G.R. Johnson, Hybrid Antimicrobial Enzyme and Silver Nanoparticle Coatings for Medical Instruments, ACS Appl. Mater. Interfaces. 1 (2009) 1553–1560. doi:10.1021/am9002155.

[34] B. Janczuk, E. Chibowski, J.M. Bruque, M.L. Kerkeb, F. González Caballero, On the consistency of surface free energy components as calculated from contact angles of different liquids: an application to the cholesterol surface, J. Colloid Interface Sci. 159 (1993) 421–428.

[35] R. Oliveira, J. Azeredo, P. Teixeira, A.P. Fonseca, The role of hydrophobicity in bacterial adhesion, in: Hidrophobicity Bact. Adhes., BioLine, 2001: pp. 11–22. http://repositorium.sdum.uminho.pt/handle/1822/6706 (accessed September 11, 2015).

[36] C.J. Van Oss, R.F. Giese, The hydrophilicity and hydrophobicity of clay minerals, Clays Clay Miner. 43 (1995) 474–477. doi:10.1346/CCMN.1995.0430411.

[37] R.X. Wang, X.M. Tao, Y. Wang, G.F. Wang, S.M. Shang, Microstructures and electrical conductance of silver nanocrystalline thin films on flexible polymer substrates, Surf. Coatings Technol. 204 (2010) 1206–1210. doi:10.1016/j.surfcoat.2009.10.030.

[38] T. de los Arcos, P. Oelhafen, U. Aebi, a Hefti, M. Düggelin, D. Mathys, et al., Preparation and characterization of TiN–Ag nanocomposite films, Vacuum. 67 (2002) 463–470. doi:10.1016/S0042-207X(02)00232-4.

[39] V.S.K. Chakravadhanula, T. Hrkac, V. Zaporojtchenko, R. Podschun, V.G. Kotnur, a Kulkarni, et al., Nanostructural and functional properties of Ag-TiO2 coatings prepared by co-sputtering deposition technique., J. Nanosci. Nanotechnol. 11 (2011) 4893–4899. doi:10.1140/epjd/e2007-00186-5.

[40] R. Escobar Galindo, N.K. Manninen, C. Palacio, S. Carvalho, Advanced surface characterization of silver nanocluster segregation in Ag-TiCN bioactive coatings by RBS, GDOES, and ARXPS., Anal. Bioanal. Chem. 405 (2013) 6259–69. doi:10.1007/s00216-013-7058-z.

[41] I. Carvalho, M. Henriques, J.C. Oliveira, C.F. Almeida Alves, A.P. Piedade, S. Carvalho, Influence of surface features on the adhesion of Staphyloccocus epidermidis to Ag–TiCN thin films, Sci. Technol. Adv. Mater. 14 (2013) 1–10. doi:10.1088/1468-6996/14/3/035009.

[42] I. Carvalho, M. Henriques, S. Carvalho, New strategies to fight bacterial adhesion, in: A. Méndez-Vilas (Ed.), Microb. Pathog. Strateg. Combat. Them Sci. Technol. Educ., Formatex Research Center, 2013: pp. 170–178.

[43] B. Alberts, A. Johnson, J. Lewis, M. Raff, K. Roberts, P. Walter, Molecular Biology of the Cell, 4th ed., Garland Science, New York, 2002. http://www.ncbi.nlm.nih.gov/books/NBK21054/ (accessed October 19, 2015).

[44] J. Ballester-Beltrán, P. Rico, D. Moratal, W. Song, J.F. Mano, M. Salmerón-Sánchez, Role of superhydrophobicity in the biological activity of fibronectin at the cell–material interface, Soft Matter. 7 (2011) 10803–10811. doi:10.1039/c1sm06102j.

[45] L. Huang, J.L. Shotwell, H. Wang, Dental implants for orthodontic anchorage., Am. J. Orthod. Dentofacial Orthop. 127 (2005) 713–22. doi:10.1016/j.ajodo.2004.02.019.

[46] H.-H. Huang, C.-H. Hsu, S.-J. Pan, J.-L. He, C.-C. Chen, T.-L. Lee, Corrosion and cell adhesion behavior of TiN-coated and ion-nitrided titanium for dental applications, Appl. Surf. Sci. 244 (2005) 252–256. doi:10.1016/j.apsusc.2004.10.144.

[47] T. Sjostrom, M.J. Dalby, A. Hart, R. Tare, R.O.C. Oreffo, B. Su, Fabrication of pillar-like titania nanostructures on titanium and their interactions with human skeletal stem cells, Acta Biomater. 5 (2009) 1433–1441. doi:10.1016/j.actbio.2009.01.007.

[48] M. Dalby, S. Yarwood, M. Riehle, H. Johnstone, S. Affrossman, A. Curtsi, Increasing fibroblast response to materials using nanotopography: morphological and genetic measurements of

cell response to 13-nm-high polymer demixed islands, Exp. Cell Res. 276 (2002) 1–9. doi:10.1006/EXCR.2002.5498.

[49] G.R. Kirkham, S.H. Cartmell, Genes and Proteins Involved in the Regulation of Osteogenesis, in: R. Reis, E. Chiellini (Eds.), Top. Tissue Eng., Eds. N Ashammakhi, 2007: pp. 1–22.

[50] L.C. Gerstenfeld, C.M. Edgar, S. Kakar, K.A. Jacobsen, T.A. Einhorn, Osteogenic Growth Factors and Cytokines and Their Role in Bone Repair, in: F. Bronner, M.C. Farach-Carson, A.G. Mikos (Eds.), Eng. Funct. Skelet. Tissue, Springer, 2007: pp. 17–45. doi:10.1007/978-1-84628-366-6_2.

[51] D.V. Shtansky, I.V. Batenina, P.V. Kiryukhantsev-Korneev, A.N. Sheveyko, K.A. Kuptsov, I.Y. Zhitnyak, et al., Ag- and Cu-doped multifunctional bioactive nanostructured TiCaPCON films, Appl. Surf. Sci. 285 (2013) 331–343. doi:10.1016/j.apsusc.2013.07.169.

8. Conclusions and future work

8.1 Conclusions

The main objective of this work was the development of multifunctional coatings to be used as electrodes with good mechanical and electrical properties as well as antibacterial activity, based on two systems, $Ti_{1-x}Ag_x$ and Ag-TiN_x. In particular, it was focused on biomedical applications and most specifically in the implementation of a smart coatings for sensors to be used in hip prosthesis.

To meet this objective it was necessary to develop the following specific tasks:

- ✓ Deposition by magnetron sputtering on piezoelectric polymer substrates two different systems, $Ti_{1-x}Ag_x$ with different Ag/Ti atomic ratio and Ag-TiN_x coatings, where the nitrogen flow was varied; and correlate the structure, piezoelectric response and sheet resistivity with the deposition parameters and the atomic composition;
- ✓ Evaluate the mechanical behavior by uniaxial mechanical stretching as well as the electro mechanical response for the two systems;
- ✓ Study the antimicrobial activity of both series;
- ✓ Evaluate the osteogenesis of $Ti_{1-x}Ag_x$ and Ag-TiN_x electrodes, using MC3T3 osteoblastic cells.

The results revealed that the deposition conditions preserved the polymer structure, for both $Ti_{1-x}Ag_x$ and Ag-TiN_x series.

XRD analysis on $Ti_{1-x}Ag_x$ series, suggested the presence of crystalline hcp-Ti phase in pure titanium coating and fcc-Ag phase in pure silver coating. For the mixture of Ag and Ti and for the zone with Ag rich coatings, similar XRD patterns suggested the formation of TiAg phase together with the Ti and Ag phase.

On the other hand, for the Ag-TiN_x series, XRD revealed the presence of crystalline fcc-TiN phase and fcc-Ag phase in samples with N_2 flow above 3 sccm. According to SEM analysis, for $Ti_{1-x}Ag_x$ and Ag-TiN_x series the coatings were homogenous and only on Ag-TiN_x electrodes with nitrogen flow above 3 sccm show that Ag nanoparticles segregate from the TiN cubic grain boundaries.

The AFM analysis suggested that $Ti_{1-x}Ag_x$ coatings have similar morphologies, while for Ag-TiN_x series roughness tends to increase for samples with N_2 flow above 3 sccm due to the presence of silver nanoparticles on the film surface.

Sheet resistivity values showed the typical behavior of a binary alloy system for the $Ti_{1-x}Ag_x$ series, with low resistivity values for Ti and Ag coatings and a slightly higher resistivity values for samples composed by a mixture of Ti and Ag. For Ag-TiN_x series, with increasing nitrogen flow, the sheet resistivity tended to be lower than in the sample without nitrogen which could be explained by the Ag distribution on the TiN matrix because silver acts as a high conductivity dopant.

Piezoelectricity within the $Ti_{1-x}Ag_x$ series showed similar values, decreasing when nitrogen is incorporated for Ag-TiN_x series. Despite this behavior, it was possible to conclude that the deposition conditions do not significantly affect the piezoelectric polymer, which maintained its characteristics for sensor applications.

The mechanical performance of the two series was assessed by uniaxial stretching and electrical resistance variation measurements during mechanical stretching. It was concluded that thin films from $Ti_{1-x}Ag_x$ and Ag-TiN_x series can be used as piezoresistive coatings, with piezoresistive properties up to 5% of strain. The thin films deposited on β-PVDF polymer exhibited a similar performance with respect to the mechanical properties, where GF increased with increasing strain, being larger in the plastic zone than in elastic one. The Ag-TiN_x samples present higher GF values compared to the other series that can be explained by the presence of Ag nanoparticles/clusters imbedded in the TiN matrix.

The antimicrobial activity of samples from both series was assessed by agar diffusion method. Only electrodes from Ag-TiN_x series presented antibacterial activity. X-ray photoelectron spectroscopy (XPS) results showed that as-deposited electrodes from Ag-TiN_x series exhibited silver clusters smaller than 4 nm. SEM analysis in this series presented some Ag segregation in the TiN matrix. After Halo test, XPS analysis showed that Ag clusters disappeared, results corroborated by SEM images showing a visible aggregation and a significant decrease in the number of Ag nanoparticles. This suggested that Ag nanoparticles aggregate and/or diffused to the agar killing bacteria or inhibiting their grown. In $Ti_{1-x}Ag_x$ series, the fact that silver is chemically bound to the titanium (Ti-Ag bond), did not prevent the samples to possess any antibacterial activity. Therefore, Ag-TiN_x electrodes are more promising candidates to be used than $Ti_{1-x}Ag_x$ electrodes for PVDF sensors.

Osteogenesis of the two series was also evaluated using MC3T3 osteoblastic cells. The results indicate that less cells attach on the Ag-TiN_x electrodes compared with $Ti_{1-x}Ag_x$ electrodes. The same behavior was observed for proliferation and differentiation tests.

So, it was possible to conclude that the presence of silver nanoparticles in the surface of Ag-TiN_x electrodes affect, in a significant way, the cell response. Considering the final function of these electrodes, for sensors to detect mechanical loads on prostheses in an early stage, it is critical to have a bad initial adhesion, so as to assess mechanical loads just identified with the prostheses. In any case, at long term, an adequate cell development is required with a specific end goal to integrate the sensor in the prostheses, since the sensor won't be removed.

Overall, the Ag-TiN_x system present the most promising behavior to be used as electrodes for this sensor application.

8.2 Future work

Despite the successful development of electrodes for sensor applications, achieving good mechanical and electrical properties as well as antimicrobial activity, several analysis should be performed to further improve the systems and perhaps, allow a commercial product.

Thus, for a future work, it is recommended to further analyze the antibacterial activity, using more complex methods, as evaluation of adhesion and biofilm formation. It is also important to quantify the metallic ion release, by inductively coupled plasma (ICP), to establish a relation between the silver ions release and cell viability of Ag-TiN_x coatings, as well as the biofilm formation. Moreover, it may be interesting to do electrical voltage measurements at the same time as the antibacterial tests and assess the sensor performance *in situ*.

In addition, TEM analysis could be used to confirm the crystalline structures of the samples, especially in the two samples selected (Ag/Ti(0.11) from $Ti_{1-x}Ag_x$ series and TiN2Ag (sample from Ag-TiN_x series).

To conclude, it should be also studied the response of the sensor after osteogenesis.